

---

# Methods<sup>1</sup>

---

## Expedition 325 Scientists<sup>2</sup>

### Chapter contents

Introduction .....	1
Sedimentological and biological assemblages .....	7
Physical properties .....	9
Paleomagnetism .....	15
Geochemistry .....	17
Chronology .....	22
Downhole logging .....	24
Microbiology .....	29
Specialist sampling of massive corals .....	30
References .....	31
Figures .....	34
Tables .....	52

### Introduction

This chapter documents the primary procedures and methods employed by various operational and scientific groups during the offshore and onshore phases of Integrated Ocean Drilling Program (IODP) Expedition 325. This information concerns shipboard and Onshore Science Party (OSP) methods as described in each transect chapter. Methods for postcruise research conducted on Expedition 325 samples and data will be described in individual scientific contributions to be published after the OSP. Detailed drilling and engineering operations are described in the “Operations” sections in each transect chapter.

### Shipboard scientific procedures

#### Numbering of sites, holes, cores, and samples

Expedition numbers for IODP are sequential, starting with 301. Drilling sites are numbered consecutively, and for a European Consortium for Ocean Research Drilling (ECORD) Science Operator (ESO)-operated platform, numbering starts with Site M0001 (the “M” indicates the ESO-operated mission-specific platform). For Expedition 325, the first site was Site M0030. Multiple holes may be drilled at a single site. For all IODP drill sites, a letter suffix distinguishes each hole drilled at one site. The first hole drilled is assigned the site number with the suffix “A,” the second hole takes the site number and the suffix “B,” and so forth. For Expedition 325, in the *Scientific Prospectus* sites were represented as 125 m radius overlapping circles. All holes were initially given the suffix “A” even if located within the same “site” circle. This was considered the best option because of the close proximity of some of the proposed holes and the requirement to differentiate between each time the seabed was penetrated. This was specified by the Great Barrier Reef Marine Park Authority (GBRMPA) in the permit citing a maximum number of drilled “holes” allowed. Where attempts were made to drill secondary holes at the same coordinates, consecutive letters were used, following the IODP naming convention (for example, Holes M0030A and M0030B).

The cored interval is measured in meters below seafloor (mbsf). Depth below seafloor is determined by subtracting the initial drill pipe measurement obtained when the seabed was tagged from the total drill pipe measurement (i.e., the drilling depth below seafloor depth scale [DSF-A]). For Expedition 325, the cored interval normally consisted of the entire drilled section, but in some cases

<sup>1</sup>Expedition 325 Scientists, 2011. Methods. In Webster, J.M., Yokoyama, Y., Cotterill, C., and the Expedition 325 Scientists, *Proc. IODP, 325*: Tokyo (Integrated Ocean Drilling Program Management International, Inc.).  
doi:10.2204/iodp.proc.325.102.2011

<sup>2</sup>Expedition 325 Scientists’ addresses.



some intervals were drilled without coring (e.g., when drilling in open hole down to the previous cored depth in Hole M0052C).

Recovered core is split into sections with a maximum length of 1.5 m and numbered sequentially from the top, starting at 1 (Fig. F1). By convention, material recovered from the core catcher of a sedimentary core is treated as a separate section labeled “CC” (core catcher) and placed below the last section recovered in the liner. The core catcher is assigned to the top of the cored interval if no other material is recovered. When recovered core is shorter than the cored interval, the top of the core, by convention, is equated to the top of the cored interval to achieve consistency in reporting depth in core.

A soft to semisoft sediment core from less than a few hundred meters below seafloor can expand upon recovery (typically 10%–15%), so the recovered interval may not match the cored interval. In addition, a coring gap typically occurs between cores (i.e., some cored interval was lost during recovery or was never cut). Thus, a discrepancy exists between the drilling meters below seafloor and the curatorial meters below seafloor. For example, the curatorial depth of the base of a core can be deeper than the top of the subsequent core for an expanding sediment.

Any sample removed from a core is designated by the distance measured in centimeters from the top of the section to the top and bottom of the sample removed. A full identification number for a sample consists of the following information: expedition, site, hole, core number, core type, section number, piece number (for hard rock), and interval in centimeters measured from the top of section. For example, a sample identification of “325-M0030A-3R-2, 35–40 cm,” represents a sample removed from the interval 35–40 cm below the top of Section 2 of Core 3R-2 (“R” designates that this core was taken using the rotary core barrel), from Hole M0030A during Expedition 325 (Fig. F1). All IODP core identifiers indicate core type. For Expedition 325, the following abbreviations are used:

X = extended nose core barrel (EXN; equivalent to IODP’s extended core barrel),

R = rotary core barrel (alien corer [ALN]; equivalent to IODP’s rotary core barrel).

The mbsf depth of a sample is calculated by adding the depth of the sample below the section top and the lengths of all higher sections in the core to the core-top datum measured with the drill string.

## Core handling during the offshore phase of Expedition 325

As soon as a core was retrieved on deck, it was immediately curated by the ESO curators. This involved marking and cutting the core into sections with a maximum length of 1.5 m. Each section was sealed at the top and bottom by attaching color-coded plastic caps: blue to identify the top of a section and clear at the bottom. A yellow cap was placed on section ends where a whole-round sample was removed for microbiology. Core section liners were permanently labeled with an engraving tool. The lengths of the core in each section and the core catcher sample were measured to the nearest centimeter; this information was logged into ESO’s Offshore Drilling Information System (OffshoreDIS). No core splitting took place during the offshore phase of Expedition 325.

### Curation procedures for HQ cores

Coring with the HQ system used metal (stainless steel) split liner halves instead of plastic liners. This required additional steps in the curation procedure to transfer the “open core” into a standard IODP butyrate liner as follows:

1. Uncover the top metal half.
2. Take an empty liner with a precut slit on one side.
3. Carefully pull the liner over the core (the liner slit faces down under the metal half).
4. Turn everything by 180° (metal half is on top now).
5. Pull the metal half out, making sure to hold the core inside the liner by covering the open liner end.
6. Leave the transferred core on the core bench for 5–10 min with the split facing down to allow any remaining drilling fluids to drain.
7. Seal the split liner with heavy-duty tape and put on the blue and clear end caps, sealing with acetone.

All cores that were transferred from metal splits were identified in the drilling information system’s core-section input form under the “remarks” field.

After curation, the core proceeded through a sequence of processing steps. Geochemists and microbiologists were given access to the cores to sample for interstitial water (IW) and microbiology. This generally required 5–10 cm whole rounds to be taken, although Rhizon syringes for IW collection

were employed if core material was suitable. With the exception of IW, microbiology, and preliminary dating, no additional sampling of the cores or core catchers was undertaken during the offshore phase of Expedition 325.

The core catcher, or a sample of the core catcher, was given to the sedimentologists and coral specialists for initial description. Shipboard sedimentologists also took the opportunity to describe core sections through the clear plastic liners, although drilling fluid and mud caking often made this difficult or impossible. Subsamples of core catcher material were taken for preliminary dating using  $^{14}\text{C}$  or U-series analysis prior to the OSP, where the results would be presented as if they were “shipboard data.” These samples were identified by the Co-Chief Scientists and were located at the top, middle, and toward the base of each hole where suitable core catcher materials were available.

Core sections were allowed to equilibrate to “container” temperature before they were run through the multisensor core logger (MSCL).

### Core handling during the Expedition 325 Onshore Science Party

After being taken out of refrigerated storage, cores were split lengthwise into a working half and an archive half. Sections containing significant lengths or well-preserved smaller sections of massive coral were treated differently (see “[Specialist sampling of massive corals](#)”). Harder cores were split with a diamond saw. Softer cores, less common during this expedition with the exception of the forereef slope site (Hole M0058A), were split with a wire or saw, depending on the degree of induration. Wire-cut cores were split from bottom to top, so investigators should be aware that older material could have been dragged up the core on the split face of each half.

Digital high-resolution images of archive halves were made with a digital imaging system, followed by discrete color reflectance measurements. Archive halves were then described visually. Total organic carbon (TOC) and X-ray diffraction (XRD) samples were taken from the cores when requested by the science party during the core description phase. If required for illustrations of particular features by the scientists, close-up crops of the high-resolution line scan images were made.

The working half of the core was sampled for both the OSP and postcruise studies. Each sample was logged into the OffshoreDIS by hole, core, section, depth, sample request number, and the name of the lead investigator receiving the sample. Samples were sealed in vials, cubes, or bags; labeled; and stored as

appropriate. Samples were routinely taken for physical properties and magnetic susceptibility measurements, which are described below.

Following initial description, sampling, and measuring, both halves of the cores were wrapped in plastic to prevent rock pieces from vibrating out of order during transit. Both halves were then placed in labeled D-tubes, sealed, and transferred to refrigerated storage at the Bremen Core Repository (BCR; Germany).

## Operations equipment

### Site locations

At all Expedition 325 sites, GPS coordinates from precruise site surveys were used as a guide for positioning. The final coordinates and coring targets were selected from within the IODP-agreed 125 m radius around the original *Scientific Prospectus* positions by the Co-Chief Scientists. Selected positions were relayed to the European Geological Survey (EGS) hydrographic surveyors onboard, and the *Greatship Maya* was then settled on position using a dynamic positioning (DP) system. In order to maintain station accurately at each site, the DP system ran for 20–30 min prior to coring at each site to build a reliable footprint model. Where adjustments to the vessel position of <1 km were made under DP, the time required to build a suitable DP model was significantly reduced. The final site position was calculated by the surveyors, using the calculated mean position of 30 readings taken every second over the first 30 s period on station after the drill pipe had tagged the seabed.

The maximum required depth of the deepest boreholes was originally 100 mbsf. Initial approval was granted by the IODP Environmental Protection and Safety Panel (EPSP) to drill to a maximum total depth of 40 mbsf on the reef sites and 100 mbsf on the forereef sites. However, these depths were amended by the EPSP to 160 m below present sea level at one chosen site on each transect (to be identified when operational offshore) in order to capture the lowest possible sea level minimum during the last glacial period.

### Drilling platform

The water depth at all the sites is relatively shallow (42.27–167.14 m lowest astronomical tide). The drilling platform, chosen by the contractor and inspected by ESO, was the *Greatship Maya*, an IMO Class II dynamically positioned vessel complete with geotechnical coring capability (Figs. F2, F3). The *Greatship Maya* had sufficient capacity by way of food, water, and accommodation for 50 days of continuous operation, so there was no requirement for a

port call for resupply. However, because the operational period was extended as a result of weather downtime due to Cyclone Ului, resupply of the vessel did occur.

### Coring rig

The vessel was equipped with a large moonpool and a Bluestone TT150 derrick and Foremost Hydraulic top drive (Fig. F4). The compact top drive onboard the *Greatship Maya* was a 150 ton Canadian-built system (Foremost Industries) that is both rugged and powerful. The design of this top drive system has been adapted to make it ideal for geotechnical or scientific drilling, sampling, and coring activities. The derrick had a mast capable of handling 9 m string lengths (Fig. F5). Wireline operation of the core barrel was conducted through the top drive. Deployment of the wireline logging tools was conducted through the mud valve at the top of the top drive, from the rooster box.

### Coring methodology

For efficient drilling/coring it is essential to apply a steady weight onto the drill bit. Vessel heave can reduce or apply excessive weight to the drill bit; therefore, the drilling system onboard was heave compensated to allow vessel movement. The drill string was suspended below the top drive and the drill string compensator. The fast line ran over a relative motion-compensating heave (2.5 m stroke cylinders) and was connected to the drawworks winch. The deadline similarly ran to the anchor point at the drill floor. Compensator loading is ~80 metric tons.

Seawater was intended as the primary drilling medium, but because of the conditions encountered (loose sand at the seabed surface and caving lithological formations downhole), it was necessary to use a biodegradable drilling mud (guar gum). Biodegradable plastic bags containing fluorescent microspheres were attached to the core barrel for the first run of each borehole and at specified sites of interest to assist the evaluation of contamination of samples for later microbiology studies.

The drillstring available included 77 joints of nominal 9.2 m long American Petroleum Institute (API) drill pipe, 5½ inch with 5½ inch full hole tool joints with a 4 inch bore inner diameter; five API drill collars, nominal length 9.2 m; and an assortment of short (pup) joints. In addition, there were four available bottom-hole assemblies (BHAs), two each API and HQ; 84 lengths of 3 m Longyear HQ drill rods; and a selection of drill bits.

Two BHAs were used, as dictated by the expected lithological conditions and core recovery rates. The

API core barrel is a versatile BHA for the API drillstring that enables rock coring to be conducted using wireline coring techniques (see “[Coring with an API BHA](#)”) and can be used with an ALN and an EXN. The EXN is deployed to recover loose sediments. It is a nonrotating core barrel that protrudes from the drive tube. This configuration allows for a push sample-like core to be collected. As with the EXN, the ALN locks into the BHA but does not have a bearing on the core barrel allowing it to rotate. Instead, the entire assembly rotates to core a hard rock sample. Both corers may be run without altering the BHA, which allows quick change-over as required. Both are recovered to deck on a wireline.

The second BHA used was a mining-type HQ-size wireline core barrel, deployed on a mining drillstring, which fit inside the API drill string and used the API drillstring as a conductor or casing (see “[Coring with an HQ string](#)”).

Initially, a camera was deployed through the API pipe to assess the seabed character and the presence of live coral. Where no live coral was identified, drillers proceeded to spud in with the API pipe. This acted like a stinger and reduced the seabed footprint, minimizing potential impacts on the seabed environment. Following coring operations at each site, the aim was to deploy the camera again to photograph any impact from the coring operation on the seabed. On a number of occasions at Hydrographer’s Passage, the postcoring camera survey proved unsuccessful because of strong seabed currents pushing the drillstring off the vertical once it was raised above the seabed. The GBRMPA was advised of this and was satisfied on those occasions that the precoring survey to ensure that no live corals were cored was sufficient.

### Coring with an API BHA

A QD Tech coring system was selected to core both rock and sediments using the API string. Two types of inner barrel assemblies were available for this project: the EXN, which is used in sediments, and the ALN, which is used in rock formation. The ALN assembly has a short or long bit option. Assemblies are directly connected to the API drillstring and recovered to deck via wireline, which has the advantage over the HQ coring system of a faster total execution time. The operation of this coring tool follows a similar procedure as the HQ rod/barrel.

#### Alien sampler

The alien sampler is an inner tube assembly for collecting core samples in hard formations that cannot be sampled using push-style samplers. The alien sampler is deployed into the drillstring and seats,

seals, and latches into the BHA at the end of the drillstring. The core sampling portion, consisting of the shoe, core lifter, inner tube, and liner, is isolated from the rotating drillstring by a swivel-bearing arrangement.

The alien sampler outer tube and coring bit rotate with the main outer bit, and flushing water is ported through the face discharge ports in the alien sampler bit. Because of the various sample types that the alien sampler may encounter, there are three core lifter types: the basket core lifter, a hard rock-style core lifter, and an integrated core lifter shoe/basket spring (a diamond coring hard rock-style core lifter with basket springs). Aluminum split liners are also available for the alien sampler. The run length of the alien sampler is as much as 3 m before recovering the inner assembly using the wireline.

#### Extended nose sampler

The extended nose sampler is an assembly for collecting core samples in sediment using direct push force. It is deployed into the drillstring and seats, seals, and latches into the BHA at the end of the drillstring. The core sampling portion, consisting of the core lifter case (shoe), core lifter, inner tube, and liner, is pushed into the formation by the drillstring and is isolated from the rotating drillstring by a swivel-bearing arrangement. This inner assembly also has a vertical movement of as much as 2 inches, depending on the amount of force required against a return spring to penetrate the material.

Liner tubes and aluminum split tubes can be used in the extended nose sampler. The run length of the extended nose sampler is as much as 3 m before recovering the inner assembly with the wireline.

#### Coring with an HQ string

In this method, API drill pipes or drillstring is used as a casing. The drillstring is lowered to the seabed with a bumper sub connected 18 m from the drill bit. The string is then washed or slowly rotated a predetermined depth into the soft overburden, and the bumper sub is opened by filling it with drill mud. The top of the API string is then hung in the elevators on the drill floor. With the casing (drillstring) in place, the HQ core barrel can be lowered through the API string and bit.

A crossover sub is used to connect the HQ rods to the top drive. The rotational speed and bit load are adjusted by the three-speed gear change and the compensator. Constant bit load is achieved by increasing and decreasing the air in the compensator. The mud flow rate is managed by controlling the revolutions per minute (rpm) of the pump.

When a single core run (maximum = 3 m) is achieved, the inner barrel is retrieved by wireline and laid on a core rack on the drill floor while a standby barrel is lowered immediately. A two-barrel setup allows coring to continue while the core is extracted from the barrel recently recovered. This barrel can then be cleaned and fitted with a fresh liner tube for the next run. This process is continued until the target depth is reached.

A supplementary method to the above can be employed when encountering sediments or sand layers by advancing the casing as coring proceeds. Advancing the casing prevents the hole from caving in, thus preventing the core barrel from getting stuck. The casing is advanced only when there is evidence of high torque during coring on the HQ rod.

The maximum core run length was 3 m. However, the length of a core run was chosen to maximize core recovery and maintain hole stability, even at the expense of overall penetration speed. In unconsolidated materials and delicate coral frameworks, the run length was reduced to 1–1.5 m to facilitate better core recovery. In some cases, coring was stopped after <1 m if increasing pressure or high torque indicated problems advancing due to lithology or a blocked bit.

#### Downhole logging tools

Downhole logging services were contracted and managed by the European Petrophysics Consortium (EPC). Details and results of the expedition logging program are given in the “Downhole measurements” section in each transect chapter.

#### Through-pipe underwater video camera

A through-pipe camera survey was conducted before and, where possible, after coring at each site to ascertain that minimal damage would be done to any living coral present at the drill site, satisfying the environmental protection requirements of GBRMPA, the EPSP, and ESO.

The British Geological Survey (BGS) provided an underwater color video camera system and a deployment frame to allow it to be lowered inside the API drill pipe (Fig. F6). It is based on diver helmet-operated systems, with an umbilical cable relaying direct feed imagery to a monitor and recording system located inside the driller’s shack on the drill floor. The system worked well, and good video coverage was obtained from a number of sites. More importantly, the video demonstrated that it is possible to drill in a reef setting with minimal disturbance to the environment.

### Seabotix remotely operated vehicle

During Expedition 325, BGS also supplied a Seabotix LBV150SE Little Benthic Vehicle (LBV) rated to 150 m water depth. Two color cameras were on board the vehicle. The main camera was mounted with a switchable high-intensity LED light array on a tilt mechanism, which allowed a 270° range of view. The second camera was a fixed-focus rear-facing unit. The LBV was propelled by four powerful thrusters: one vertical, one lateral, and two horizontal. This configuration afforded four-axis maneuverability with a top speed of 3 kt and the ability to work in currents up to 2 kt. The system enabled visual inspections of the drillstring and seabed template with relation to the reef structures and seabed features to be carried out, with video imagery being relayed in real time to recording equipment on deck, thereby complementing the suite of pre- and postdrilling downpipe camera imagery. Because of the strong currents experienced at Hydrographer's Passage, it was not possible to launch the LBV at all sites.

### YSI Environmental 6600 V2-4 Sonde

The 6600 V2-4 Sonde was used to collect simultaneous measurements of conductivity (salinity), temperature, depth, pH, dissolved oxygen, and turbidity to monitor present-day oceanographic conditions at the drilling sites. In total, 40 profiles were taken (Table T1) across the four transects. Where possible, measurements were taken at various states of the tidal cycle (falling, rising, and slack water). However, in many cases, it was only possible to take one measurement because of the time on station before moving to a new location. In addition, on many occasions, especially at Hydrographer's Passage, the currents proved too strong to safely deploy the sonde. Sensor specifications are detailed in Table T2.

### Data handling, database structure, and access

Two overlapping phases of data management were used during Expedition 325. The first phase was the capture of metadata and data during the expedition (offshore and onshore). Central to this was the Expedition Drilling Information System (GBREC-DIS). The second phase was the long-term, postexpedition archiving of Expedition 325 data sets, core material, and samples. This was done by the World Data Center for Marine Environmental Sciences (WDC-MARE) and the BCR. The Publishing Network for Geoscientific and Environmental Data (PANGAEA) is the geoscience information system used by WDC-MARE, whereas the BCR uses the Curation Drilling Information System (Curation-DIS).

Offshore, the GBREC-DIS was used to capture drilling information, core and sample curation information, core catcher photographs, and primary measurement data (e.g., MSCL, downhole logging data, and additional data such as initial visual core descriptions (VCDs) of core sections (in liner) and core catchers and IW analysis. This process was replicated during the OSP, where a broader range of measurements and observations was captured (for example, line-scan images, color reflectance data, and visual core descriptions of the cut cores). Corelyzer was used to visualize the data (high-resolution line scan images and MSCL data).

Also, expedition scientists produced a variety of spreadsheet files, text documents, and graphics containing data, descriptions, and interpretations in different formats, both offshore and onshore. These files were stored in a structured file system on a file server.

Following the OSP, Expedition 325 data were transferred to WDC-MARE. This process was completed by the time this volume was published. Until the end of the moratorium period, Expedition 325 scientists could access the data through a password-protected data portal.

After the moratorium, the data are available to the public through the IODP Scientific Earth Drilling Information System (SEDIS) portal. WDC-MARE will continue to acquire, archive, and publish new results derived from Expedition 325 samples and datasets. Expedition core and sample metadata will be transferred to the BCR Curation-DIS and linked to the IODP Sample Materials Curation System (SMCS).

### Hardware installation

The ExpeditionDIS was implemented in SQLServer-2000 with Microsoft-based client PCs connecting to the system through a Microsoft Access-like user interface. For the offshore phase of the expedition, the ExpeditionDIS was installed on a server on the *Greatship Maya*. A second server was used as a hot-standby and data back-up system. Incremental backups to the secondary server were automatically made twice per day, and additional full backups to an external hard drive were also regularly made. These backups comprised the ExpeditionDIS and the shared file server. Automated database backups were also done twice per day.

A similar setup was used during the onshore phase. Two servers were used for the installed ExpeditionDIS and for handling files. ESO laptops were set up to provide access to the ExpeditionDIS in all used offices. Networked printers were also available via a

print server. Automated database and complete file server backups were also done twice per day. The expedition reports–related files were also backed up more frequently (an additional two times per day).

## Sedimentological and biological assemblages

### Visual core descriptions

Offshore sedimentologists and coral specialists conducted preliminary visual inspections and prepared written descriptions of the intact cores and core catcher material recovered during the expedition. Intact cores were examined visually, either through plastic core liners or uncovered when drilled using metal splits, along with a hand lens when necessary. More detailed observations of individual corals, bioclasts, and other components were made using a binocular microscope. These observations were recorded on visual core description (VCD) forms and then entered into the OffshoreDIS. Section description barrel sheets were generated from the information entered into the OffshoreDIS.

Onshore sedimentologists conducted visual inspections and observations of the archive halves of the cores and prepared written descriptions. Note that a single core can be composed of as many as three sections plus the core catcher. Onshore description of the coral fauna by the coral specialists within each cored interval was based mainly on observations of the archive halves of the cores. Section units were defined and numbered on the basis of general lithological changes and/or changes in the dominant hermatypic coral type (identified to family, genus, and/or growth form). This allowed the coral specialists and sedimentologists to map the preliminary stratigraphic positions of all visible corals on the VCD forms (Figs. F7, F8). The identity, general appearance, growth direction, and context of coral specimens were described from the top to bottom of each core. The following properties were described:

- Core disturbance and intervals of downhole sediment contamination in the upper parts of some cores;
- Lithologies;
- Sedimentary boundaries (e.g., lithological changes, depositional discontinuities, unconformities, erosional surfaces, hardgrounds, etc.);
- Major components;
- Minor components;
- Individual corals;
- Microbialites;

- Coralline algae;
- Mollusks, worms, bryozoans, larger foraminifera, and so on;
- Bioerosion and fossil preservation;
- Diagenesis and other features (e.g., dissolution, cementation phases, staining, geopetal fabrics, etc.).

### Core disturbance

Highly disturbed intervals were marked on VCD forms, and disturbance of the core caused by fracturing and/or grinding during drilling was recorded. In the upper part of some cores, sedimentary breccias were clearly identifiable as downhole contamination (Fig. F9).

### Lithology

Grain size was defined using terms and symbols from Wentworth (1922):

- cb = cobbles (256–64 mm).
- p = pebbles (64–4 mm).
- g = granules (4–2 mm).
- vc = sand, very coarse (2–1 mm).
- c = sand, coarse (1–0.5 mm).
- m = sand, medium (0.5–0.25 mm).
- f = sand, fine (0.25–0.125 mm).
- vf = sand, very fine (0.125–0.0625 mm).
- M = mud (<0.0625 mm) (true for fine carbonate sediment).
- s = silt (0.0625–0.0039 mm).
- C = clay (<0.0039 mm).

Overall lithology/texture was defined for carbonate sediments following Dunham's (1962) classification as modified by Embry and Klovan (1972). This classification distinguishes the following lithologies (see Fig. F10 for examples):

- Boundstone = original components organically bound during deposition.
- Bindstone = framework bound together by encrusting organisms.
- Framestone = rigid framework of organisms.
- Bafflestone = bound by organisms that act as baffles.
- Rudstone = granule/pebble-sized grains >2 mm, grain-supported textures with no matrix between the grains.
- Floatstone = granule/pebble-sized grains >2 mm, matrix supported.
- Grainstone = sand-sized grains <2 mm, grain-supported textures with no mud between the sand grains.

- Packstone = sand-sized grains <2 mm, grain-supported textures with mud between the sand grains.
- Wackestone = mud-supported textures with sparse sand-sized grains floating in the mud.
- Mudstone = mud-supported textures with sparse rare (<10%) sand-sized grains.

“Framework” is a lithology with in situ corals encrusted with thick coralline algal crusts or microbialites, and one where corals may make up only a small percentage by volume of the entire rock (see “**Major components of a core**”). Framework is a generic term that is *not* based on the most voluminous component (e.g., microbialite).

Any noncarbonate sediments and their lithified equivalents were also mentioned and described.

### Sedimentary boundaries

Lithological changes represented by discontinuities, unconformities, bioerosion, boring, and other features (e.g., staining, cementation, or dissolution) associated with such boundaries were marked on the VCD forms.

### Major components of a core

The major components of a core are defined as those that contribute to the highest percentage by volume of the sediment and/or rock. Framework lithologies can include corals, microbialites, or coralline algae as major components or may contain a mixture of these organisms. Major component categories used during the Onshore Science Party were modified slightly from those used in offshore descriptions. Terms and codes used to describe major and minor components are listed in Table T3.

### Coral descriptions

#### Coral taxonomy

Both offshore and onshore coral identifications generally followed the usage of Veron (2000) but were usually done only to family or genus, either because species-level taxonomic characters were not preserved or because there was insufficient time for careful examination. Many specimens were sampled for later identification. A few species were easily recognizable, and these were identified to species level. Uncertain identifications pending further study are marked “?”.

The most important taxonomic change from the offshore descriptions involved the common robustly branching to massive frame-building corals that were listed in the offshore reports as *Acropora palifera*, *Acropora cuneata*, or simply “massive *Acropora*.”

Recent genetic work (Wallace et al., 2007) demonstrates that these species belong to a different (but related) genus, *Isopora* Studer, 1878. Because the two species are morphologically very similar, they are described in the onshore reports as either *Isopora palifera/cuneata* or as “massive *Isopora*.”

#### Coral growth forms

Coral growth forms were described as

- Encrusting (<5 cm thick) or massive (>5 cm);
- Foliaceous (free margins <2.5 mm thick) or platy (free margins >2.5 mm);
- Branching-fine (<1 cm average diameter), medium (1–3 cm), robust (3–5 cm), or columnar (>5 cm);
- Tabular or discoid (free-living); or
- Fragments.

#### Coral context

Special attention was given to establishing the context of each coral within each cored section. A combination of criteria (Blanchon and Blakeway, 2003; Webster and Davies, 2003; Webster et al., 2004) was used to distinguish in situ corals from allochthonous rubble and/or drilling disturbance. These criteria included

- Presence or absence of fresh breakage surfaces;
- Presence or absence of severe surface abrasion and rounding of coral colonies;
- Orientation of well-preserved corallites;
- Orientation of coral skeletal characters, including growth axes;
- Presence or absence of thicker (>5 mm) coralline algal crusts capping upper surfaces;
- Presence or absence of attached substrate at base of coral; and
- Presence or absence (and orientation) of macroscopic sediment geopetals in cavities.

Based on these criteria, each larger individual coral was assigned a context:

- IS = in situ (convincing supporting evidence).
- ISX = not in situ (ISX) = convincing nonsupporting evidence.
- IS? = possibly in situ (IS?) = inconclusive supporting evidence.
- ISN = status not known (ISN) = inadequate evidence either way.

#### Microbialite descriptions

Some cores had laminated or clotted micritic sediment interpreted as microbialites (Camoin and Montaggioni, 1994; Camoin et al., 1999, 2006). Three



general morphologies were distinguished: laminated, dendritic, and undetermined. For microbialites that grew into open cavities, the morphology of the surfaces (knobbly versus smooth) was also distinguished.

### Larger benthic foraminifera

The cores were examined for the presence of larger benthic foraminifera (arbitrarily defined as benthic foraminifer tests >2 mm in diameter) using a Stemi 2000 binocular microscope. In this volume, if not otherwise qualified, “larger foraminifera” refers to larger benthic foraminifera (Hallock, 1985). Where present, larger foraminifera were identified to various taxonomic levels from species to order and summarized in tables for each transect. Wherever possible, the degree of preservation was noted.

### Diagenesis and other features

Where applicable, occurrences of such features as open cavities, geopetal infills, color staining, cementation, and diagenetic alteration of components were identified. Dissolution cavities were present in some cores. Some of these cavities were filled locally by internal bioclastic (marine) sediment, whereas other cavities were lined by cement. The morphology of this cement (e.g., whether it had a “speleothem” shape, acicular or fibrous morphology, and/or color staining) was described, as these features are indicative of subaerial exposure surfaces.

## Physical properties

The principal objective of the physical properties measurement program for Expedition 325 was to collect high-resolution data that will allow

- Characterization of lithostratigraphic units and formation properties,
- Facilitation of hole-to-hole correlation and the retrieval and construction of complete composite stratigraphic sections together with lithological and sedimentological descriptions for each hole, and
- Provision of data for construction of synthetic seismograms and investigation of the characteristics of major seismic reflectors.

Off shore, the physical properties program involved collecting high-resolution, nondestructive measurements on whole cores using a GEOTEK multisensor core logger (MSCL). The MSCL is equipped with four sensor types in order to measure gamma density, transverse compressional wave (*P*-wave) velocity, noncontact electrical resistivity (NCR), and magnetic susceptibility. Note that “gamma density” refers to

the bulk density of the core as derived from the collimation of gamma rays across the core (see “[Gamma density](#)”).

On shore, physical properties measurements included digital line-scan images and color reflectance. Lower resolution thermal conductivity measurements on unsplit cores, using a full-probe needle point inserted into whole cores, were conducted prior to the Onshore Science Party (OSP). Discrete samples taken from split cores during the OSP were measured for *P*-wave velocity and moisture and density (MAD). *P*-wave velocities were mostly measured on the same sample (in coral formations) or on a sample from the same depth (in sediments) as the MAD measurements. The resolution of these measurements is approximately one per section from the working half of split cores. Results from discrete sampling can be used to calibrate the high-resolution, nondestructive measurements made offshore on whole cores with the MSCL.

## Offshore petrophysical measurements

### Multisensor core logger

The MSCL has four primary measurement sensors mounted on an automated track that sequentially measure gamma density, *P*-wave velocity, NCR, and magnetic susceptibility at a 1 cm sampling interval. Two secondary measurement sensors are also present, which allow the primary measurements to be corrected for core diameter and temperature. Whole-core round sections were measured with the MSCL set up in horizontal mode. Automated measurements were taken on all core sections after they equilibrated to ambient temperature. Core catcher pieces and core shorter than 15 cm were not included in the logging process.

The quality and validity of the MSCL data are a function of both core quality and sensor precision. Optimal measurements for all sensors require a completely filled core liner and fully fluid-saturated cores. In sections where the core liner is insufficiently saturated, the quality of the measurements is compromised (see “[Quality assurance and quality control](#)” for an expanded discussion of this). In terms of sensor precision, gamma density and magnetic susceptibility sensors are affected by measurement time, whereas *P*-wave velocity and resistivity measurements are affected by temperature (see “[P-wave velocity](#)” and “[Noncontact electrical resistivity](#)”). To provide high-resolution data during Expedition 325, a downcore measurement sampling interval of 1 cm for all sensors was chosen on the basis of the amount of core and time available, coupled with the goal of attaining optimal resolution of data.

Cores were allowed to equilibrate to room temperature for a minimum of 6 h prior to measuring.

A full calibration of the MSCL sensors (Table T4) was conducted at the start of the expedition, every time the system was rebooted (for example, after power failure or after transit), and when calibration checks revealed unacceptable departures from full calibration values (see “[Quality assurance and quality control](#)”). Checks on the full calibration were then performed approximately once every 5–6 cores or every 6 h. These calibration checks involved logging three calibration reference pieces (magnetic susceptibility piece, standard core liner saturated with distilled water, and standard core liner saturated with 3.5 g/L salinity fluid) and comparison with the values derived during the full calibration. This allows the functionality of the four primary sensors to be assessed quickly.

### Measurement principles

#### Gamma density

Gamma density is measured by determining the attenuation of gamma rays (mainly by Compton scattering) that pass through the cores and is used as a proxy for bulk density. The degree of attenuation is proportional to the electron density in the gamma path (GEOTEK MSCL Manual; [geotek.co.uk/downloads/](http://geotek.co.uk/downloads/)). Gamma attenuation coefficients vary as a function of atomic number, but as most rock-forming minerals have similar and low atomic numbers, the correlation between gamma density and bulk density is generally very good.

A small (370 MBq)  $^{137}\text{Cs}$  source (half life = 30.2 y) was used to produce a gamma beam with primary photon energies of 0.662 MeV. The 5 mm diameter collimator was used throughout MSCL measurement operations during Expedition 325. The sampling interval was set at 1 cm with count time set at 10 s (the same as for the magnetic susceptibility sensor). The resolution with this setup is 0.5 cm.

Calibration of the system for Expedition 325 was completed using a stepped water/aluminum density standard (provided by GEOTEK). Initial calibration was performed using a standard core liner (~0.3 m length) containing the stepped aluminum calibration piece centered inside the liner and filled with distilled water. Gamma counts were taken for 30 s through each of the five aluminum steps of known thicknesses (6, 5, 4, 3, and 2 cm). In addition, the gamma counts of a liner filled entirely with distilled water were recorded. Regular calibration checks (every 5–6 cores) were conducted during logging, using the distilled water calibration piece. All data were handled using the processing parameters from these

wet calibrations. Dry calibrations (air/aluminum) were also conducted, and the processing parameters arising from these are available should reprocessing be required.

#### P-wave velocity

Transverse *P*-wave velocity was measured using two *P*-wave transducers aligned perpendicular to the core axis (in whole-core setup). A compressional acoustic wave pulse centered on a frequency of 230 kHz was transmitted horizontally across the core at each sample point (1 cm sampling interval). The *P*-wave transducers also function like displacement transducers, monitoring the variations in the outside diameter of the liner. These variations are ultimately used in processing of the gamma density, *P*-wave velocity, and magnetic susceptibility datasets (NCR is not affected by core diameter). Initial calibration was performed using a distilled water saturated standard core liner piece (~0.3 m length) at room temperature. This was repeated as necessary, following checks conducted by logging the calibration piece at regular intervals during the core logging process (calibration check pieces run every 5–6 cores or every 6 h, as with the other sensors).

This measurement is critically affected by the quality of the core. The data quality is poor where under-sized core causes a separation between the core material and core liner and also where the core is insufficiently water-saturated to allow for successful propagation of the acoustic pulse through the core. Prior to Expedition 325, it was decided that core liners would not be resaturated. As a result, core liners were often insufficiently saturated, and *P*-wave measurement was often unsuccessful because of poor acoustic coupling.

#### Noncontact electrical resistivity

Electrical resistivity of sediment cores was measured using the noncontact resistivity sensor. The measurement is based on a technique using two sets of coils, allowing for the comparison of readings from the core (one set of coils) with readings from taken in air (one set of coils). This makes measurement of the very small sensor responses possible. In terms of operation, the transmitter coil induces a high-frequency magnetic field in the core. This magnetic field induces electrical currents in the core that are proportional to the core's conductivity (inversely proportional to the resistivity of the core). Very small magnetic fields are then regenerated by these electrical currents, and these fields are then measured by the receiver coil. The spatial resolution of the measurement is ~2 cm.

Initial calibration was performed using six standard core liner sections (~0.3 m in length) containing

fluid of known salinity. The six standards were made up to concentrations of 35, 17.5, 8.75, 3.5, 1.75, 0.35, and 0 g/L. This calibration procedure was repeated as necessary following regular checks every 5–6 cores (or every 6 h) by logging a piece of core liner filled with fluid of salinity in the middle of the anticipated salinity range (3.5 g/L) of the logged core.

#### Magnetic susceptibility

Whole-core bulk magnetic susceptibility was measured on the MSCL using a Bartington MS2 system composed of a MS2 meter coupled to a MS2C sensor coil. The sensor coil has a diameter of 88 mm, corresponding to a loop diameter of 80 mm. The 80 mm loop used for Expedition 325 is a nonstandard loop operating at a frequency of 513 Hz (standard 80 mm loops usually operate at 565 Hz). A correction factor ( $\times 0.908$ ) is therefore applied to the processed data. The MS2 system operates on two fixed sensitivity levels,  $\times 0.1$  and  $\times 1$ . These sensitivity levels correspond to count times of 10 and 1 s, respectively. For Expedition 325, all cores were measured for magnetic susceptibility using the  $\times 0.1/10$  s setting because the cores were expected to have very low magnetic susceptibility, giving a poor signal response, and measurements can be optimized in this instance by increasing the count time. Measurements were made at a sampling interval of 1 cm. The sensor automatically zeroes and takes a free air reading at the start and end of each run in order to account for instrument drift by subtraction of a linear interpolation between readings. Magnetic susceptibility data were recorded as corrected volume specific units ( $\times 10^{-5}$  SI).

The accuracy of the magnetic susceptibility sensor was checked using a calibration standard (made of impregnated resin) with a bulk susceptibility of  $213 \times 10^{-6}$  cgs. This calibration piece was centered within a short section of core liner and logged at regular intervals during the core logging process to check functionality of the sensor.

Because of an intermittent sensor problem, the 80 mm loop was changed to a 90 mm loop for Hole M0047A and for all further holes. The slightly larger loop diameter means that the loop/liner diameter ratio is larger, and the quality of the data may therefore be affected.

#### Quality assurance and quality control

A quality assurance/quality control (QA/QC) check was carried out in three stages: during the offshore phase of the expedition, before the OSP, and during the OSP. During the offshore phase, QA/QC involved core quality description, use of hard copy and electronic MSCL log sheets and calibration sheets, and

repeat MSCL logging of selected cores as described below. Postoffshore systematic cross-checks of electronic calibration, data files, and processed data were made. The final dataset was made available during the onshore phase as raw, processed, and filtered data.

The quality of the MSCL data is greatly affected by the quality of the core being measured. Core quality issues including undersized cores, small segments, and rubble were all prevalent in the Expedition 325 cores. The impact on the measurements is such that data are often underestimated or erratic, and as such, the dataset should be treated with caution.

In addition to sensor calibrations and calibration checks, a QA/QC repeat measurement plan was in place during the offshore phase of the expedition. Twenty-six core sections were relogged while offshore, with sections selected from a variety of depths but otherwise at random to avoid any bias. Gamma density and noncontact resistivity data were the most repeatable of the measurements. Those which gave large differences between the original and repeat measurements can be attributed to core quality issues. The magnetic susceptibility repeated measurements were much closer in value to the original measurements after the loop change (see “[Magnetic susceptibility](#)”). Those repeated measurements taken on the 80 mm loop had good agreement in terms of trends but not in terms of absolute values of the original data. Where available (three core sections), the repeated *P*-wave velocity data was very close in value and trend to the original dataset.

A roll test was also conducted on a section that highlighted the effect of core orientation on different measurements. NCR gave the greatest variation in repeated results, owing to a combination of depth of investigation and core heterogeneity. Gamma density exhibited good agreement in opposite pairs of results (north–south and east–west), which can be explained by the way in which the sensor works. Magnetic susceptibility gave consistently good agreement between all four roll test measurements, which, as with gamma density, can be attributed to the way the sensor operates.

#### Onshore petrophysical measurements

Onshore petrophysical methods are described in the order in which they were undertaken. Thermal conductivity required measurement on whole cores, and the measurements were therefore taken in advance of the OSP. Line-scanning and color reflectance measurements were conducted on split core sections, and it was necessary to do these measurements as soon after splitting as possible to preserve the integrity of the images and data. The remaining measure-

ments (discrete *P*-wave and MAD) were conducted on discrete samples taken from the split cores and were therefore done last.

### Thermal conductivity

Thermal conductivity was measured with the TeKa TK04 system using the needle-probe method in full-space configuration for soft sediments (Von Herzen and Maxwell, 1959). The needle-probe contains a heater wire and calibrated thermistor. It is assumed to be a perfect conductor because it is significantly more conductive than the sediments that it is measuring. Cores were measured cold, at a temperature of 4°–6°C in the reefer at the Center for Marine Environmental Sciences (MARUM) at Bremen University (Germany).

Thermal conductivity of whole cores from Expedition 325 was measured by inserting the needle-probe into the sediment through a small hole drilled into the core liner. The needle was always inserted parallel to the splitting plane of the core to ensure minimum disturbance of cores. Generally, the coefficient of thermal conductivity ( $k$  [W/(m·K)]) is calculated from the following:

$$k(t) = (q/4\pi) \times \{[\ln(t_2) - \ln(t_1)]/[T(t_2) - T(t_1)]\},$$

where

$T$  = temperature (K),

$q$  = rate of heat flow through the material (W/m),  
and

$t_1$  and  $t_2$  = time interval (normally 80 s duration)  
along the heating curve(s).

The correct choice of  $t_1$  and  $t_2$  is complex. Commonly, thermal conductivity is calculated from the maximum interval ( $t_1$  and  $t_2$ ) along the heating curve where  $k(t)$  is constant. In the early stages of heating, the source temperature is affected by the contact resistance between the source and the full space, and in later stages, it is affected by the finite length of the heating source (assumed infinite in theory). The special approximation method employed by the TK04 software is used to develop a best fit to the heating curve for all of the time intervals where

$$20 \leq t_1 \leq 40,$$

$$45 \leq t_2 \leq 80,$$

and

$$t_2 - t_1 > 25.$$

A good measurement results in a match of several hundred time intervals along the heating curve. The

best solution (output thermal conductivity) is that which most closely corresponds to the theoretical curve. Numerous measuring cycles were automatically performed at each sampling location, and, when obtained, the best five were used to calculate an average thermal conductivity.

Thermal conductivity measurements were taken at one location within a core, and cores were sampled where appropriate. Most of the Expedition 325 cores were corals, which are not appropriate for thermal conductivity measurement owing to voids in the core. Measurements were taken primarily in soft sediments, into which the TK04 needles could be inserted without risk of damage. However, if sediments were partially or completely lithified, a small hole was drilled into the core prior to inserting the TK04 needle.

### Digital imaging

Digital linescan images of the split cores were obtained during the OSP using the Avaatech Superslit X-ray fluorescence (XRF) core scanner in operation at MARUM and supported by the DFG-Leibniz Center for Surface Process and Climate Studies at the University of Potsdam (Germany). The XRF scanner has an option for linescan camera and linear light source, and it should be noted that XRF was not taken on the cores. The linescanner produces high-resolution color images and also outputs accurate color data in red-green-blue (RGB) and Commission Internationale d'Eclairage lightness, a (green to red chromacity), and b (blue to yellow chromacity) (CIE-Lab) units because of individual charge-coupled device pixel calibration. The Linescan Program uses the Stemmer Common Vision Blox platform to acquire and process color images.

The camera system contains a three charge-coupled device camera with beam-splitter and a manual controlled Pentax 50 mm lens. The image resolution is ~150 pixel/cm in the crosscore and downcore directions. With an exposure time of 5 ms, a scan speed of 125 mm/s was achieved. The image coverage in the crosscore direction is ~13.5 cm and in the downcore direction a maximum 153 cm.

Every split core was imaged with a color/gray chart beside it, and this scan is available as the original file. Three output files are generated for each core section: a high-resolution bitmap file (.BMP), a compressed image file (.JPEG), and a numeric text file (.TXT). Numeric data are in RGB units. The linescan system was calibrated every 24 h with black and white calibration. All split cores were measured using aperture setting  $f/5.6+$  (a fixed value between 5.6 and 8) and white calibration level  $f/11+$  (a fixed value between 11 and 16). Consistency of equipment settings

was chosen over custom settings in order to ensure uniformity of the dataset. Software features necessitate the length of linescan images to be a couple of centimeters longer than the curated core length. For Expedition 325, bitmap picture files were modified to match the length of the cores after the image was taken. Where a whole-round sample had been removed from the core, a foam placer was inserted in its place. The numeric data files were corrected to the same length as the modified .BMP picture files. Both original and corrected files were uploaded to the database. All images were checked by the operator to ensure that the full core section had been captured by the scan before acceptance of data.

### Diffuse color reflectance spectrophotometry

Archive halves were typically measured at 2 cm intervals using a handheld Minolta spectrophotometer (model CM-2600d). Interval spacing was adjusted appropriately depending on the nature of the core. White calibration of the spectrophotometer was carried out twice per day, and a calibration for zero was performed once per day on starting up the machine. Prior to measurement, the core surface was covered with clear plastic wrap (Hostaphan) to maintain a clean spectrometer window.

Spectrophotometric analyses produce three types of data:

1.  $L^*$  (lightness),  $a^*$ , and  $b^*$  values, where  $L^*$  is a total reflectance index,  $a^*$  is the green (–) to red (+) chromaticity, and  $b^*$  is the blue (–) to yellow (+) chromaticity (Minolta Spectrophotometer CM-2600d Manual; [www.konicaminolta.eu/fileadmin/CONTENT/Measurement\\_Instruments/Download/NEU\\_Owners\\_Manuals/CM-2600d\\_2500d\\_IM\\_English.pdf](http://www.konicaminolta.eu/fileadmin/CONTENT/Measurement_Instruments/Download/NEU_Owners_Manuals/CM-2600d_2500d_IM_English.pdf));
2. Munsell color values; and
3. Intensity values for 31 contiguous 10 nm wide bands across the 360–740 nm interval of the light spectrum with a reflectance range from 0% to 175% and a resolution of 0.01% (Minolta Spectrophotometer CM-2600d Manual).

When utilizing the spectrophotometric measurements, it is recommended that detailed examination of core photos/images and disturbance descriptions/tables is undertaken in order to cull unnecessary or spurious data. However, this screening process was minimized by targeting appropriate locations along the core for measurements with the handheld sensor. Measurements were taken with the instrument horizontal against the split core surface. The location in depth of the measurement was recorded. Measurements were taken in the most homogeneous areas at each depth downcore in order to obtain as pure a color reflectance signal as possible.

### P-wave velocity from discrete samples

*P*-wave velocity in material removed from a split core can be derived from the traveltime of acoustic waves passing through a sample of known thickness. *P*-wave velocity varies with the lithology, porosity, saturation, and bulk density of the material, as well as state of stress and degree of fracturing. In marine sediments and rocks, velocity values are also controlled by the degree of consolidation and lithification, fracturing, occurrence and abundance of free gas and gas hydrates, and so on. Together with density measurements, sonic velocity is used to calculate acoustic impedance, or reflection coefficients, which can be used to estimate the depth of reflectors observed in seismic profiles and ultimately to construct synthetic seismic profiles.

*P*-wave velocity was measured during the OSP using a GEOTEK *P*-wave logger for discrete samples (PWL-D). The equipment consists of a mechanical section containing the transducers (between which the sample to be measured is placed), a set of electronics, and a computer. The two transducers also contain receivers. Acoustic coupling is achieved through solid neoprene surfaces (pads on the transducers) and can be improved by applying downward pressure on the sample between transducers and/or by wetting the neoprene with distilled water. A laser distance transducer measures the thickness of the sample. The PWL-D system can measure velocities on cubic or cylindrical, consolidated or lithified core specimens. Poorly consolidated samples are not suitable for measurement with the PWL-D because they tend to crumble when placed between the transducers. The system allows measurement on split cores in the direction perpendicular to the split core surface.

The basic velocity equation is

$$v = d/t,$$

where

$d$  = distance traveled through the material (m) and  
 $t$  = traveltime of the *P*-wave through the material.

The PWL-D was calibrated at the start of each set of samples measured. Calibration involved measurement of a sample of known length and *P*-wave velocity, and a measurement was also taken with the transducers touching (zero distance). In order to monitor drift of the measurements, the velocity of the calibration piece was also noted at the end of each sample run.

Time delays that are subtracted to correct the traveltime are the delay related to the transducers and electronics ( $t_{\text{delay}}$ ) and the delay related to the peak detection procedure ( $t_{\text{pulse}}$ ). Delays were determined

during calibration with zero distance. For routine measurements on discrete samples with the PWL-D system, the equation for the velocity is

$$v_{\text{core}} = 1000 \cdot d_{\text{core}} / (TOT - PTO),$$

where

- $v_{\text{core}}$  = velocity through sample (m/s),
- $d_{\text{core}}$  = measured thickness of the sample (mm),
- $TOT$  = measured total traveltime ( $\mu\text{s}$ ), and
- $PTO$  = delay correction ( $\mu\text{s}$ ).

A pulse is sent to the transmitter sensor, which generates an ultrasonic compression wave at  $\sim 230$  kHz, which then propagates through the sample and is received by the receiver sensor. The received signal is processed through an analog to digital converter before being displayed in the software display. The signal is digitized at a sampling frequency of 12.5 MHz.

In the software, a threshold detector determines the first positive or negative excursion on the received pulse and can be adjusted by the operator. The pulse timing is achieved by measuring the time to the first zero crossing after the threshold has been exceeded. In this way, the traveltime measured is approximately one half of the wavelength after the start of the pulse but is measured without any errors caused by signal amplitude. A delay can be used to define the point at which the software should start its threshold detection. The delay should be set before the start of the signal.

Sample quality strongly affects the ability to acquire  $P$ -wave velocity data. It was important during Expedition 325 to prepare the sample correctly in order to get good contact between the transducers. Where appropriate, preparation involved cutting the sample to ensure there were two flat, parallel surfaces to aid in good acoustic coupling with the transducers.  $P$ -wave velocity is also sensitive to temperature (Leroy, 1969), with  $P$ -wave velocity increasing with increasing temperature. Temperature was recorded during every measurement. The  $P$ -wave system was calibrated before every measuring session.

$P$ -wave measurements were made on discrete samples taken, on average, once per section. In areas of coral material, one discrete sample was collected and analyzed for both MAD and  $P$ -wave. In areas of sediment, separate  $P$ -wave and MAD samples were taken, in most cases, at the same depth or near each other. It was not possible to measure all samples because some samples were not well consolidated and crumbled when placed between the transducers. Measurements were performed first on samples straight from the sampling table ("initial"), followed by samples dried in the oven for 24 h ("dry"), and then finally fluid-saturated samples ("resaturated"). Saturation of

pore spaces was achieved by placing the sample in a saline solution of 35 g/L ("seawater") for 24 h while in a vacuum. The  $P$ -wave measurement was performed three times at each stage (initial, dry, and resaturated) for each sample for more reliable results.

Data files are in tab-separated value (.TXT) format and contain a header with the core followed by the measured data and the calculated velocity and sample stage (initial, dry, and resaturated). The waveform is recorded in two columns containing the time base and voltage changes.

### Moisture content and density

MAD measurements (bulk density, dry density, grain density, water content, porosity, and void ratio) were determined from measurements of the wet and dry masses of core plugs and dry volumes.

Discrete samples of  $<10$  cm<sup>3</sup> were taken from the working-half sections and transferred into previously weighed and calibrated 10 mL glass beakers. Samples were taken at an interval of one sample per section, in a zone of geological interest, where core quality allowed. In areas of coral material, only one discrete sample was taken per section for both MAD and  $P$ -wave analyses. However, in areas of sediment, a further 3 to 15 cm<sup>3</sup> sample was collected as close as possible to the MAD sampling point for discrete transverse  $P$ -wave velocity measurements.

Wet samples were weighed to a precision of 0.001 g using an electronic balance ( $M_{\text{wet}}$ ). Samples were dried in a convection oven at  $105^\circ \pm 5^\circ\text{C}$  for a period of 24 h followed by cooling to room temperature in a dessicator. Dry sediments were successively weighed ( $M_{\text{dry}}$ ) and measured using a Quantachrome pentapycnometer (helium-displacement pycnometer) with a precision of 0.02 cm<sup>3</sup>. This equipment allowed the simultaneous analysis of four different samples and one standard (calibration spheres). Volume measurements were repeated a maximum of five times, or until three consecutive measurements exhibited  $<0.02\%$  standard deviation with a purge time of 1 min. Volume measurements were averaged per sample ( $V_{\text{dry}}$ ). Calibration spheres were cycled from cell to cell of the pycnometer during each run to check for accuracy, instrument drift, and systematic error.

The mass of the evaporated pore water ( $M_{\text{pw}}$ ) is given by

$$M_{\text{pw}} = M_{\text{wet}} - M_{\text{dry}}$$

The volume of pore water ( $V_{\text{pw}}$ ) is given by

$$V_{\text{pw}} = M_{\text{pw}} / \rho_{\text{pw}},$$

where  $p_w$  = pore water density at standard laboratory conditions ( $1.024 \text{ g/cm}^3$  and 3.5% salinity).

Salt precipitated in sample pores during the drying process is included in the  $M_{\text{dry}}$  and  $V_{\text{dry}}$  values, resulting in the following approximations:

- The mass of solids including salt ( $M_{\text{solid}}$ ) is given by the dried mass of the sample ( $M_{\text{dry}} = M_{\text{solid}}$ ).
- The volume of solids including salt ( $V_{\text{solid}}$ ) is given by the measured dry volume from the pycnometer ( $V_{\text{dry}} = V_{\text{solid}}$ ).
- The wet volume ( $V_{\text{wet}}$ ) is given by

$$V_{\text{wet}} = V_{\text{solid}} + V_{\text{pw}}$$

For all sediment samples, water content ( $w$ ) is expressed as the ratio of the mass of pore water to the wet sediment (total) mass:

$$w = M_{\text{pw}}/M_{\text{wet}}$$

Wet bulk density ( $w$ ), dry bulk density ( $d$ ), sediment grain density ( $g$ ), and porosity ( $\phi$ ) are calculated from the previous equations (density is given in  $\text{g/cm}^3$ ):

$$w = M_{\text{wet}}/V_{\text{wet}}$$

$$d = M_{\text{solid}}/V_{\text{wet}}$$

$$g = M_{\text{solid}}/V_{\text{solid}}$$

and

$$\phi = V_{\text{pw}}/V_{\text{wet}}$$

Expedition 325 samples were selected from the least disturbed intervals. However, it was not possible to ensure that all were completely uncontaminated by fluid inundation during the core splitting and sampling process.

Porosity values derived from MAD measurements may be underestimated in particular coral units. This is a consequence of the high permeability of these sediments, which allow fluid to drain from the cores during the weighing process. Finer grained sediment cores are less susceptible to such draining, and as such, the porosity estimates are more accurate.

## Paleomagnetism

### Magnetic susceptibility

Magnetic susceptibility is an indicator of the strength of the transient magnetism within a sample in the presence of a magnetic field (Nagata, 1961). All mineral grains are “susceptible” to be magnetized

when submitted to a magnetic field, and the level of magnetic susceptibility is a function of the concentration and composition of the “magnetizable” materials in a sample. Materials that create an opposite magnetic field (low), which has a negative magnetic susceptibility, are called “diamagnetic,” consisting mainly of organic matter, glass, pure carbonate, and water. Materials that react with (and are slightly attracted to) the applied magnetic field are called “paramagnetic.” Examples of these are aluminum, sodium, magnesium, and most of the clay minerals. The important paramagnetic minerals in marine sediments include clay minerals (e.g., illite, chlorite, and smectite), ferromagnesian silicates (e.g., biotite, tourmaline, pyroxene, and amphiboles), iron sulfides (e.g., pyrite and marcasite), iron carbonates (such as siderite and ankerite), and other iron- and magnesium-bearing minerals (Ellwood et al., 1989, 2000, 2007). When a material is able to keep its own magnetization, it is called “ferromagnetic” (e.g., magnetite and hematite).

The study of susceptibility in contrast with rock magnetic analyses provides quantitative and qualitative information about the paramagnetic and ferromagnetic materials in the sediments. Therefore, the presence of cyclic trends in magnetic susceptibility recorded in marine environments can be related to fluxes of detrital sediments resulting from environmental changes attributed ultimately as Milankovitch-driven cyclicity derived from variations in the orbital parameters of the Earth (deMenocal et al., 1991; Weedon et al., 1999; Ellwood et al., 2000, 2007). This can in turn be related to periodical enhancement or reduction of either detrital or eolian origin components, or both, which are transported to the marine environment and distributed by ocean currents (Ellwood et al., 2006). Therefore, this cyclic appearance of magnetic susceptibility due to astronomical causes can be used as a chronological control on geologic timescales (Jovane et al., 2006, 2010). However, the astronomical forcing “footprint” is often superimposed upon other high-frequency local and temporal signals (i.e., tectonic, eustasy, sea level changes, etc.), that also affect the fluxes of magnetic material into the marine environment.

Magnetite and greigite can be produced as intracellular crystals inside of the magnetotactic bacteria. These particular bacteria live in the oxic–anoxic transition zone of waters and sediments (Kopp and Kirschvink, 2008). How this component relates to corals and coral reef systems has never been studied.

Low-field magnetic and mass-specific susceptibility ( $\chi$ ) was measured on minicores, discrete standard IODP paleomagnetic plastic boxes ( $2 \text{ cm} \times 2 \text{ cm} \times$

2 cm), and selected coral samples at the Bremen Core Repository, using a KLY 2 (AGICO) Kappabridge with an operating frequency of 920 Hz and a magnetic induction of 0.4 mT (noise level of  $2 \times 10^{-10}$  m<sup>3</sup>/kg). Low-field bulk magnetic susceptibility values obtained have been iteratively checked with MSCL and color reflectance data in order to study their relationship with continuous proxies (e.g., density, volume-specific magnetic susceptibility, and resistivity) and the color of the sediments. Samples were obtained as 2.5 cm (1 inch) minicores drilled perpendicular to the split face of the rock cores. Samples were spaced at irregular intervals of ~1 m in the rubble material sections, with the object of collecting at least one specimen per section depending on sample availability. When material was rubble coral, loose pieces of the corals were collected. For sections that comprised continuous material, discrete minicores were collected with a spacing interval of 10 cm. Low-field magnetic susceptibility data were recorded as corrected mass-specific units ( $\times 10^{-8}$  m<sup>3</sup>/kg). Additionally, the diamagnetism of sample holders and paleomagnetic boxes (if used) has been removed in relation to the very low susceptibility values of the corals and sediments studied. The accuracy of the Kappabridge was checked using a calibration standard with a bulk susceptibility of  $1165 \times 10^{-6}$  SI. This calibration piece was run in the Kappabridge every six core sections.

Oriented paleomagnetic samples were recovered, where possible, from all core intervals in which the up-down orientation had been preserved. Unfortunately, some intervals were composed exclusively of coral rubble material, so the azimuthal orientation of each individual core section was often random, and shorter intervals within each core section were obviously rotated relative to each other. As a result, any potential paleomagnetic analysis is limited to measure inclination and relative paleointensity.

### Natural remanent magnetization and environmental magnetism

One important aspect of the Expedition 325 program is the recovery of high-quality paleomagnetic data to improve the existing paleointensity stacked curve (Valet et al., 2003, 2005). Results from IODP Expedition 310 demonstrate that these records can be recovered from corals and recent carbonate sediments of coral reefs such as Tahiti (e.g., Lund et al., 2010; Ménabréaz et al., 2010). Therefore, paleomagnetism and magnetostratigraphic studies are important observations needed to fulfill the expedition objectives of obtaining

1. The origin of the magnetic components,

2. A magnetic record (magnetic susceptibility and rock magnetism) useful for correlation between cores,
3. Well-intercalibrated paleointensity records, and
4. Information regarding environmental changes of sediments and corals in relation to sea level changes and climate.

There are some fundamental conjectures in using paleomagnetic directions to resolve the core azimuth of the material recovered. The direction and the inclination of the geomagnetic field in which the characteristic remanent magnetization was acquired must be known and should show a normal inclination. Coral and sediment samples collected during Expedition 325 encompass the time intervals from the present day back to a maximum of >30 calibrated years before present (cal y BP; years before 1950 AD), which is long enough for the Earth's magnetic field to be modeled satisfactorily by a geomagnetic axial dipole for the timescales of Quaternary to Neogene (McElhinny, 2007). The carbonate sediments collected are recent and unconsolidated; thus, the presence of a potential shallowing of inclination can be excluded. The sample interval resolution is sufficiently long for geomagnetic secular variation to be averaged out, and in principle we know that the bedding is horizontal. Thus, cleaned paleomagnetic data will be characterized by shallow inclinations, consistent with the sites being near the paleoequator (15°–20°S; paleolatitude = ~28° to ~36°), and by normal inclinations.

Magnetic minerals in a carbonate setting are driven by detrital origin relative to environmental changes in the nearby continent (Verosub and Roberts, 1995). However, other contributions must be considered, as magnetic minerals can also be supplied into the system from biogenic or other origins such as (1) magnetotactic bacteria production (Kopp and Kirschvink, 2008), (2) precipitation, (3) dehydration, (4) crystallization as authigenic oxides (e.g., magnetite) and as hydroxides (e.g., goethite and hematite), or (5) chemical or microbial reduction (anoxic basin and fecal pellets) (Jovane et al., 2009).

Paleomagnetic analysis was performed at the University of Bremen. Samples contained in discrete standard IODP paleomagnetic plastic boxes (2 cm × 2 cm × 2 cm) were measured using the pass-through 2G Enterprises automated cryogenic magnetometer (Model 755), with internal diameter of 4.2 cm and equipped with three direct-current superconducting quantum interference device (DC-SQUID) sensors (noise level  $\leq 1 \times 10^{-9}$  emu). Natural remanent magnetization (NRM) was measured on selected box samples with the highest magnetic susceptibility. Standard stepwise alternating-field (AF) demagneti-



zation was also conducted at steps of 0, 5, 10, 15, 20, 25, 30, 35, 40, 50, and 60 mT to obtain a NRM record of the samples studied. We recognize that only a few samples are characterized by high NRMs, and these appear to be associated with layers of high values of magnetic susceptibility among the different lithological facies. Demagnetization data that were obtained from the AF stepwise method have been examined using orthogonal vector component diagrams (Zijderveld, 1967; Kirschvink, 1980).

The demagnetization method used does not remove the magnetization for the entire core section. Other methods, such as thermal demagnetization experiments, could be used to remove the overprinting that may be related to the presence of high-coercivity magnetic minerals such as hematite and goethite, and so reduce the NRM intensity. However, the overprinting cannot be erased with standard AF demagnetization, and there are still uncertainties regarding how the secondary overprint was acquired and why some samples do not demagnetize at all and others have the potential for demagnetization. The component of any drilling-related overprint that may remain will have a negative effect on both inclination and declination results. However, samples for which data analysis suggests no overprinting, or for which much of the drilling overprint has been removed, will be used to conduct further studies, such as paleointensity experiments.

In order to investigate the environmental magnetic signal carried by the finer magnetic materials in question, we conducted anhysteretic remanent magnetization (ARM). Environmental magnetism provides qualitative and quantitative information of concentration, composition, and grain size of the magnetic particles, which can be directly related to the sedimentary processes or geological systems. The initial approach to study the environmental magnetic signal is to define rock magnetic parameters such as quantity, quality, and dimension of magnetic grains by means of ARM experiments. This is an induced artificial magnetization comprising the demagnetization of 100 mT with a superimposed 50  $\mu$ T direct-current bias. In relation to the physical properties, ARM experiments magnetically excite only the finer magnetic minerals, and for this reason, when ARM data are normalized for the concentration of the total magnetic minerals, the results are able to provide information of the magnetic grain size.

## Geochemistry

### Shipboard sampling procedures

#### Offshore interstitial water sampling using rhizon samplers

Rhizon sampling was undertaken where the structure of the sediments allowed the insertion of rhizon samplers. A standard 3.8 mm diameter drill bit was used to drill a hole in the plastic liner. A spacer on the drill bit prevented the bit from penetrating the core material. Core catcher materials were sampled in a split liner after they were delivered from the drill floor. If necessary, a 2.5 mm wide stainless steel stick was used to prepare a hole in the sediment. Rhizon samplers were placed in a beaker with pure water prior to use. Sample vials were prepared with preservatives (Table T5).

Rhizon samplers were carefully pushed into the sediment and connected to a 50 or 20 mL disposable syringe. A vacuum was established by pulling the syringe plunger and keeping it open with a wooden spacer. The sampling interval was variable and determined by the availability of suitable core material and the amount of drill mud contamination. If the pore water flow through a rhizon sampler was slow, the syringe was taped to the liner to allow core curation procedures to continue. Alternatively, the rhizon samplers were removed and cores were logged and resampled with fresh rhizon samplers after logging.

Where drill mud contamination was negligible, 30 min to 2 h was required for the syringe to fill with pore water. If there was still pore water flow, the syringe was emptied into a 20 mL scintillation vial (Greiner; polypropylene) and reattached. Filtering was generally not necessary because the maximum pore width of the rhizon samplers is 0.2  $\mu$ m. Broken rhizon samplers can easily be detected, as the vacuum cannot be maintained when the porous tube is damaged. If detected early, damaged rhizon samplers were replaced. Samples collected from broken rhizon samplers were refiltered with 0.45  $\mu$ m disposable syringe filters (Nalgene 25 mm; nylon). When pore water collection was very slow, two rhizon samplers were used in the same sampling interval to speed up the sampling procedure. Rhizon samplers retain 130  $\mu$ L of liquid when wet and are prepared for use by being placed in a beaker with pure water. Ideally, the first drops of residual water would have been dis-

carded to avoid collecting it. However, at very low expected sample volumes it was decided to leave this water in the sample and account for the dilution. Approximate sample volumes were measured volumetrically using the syringe grading. Gravimetric measurement was not possible because of the ship movement.

### Effect of drilling procedures on interstitial water quality

Cuttings were flushed from both the HQ and American Petroleum Institute pipes with drill mud composed of guar gum mixed with seawater. Guar gum is a natural, biodegradable polysaccharide that gels in the presence of calcium ions. Guar gum is nonionic and stable in seawater. Upon microbial degradation, the mixture, if undisturbed, becomes acidic (pH ~4).

The ship had a dedicated pump to transfer seawater from the moonpool to the mud tank in order to pre-mix the drill mud. During the drilling process, drill mud flushes the barrel and leaves the pipe through mudways between the barrel shoe and the inner side of the drill bit. Thus, porous or coarse sediments might be expected to contain pore waters mixed with drill mud. Drill mud can clog rhizon samplers, resulting in slow flow rates. This was especially true in the loose sands and disturbed sediments.

Random sampling of seawater from different holes and transects and different drill mud compositions were acquired for reference. Both the guar gum powder and the different substances used on the drill bit and the barrel were sampled as well, in order to provide baseline tracer references for possible contamination. However, because of the filtering effect of the rhizon samplers, the pore water collected was free of contamination.

### Seawater sampling

Seawater samples from 2–3 sites along each of the four transects were collected in order to measure oxygen isotopes, carbon isotopes of dissolved inorganic carbon, and uranium concentrations. Samples were collected from the sea surface using a bucket deployed over the side of the vessel, attached to a line. At some sites, they were collected at the same time and from the same side of the vessel as the conductivity, temperature, and density profiling.

For oxygen isotope analyses, crimp glass vials were filled with 20 mL of unfiltered seawater, leaving a small headspace to prevent breakage during shipping. For carbon isotope analysis, 20 mL of unfiltered seawater was placed into a crimp glass vial, and 0.2 mL of mercuric chloride ( $\text{HgCl}_2$ ) solution was added. Again, headspace was required to prevent the

glass vial from breaking because of temperature changes. For uranium concentration analyses, 2 mL of concentrated ultra pure nitric acid was added to 200 mL of filtered seawater and stored at room temperature.

### Sample labeling

Both the syringes and sample vials were hand labeled with hole, core, section, and sampling depth information. All sample information was entered into the OffshoreDIS. The primary sample label was used for the anion 8 mL Nalgene vial. Additionally, all samples and sample splits were labeled with a sequential number in red. This number is useful to quickly label temporary sample containers in the laboratory and for sorting samples. The sequential number was entered into the remarks field of the OffshoreDIS. Samples that were preserved with nitric acid were also marked with a red identifying dot on the lid.

Samples were collected in the curation container and measured for pH, alkalinity, ammonia, and approximate salinity in the geochemistry container. Results were compiled to calculate alkalinities and calibrated ammonia concentrations. These results, the total sample and split-sample volumes, and the type and amount of added preservatives were entered into the OffshoreDIS. Split-sample labels from the OffshoreDIS were glued to the appropriate vials and covered with transparent tape. If label fields failed to print correctly, they were hand corrected with a permanent marker. Samples other than pore water were only hand labeled.

### Sample splitting

When possible, water samples split from the primary sample vial were subsampled using a syringe. Where exact amounts were needed (e.g., alkalinity and sulfide), adjustable pipettes (Eppendorf 5000  $\mu\text{L}$  and Eppendorf 1000  $\mu\text{L}$ ) were used to transfer samples from the primary sample vial. Samples for isotope analyses were put into vials and sealed without headspace (unlike the strategy for seawater). Table T5 shows the sample-split priority.

The minimum sample amount from which all offshore parameters were measured was ~500  $\mu\text{L}$ . Alkalinity and pH were measured from a 200  $\mu\text{L}$  sample split, and ammonia was measured from a 1:5 dilution (200  $\mu\text{L}$  sample + 800  $\mu\text{L}$  pure water). Salinity can be optionally measured from a ~100  $\mu\text{L}$  sample split. Because rhizon samplers contain 130  $\mu\text{L}$  of pure water when wet, this amount was considered a dilution of the original sample. When the total sample volume collected was low, the remaining sample, after alkalinity titration, was stored in case addi-

tional samples were needed. The exact amount of acid added to the alkalinity sample was recorded on the label.

### Pure water

Pure water was generated in the curation container from the ship's tap water with a Seradest USF 3000 purifying cartridge. The conductivity of the water was controlled to be  $<0.1 \mu\text{S}$  ( $>10 \text{ M}\Omega\text{cm}$ ) by an LFM C1 conductivity detector. Pure water for laboratory use was produced in batches of 10 L and stored in a carboy. For microbiological use, the pure water was additionally treated with an Aquafine ultraviolet disinfection unit to remove any microbial contamination from the cartridge and filtered with a  $0.2 \mu\text{m}$  filter cartridge. The casing of the ultraviolet disinfection system is made up of a quartz tube and stainless steel and, therefore, sterile pure water is potentially not completely metal free. Both pure water and tap water were sampled repeatedly.

### Sample temperature

In situ temperatures of the samples could not be measured; however, water temperatures at the sites were generally around  $28.5^\circ\text{C}$ , as measured using a YSI 6600V2 conductivity, temperature, and density probe accurate to  $\pm 0.15^\circ\text{C}$ . Temperatures in the geochemistry container were well controlled to between  $23^\circ$  and  $25^\circ\text{C}$ . For pH measurement, temperature compensation was done using the container temperature, measured with an external temperature sensor. Because measurements were performed in 1.5 or 2 mL Eppendorf vials, temperatures were expected to be equilibrated to ambient temperature. In certain weather situations, however, the air conditioning in the laboratory container failed, causing the ambient temperature to rise well above  $25^\circ\text{C}$ . Measurements under such circumstances were avoided, but if they were unavoidable, were noted.

### pH value

Sample pH was measured with a Mettler Toledo In-Lab 423 microcombination glass electrode with a 3 mm tip connected to either a WTW pH 340i pH meter or a Radiometer TIM840 Autotitrator. The pH value and alkalinity were determined from 0.7 mL of sample in 2 mL Eppendorf cups. When the sample volume was smaller, the amount required could be reduced to a minimum of  $200 \mu\text{L}$  using a conical 1.5 mL Eppendorf cup. A constant reading was achieved by turning the vial around the electrode with a special magnetically driven vial holder rather than stirring the sample with a stir bar. The pH meter was calibrated once a day using AppliChem color coded National Bureau of Standards (NBS) scale pH buffer

solutions of  $\text{pH} = 4.01$  and  $7.00$ . Temperatures were monitored with a pt1000 T-sensor next to the sample vial. The instrument shows the pH with a resolution of  $0.001 \text{ pH units}$  and the measurement has an accuracy of better than  $\pm 0.02 \text{ pH units}$ .

### Alkalinity

Alkalinity was determined by titration with  $0.01 \text{ M HCl}$  where the equivalence point was detected by titrating known amounts of sample (usually  $0.7 \text{ mL}$ ) while measuring the pH value. A Radiometer TIM840 Autotitrator with a  $5 \text{ mL}$  burette was used for titration and stopped at  $\text{pH} < 3.9$ . The algorithm used to calculate alkalinity accounts for the activity of seawater and dilution by the titration solution so that the results are comparable for different end-point pH values. The measurement has an accuracy of better than  $0.2 \text{ mM}$ .

For the titration, a  $0.3 \text{ mm}$  internal diameter polytetrafluoroethylene (PTFE) tube from the digital burette was placed in the liquid before the titration started. Both the PTFE tube and the pH electrode were rinsed with pure water and carefully dried with laboratory tissues before the measurement. The magnetically driven rotating vial holder is described in more detail in the ESO curation container cookbook. The algorithm is a corrected version of the algorithm of Grasshoff (1983):

$$\text{ALK [M]} = (10^{-\text{pH}_{\text{initial}}}/f_{\text{H}^+_{\text{initial}}}) + [(c_{\text{HCl}} \cdot V_{\text{HCl}})/V_0] - (10^{-\text{pH}_{\text{final}}}/f_{\text{H}^+_{\text{final}}}) \cdot [(V_0 + V_{\text{HCl}})/V_0]$$

where

- $\text{pH}_{\text{initial}}$  = original pore water pH,
- $\text{pH}_{\text{final}}$  = pH at end-point of titration (usually  $\text{pH} 3.95$ ),
- $f_{\text{H}^+}$  = activity coefficient of  $\text{H}^+$  (for standard seawater this is  $0.755$ ),
- $c_{\text{HCl}}$  = concentration of titration solution (usually  $0.01 \text{ M}$ ),
- $V_{\text{HCl}}$  = titration volume depending on alkalinity of sample, and
- $V_0$  = initial volume of sample (usually  $0.0007 \text{ L}$  [ $700 \mu\text{L}$ ]).

### Ammonium

Ammonium was detected using the PTFE tape gas separator technique, as described in the curation container cookbook (modified after Hall and Aller, 1992). With this technique, ammonium is stripped from a  $100 \mu\text{L}$  sample by an alkaline carrier solution ( $0.2 \text{ M}$  sodium citrate in  $10 \text{ mM NaOH}$ ), passes a  $200 \text{ mm} \times 5 \text{ mm}$  PTFE membrane as ammonia ( $\text{NH}_3$ ), and is redissolved as  $\text{NH}_4^+$  in an acidic solution ( $1$

mM HCl). The  $\text{NH}_4^+$  causes a conductivity signal in the acidic carrier that is detected with an Amber Science 1056 conductivity meter with a model 529 temperature-compensated microflow-through cell. The conductivity signal was recorded with a Knauer strip-chart recorder, and peak height was analyzed manually. This method is very precise and stable, practically insensitive to matrix changes, and shows a linear conductivity response for ammonium concentrations between 10 and 1000  $\mu\text{M}$ . The detection limit is 5  $\mu\text{M}$ , and accuracy is <2%.

Generally, measurements were made on the original sample, which was only diluted if the sample volume was extremely low or the ammonium concentration exceeded the calibrated range (>1.6 mM). Ammonia calibration standards were freshly prepared from a 55.6 mM (1000 ppm) standard solution using artificial seawater as a matrix.

A 300–400  $\mu\text{L}$  sample split was taken from the primary sample vial with a Hamilton 1000  $\mu\text{L}$  precision glass syringe and injected onto a 100  $\mu\text{L}$  loop with a Rheodyne high-pressure liquid chromatography valve. The valve was then opened to the carrier solution stream to start the analysis. The Hamilton syringe was rinsed with pure water twice before and after analysis.

### Salinity

Salinity was optionally measured using a Krüss Optronic digital refractometer. The measurement precision for the refractometer is 0.1%, so the data can only be used to detect samples with salinities that differ significantly from seawater. The zero point calibration was performed with pure water. The refractometer was calibrated externally by measuring International Association for the Physical Sciences of the Ocean (IAPSO) standard seawater with a salinity of 34.99.

### Headspace sampling

Headspace gas samples were taken and preserved, but methane concentrations were not measured offshore. Ideally, 5 mL sediment was sampled from the working half of the core using a cut-off disposable syringe. The amount was noted in both the laboratory book and in the OffshoreDIS. The sample was immediately transferred into a 20 mL headspace vial containing 10 mL of brine. The receiver solution was composed of a 333 g/L NaCl brine with 24 mg/L  $\text{HgCl}_2$  to prevent microbial degradation of the sample. The absolute amount of  $\text{HgCl}_2$  in one vial is 0.24 mg. The vials were crimp sealed, labeled, and stored in a padded box. All gas samples collected were la-

beled with a red sequential number that matched the sequential numbers of the corresponding pore water samples.

### Onshore geochemistry of interstitial water

A total of 118 interstitial water samples (18, 20, 2, and 78 from transects HYD-01C, HYD-02A, RIB-02A, and NOG-01B, respectively) were taken from the cores using rhizon samplers, along with 35 reference water samples (i.e., pure water used onboard for chemical analysis, rain water, tap water, seawater from the drilling site, and filtrate of drilling mud). Alkalinity, pH, salinity, and ammonium were measured from the interstitial water onboard. With the assistance of the technical staff at the University of Bremen, an additional 30 chemical species were measured in the interstitial water. Chloride, bromide, and sulfate were measured by ion chromatography. Na, Al, As, B, Ba, Be, Ca, Cd, Co, Cr, Cu, Fe, K, Li, Mg, Mn, Mo, P, Pb, S, Si, Sr, Te, Ti, V, Zn, and Zr were measured by inductively coupled plasma–optical emission spectrometry (ICP-OES).

### Interstitial water analyses

Using analytical equipment housed in the Department of Geosciences, University of Bremen, aliquots of interstitial water samples taken during drilling operations were analyzed for a suite of dissolved species to complement shipboard analyses (Expedition 302 Scientists, 2006).

### Cations measured by inductively coupled plasma–optical emission spectrometry

Dissolved cations were measured using a PerkinElmer Optima 3300 R simultaneous ICP-OES. Cation aliquots of pore water samples used for these analyses were acidified directly on board following shipboard sampling with 1% (10  $\mu\text{L}$  acid/1 mL sample) of concentrated  $\text{HNO}_3$ .

During the Onshore Science Party, pore water aliquots were diluted 1:100 for measurements of Na, 1:10 for other major elements (Al, B, Ba, Ca, Fe, K, Li, Mg, Mn, P, S, Si, Sr, and Ti), and 1:40 for trace elements (Al, As, Be, Cd, Co, Cr, Cu, Mn, Mo, Ni, P, Pb, Te, Ti, V, Zn, and Zr) using a 1.0%  $\text{HNO}_3$  solution (prepared with subboiled distilled  $\text{HNO}_3$  and 18 M $\Omega\text{cm}$  water). Major and trace elements were analyzed using a cross-flow nebulizer and CETAC USN 5000AT ultrasonic nebulizer, respectively. For measurements of major and trace elements, measuring the intensity at each wavelength was performed in

triplicate. Wavelengths used for identifying major and trace elements are shown in Table T6.

In all cases, standardization was done against multi-element solutions prepared from commercial standards and adjusted to a NaCl concentration similar to that in the seawater matrix of the samples, as shipboard salinity measurements determined all samples had seawater-like salinities. Calibration standards for major elements were prepared with high-purity single-element standards (Spectrascan by Teknolab, Norway) using a 0.5 M NaCl (Merck certipur) solution as the matrix. Calibration standards for trace element analyses were prepared by multiple dilutions of a multi-element standard (Merck Certipur multi-element standard IV) prepared with a 0.6 M NaCl solution as the matrix. Measurement precision is  $\pm 3\%$  and  $\pm 5\%$  for major and trace elements, respectively.

### Anions measured by ion chromatography

Unacidified aliquots of the samples were diluted 1:100 using 18 M $\Omega$ cm water. Concentrations of Cl, Br, and S were measured using 861 Advanced Compact IC with Sequential Compression by Metrohm AG and an IC-Anion column Metrosep A Supp 5 (100 mm run length) at the University of Bremen. Measurement precisions for Cl, Br, and S were  $\pm 0.6\%$ ,  $\pm 3.5\%$ , and  $\pm 2\%$  ( $1\sigma$ ), respectively. Dilutions of IAPSO seawater served as a certified reference material. Calibration standards were prepared from certified commercial single-anion standards (CertiPUR by MERCK).

## Onshore analysis of sediments

### X-ray diffraction methods

To determine the mineralogy of the deep foreereef slope at Noggin Pass (transect NOG-01B), samples from Hole M0058A were taken every 50 cm for the entire length of the hole. Samples were freeze-dried and ground in agate mortars to ensure sample homogeneity and a fine grain size ( $<20\ \mu\text{m}$ ) so as not to introduce mineral orientation biases during measurement. X-ray diffraction measurement and pattern analyses were performed in the Crystallography research group laboratories (University of Bremen, Central Laboratory for Crystallography and Applied Material Sciences, ZEKAM, Department of Geosciences). X-ray diffraction was measured on a Philips X'Pert Pro multipurpose diffractometer equipped with a Cu-tube ( $K\alpha\lambda\ 1.541$ , 45 kV, 40 mA), a fixed divergence slit of  $0.2503^\circ$ , a 16 sample changer, a secondary Ni-filter, and the X'Celerator detector system. Measurements were performed as a continuous scan from  $3.0060^\circ$  to  $84.9800^\circ 2\theta$  with a step size of

$0.0170^\circ 2\theta$  (calculated time per step was 50.1650 s). Mineral identification was performed using the Philips software X'Pert HighScore, which gave a semi-quantitative value for the weight percent of each identified mineral on the basis of relative intensity ratio (RIR) values. RIR values are calculated as the ratio of the intensity of the most intense reflex of a specific mineral phase to the intensity of the most intense reflex of pure corundum ( $I/I_c$ ) referring to the "matrix-flushing method" of Chung (1974).

Replicate measurements of three samples suggest that the analytical uncertainty is  $\pm 3\ \text{wt}\%$  for aragonite;  $\pm 2\ \text{wt}\%$  for calcite and Mg calcite;  $\pm 5\%$  for quartz;  $\pm 5\%$  for total feldspars; and  $\pm 7\%$  for total clays. Unfortunately, RIR values are sparse for clay minerals and long chain organic compounds, hampering the quantification in this case. Clay mineral identification and quantification is also hampered in these samples by the low clay weight percent and the tendency of the peak positions of the clay minerals to be sensitive to the chemical composition of the clay minerals (Vogt et al., 2002; Vogt, 2009). Interpretation of clay mineralogy and abundance should therefore be treated with caution and assumed to be of a qualitative nature. The quantification of weight percent Mg calcite is also hampered here by the reference data being limited to only two examples of Mg calcite ( $[\text{Mg}_{0.10}\text{Ca}_{0.90}]\text{CO}_3$  and  $[\text{Mg}_{0.14}\text{Ca}_{0.86}]\text{CO}_3$ ). Where the Mg content of Mg calcite deviates from those of the reference data, additional uncertainty will be introduced into the estimation of weight percent for Mg calcite.

### Total organic carbon methods

To determine the concentration of total organic carbon (TOC) of the deep foreereef slope at Noggin Pass (transect NOG-01B), samples were taken every 50 cm for the entire length of Hole M0058A. Selected sediment samples were analyzed for total carbon and TOC concentrations using a LECO CC-125 carbon-sulfur analyzer at the University of Bremen. Total inorganic carbon was calculated as the difference between total carbon and TOC. Sediment samples were freeze-dried and finely ground by hand in an agate mortar. Approximately 50 mg of dried, ground sample was weighed in a ceramic cup and heated in a furnace. The evolved  $\text{CO}_2$  was then measured with a nondispersive infrared detector. A second aliquot of 1 g was weighed in a ceramic cup, reacted with 12.5% HCl twice, washed with deionized water twice, and reanalyzed as above. The  $\text{CO}_2$  measured in the second run was assumed to come from organic carbon. The analytical precision is about  $\pm 0.02\%$ .

## Chronology

The aim of preliminary dating was to provide a rapid overview of the ages of the material recovered during the offshore phase of Expedition 325. These dates are intended to aid the onshore phase of the expedition and, in particular, the sampling of the core material so that more focused sampling strategies can be implemented to achieve the scientific objectives of individual science party members. We hope that this dataset will act as a starting point for collaborations within the science party. The data will also enable more effective outreach to the scientific community in the period immediately following the science party before more comprehensive chronologies become available.

### Sampling

Subsamples of core catcher material were taken during the offshore phase under the direction of the Co-Chief Scientists. Coral and mollusk material was selected based on the likelihood of the calcium carbonate being suitable for U-Th or radiocarbon dating (no visible diagenetic textures and free of detrital contamination) and from an important core section so as to constrain the basic chronology of each hole. A total of 20 coral samples were sent to the University of Oxford (United Kingdom) for U-Th dating, and 48 samples were sent to the University of Tokyo (Japan) for sample preparation and then the Australian National University (Australia) for radiocarbon analysis. To ensure that the chronological control on the lower portions of holes was not limited by the range of the radiocarbon chronometer (~50 cal y BP), the deeper samples from each hole were selected for U-Th analysis and the shallower samples were analyzed for radiocarbon.

### U-Th measurements

Samples were reduced to pieces ~5 mm in size, ultrasonically cleaned in Milli-Q (18 MΩcm) water, and examined for detrital contamination. Approximately 0.3 g of the cleanest coral aragonite was picked for U-Th analysis, and a similar amount was set aside for radiocarbon analysis. Sample preparation was the only screening performed on the subsamples, in contrast to the normal approach to U-Th dating where samples are rigorously screened for diagenetic alteration prior to analysis. This omission of sample screening greatly improved the timely throughput of the samples, allowing the data to be used to assess

the ages of samples to the accuracy required to improve sampling strategies during the OSP.

Coral subsamples for U-Th analysis were weighed, spiked with a mixed  $^{229}\text{Th}$ : $^{236}\text{U}$  tracer (Robinson et al., 2004a), and dissolved in  $\text{HNO}_3$ . Once dissolved, samples were refluxed in a mixture of 3:1  $\text{HNO}_3(\text{conc})$ : $\text{HCl}(\text{conc})$  (reverse aqua regia) overnight to remove organic matter and ensure sample tracer equilibrium. Samples were converted to nitrate form, followed by separation of U and Th from each other and the sample matrix (Negre et al., 2009).

U and Th isotopes were measured using a Nu Instruments multicollector inductively coupled plasma-mass spectrometer (MC-ICP-MS) at the University of Oxford. U was measured statically with  $^{234}\text{U}$  in an ion counter, and all other isotopes were counted in faraday collectors. All machine biases were accounted for by bracketing each sample measurement with measurements of the NBS 112a uranium standard, with the mass 234 beam intensities matched between samples and standards. Th was measured dynamically, with both  $^{230}\text{Th}$  and  $^{229}\text{Th}$  measured sequentially in an ion counter, and differences in beam intensity between measurement steps were normalized through measurement of  $^{232}\text{Th}$  in faraday collectors during each step. Again, machine biases were corrected using a bracketing standard and, in this case, an internal  $^{229}\text{Th}$ : $^{230}\text{Th}$ : $^{232}\text{Th}$  (ThIS-2; Mason and Henderson, 2010) standard was used.

### $^{14}\text{C}$ measurements

Coral and mollusk samples for radiocarbon measurements were further divided using a dental drill to obtain calcium carbonate with minimal diagenetic alteration. Subsamples (~50 mg) were ultrasonically cleaned in Milli-Q water and then dried in an oven, and ~40%–50% of the material was etched prior to conversion to  $\text{CO}_2$ . Neither stepwise dissolution (Yokoyama et al., 2000) nor X-ray diffraction measurements were conducted to screen for diagenesis in order to maintain the same constraints imposed as for U-series dating.

All cleaned calcium carbonate samples were placed in test tubes and dissolved in phosphoric acid. The evolved  $\text{CO}_2$  was then cleaned in an ultra vacuum preparation line and reduced to graphite in a hydrogen atmosphere (Yokoyama et al., 2007, 2010). Radiocarbon in the graphite was then measured by accelerator mass spectrometry (AMS) (Fallon et al., 2010; Yokoyama et al., 2010).

## Data

U and Th isotope ratios and age determinations are shown in Table T7, and uncalibrated radiocarbon ages are presented in Table T8.

## Age interpretations

### U-Th

#### Closed system ages

U-Th ages of samples can be calculated using the age equation of Broecker (1963) under the assumptions that the sample has remained a closed system to  $^{238}\text{U}$ ,  $^{230}\text{Th}$ , and their intermediate nuclides, and that the sample had no initial  $^{230}\text{Th}$ . The results of these calculations, as well as the backcalculated ( $^{234}\text{U}/^{238}\text{U}$ ) at the time the coral grew ( $^{234}\text{U}/^{238}\text{U}_i$ ), are shown in Table T9.

#### Initial Th correction

The assumption that the coral samples contained no initial  $^{230}\text{Th}$  is not always valid. In some of the coral samples,  $^{232}\text{Th}$  concentrations are elevated relative to that expected for pristine coral aragonite ( $>0.1$  ppb), suggesting that there has been some incorporation of Th. High  $^{232}\text{Th}$  concentrations (as much as 110 ppb in Sample 325-M0033A-15R-2, 8 cm) suggest that a significant continental detrital component is present (it is unlikely that  $^{232}\text{Th}$  incorporation from seawater alone could cause such an enrichment). The incorporation of  $^{232}\text{Th}$  into the coral when it formed would have been associated with the incorporation of some  $^{230}\text{Th}$  as well. This initial  $^{230}\text{Th}$  requires accounting for during interpretation of the age. If all of the initial Th was derived from continental detrital material, then one could use the crustal average  $^{230}\text{Th}/^{232}\text{Th}$  value (1.030; median of GEOROC Database [[georoc.mpch-mainz.gwdg.de/georoc/](http://georoc.mpch-mainz.gwdg.de/georoc/)]) and use the  $^{232}\text{Th}$  concentration in the sample to assess the amount of initial  $^{230}\text{Th}$ . The effect of correcting for this initial  $^{230}\text{Th}$  using a crustal value is shown in Table T10 and Figure F11 (an uncertainty of 100% is associated with each estimate of initial  $^{230}\text{Th}$  to account for the uncertainty in the  $^{230}\text{Th}/^{232}\text{Th}$  of the contaminant). However, it is possible that samples with lower  $^{232}\text{Th}$  concentrations incorporated a significant portion of their Th from seawater, which has a much higher  $^{230}\text{Th}/^{232}\text{Th}$  value (9.250; Robinson et al., 2004a), leading to larger corrections. Thorium incorporation from seawater can be considered a worst case scenario and is illustrated in Table T10 and Figure F11. Typically, where  $^{232}\text{Th}$  is high, crustal contamination is more likely, and therefore the correction for initial  $^{230}\text{Th}$  is small. Likewise, samples with lower  $^{232}\text{Th}$ ,

where incorporation of Th from seawater may be more significant, still have a small initial  $^{230}\text{Th}$  correction because of the low  $^{232}\text{Th}$  content. For both cases illustrated here, the initial  $^{230}\text{Th}$  has been shown to only be a significant correction for samples with  $^{232}\text{Th} > 5$  ppb, and in the worst case scenario (i.e., incorporation of Th from seawater), the correction reduces ages by ~500 y with the exception of samples from Sections 325-M0032A-8R-CC and 325-M0033A-15R-CC.

#### Open system U-Th behavior

The  $^{234}\text{U}/^{238}\text{U}_i$  for all samples that yielded ages are close to the value of 1.147 for modern seawater and coral (Delanghe et al., 2002; Robinson et al., 2004a; Andersen et al., 2007). A clearly defined trend of lower initial  $^{234}\text{U}/^{238}\text{U}$  with increasing age between 10 and 30 calibrated years before present (cal y BP; years before 1950 AD) is in agreement with previous observations (Yokoyama and Esat, 2004; Esat and Yokoyama, 2006). This agreement gives some qualitative indication of the reliability of the closed system assumption and, hence, the accuracy of the ages. There is, however, some variability in the  $^{234}\text{U}/^{238}\text{U}_i$ , which may be the result of the lower  $^{234}\text{U}/^{238}\text{U}$  of seawater during glacial times (Yokoyama and Esat, 2004; Robinson et al., 2004b; Esat and Yokoyama, 2006, 2010) and/or some open system behavior of the corals.

#### Calibrated $^{14}\text{C}$ ages

To account for variability in the  $^{14}\text{C}$  content of the atmosphere over time, radiocarbon ages have been calibrated using the marine09 calibration curve (Reimer et al., 2009) and a  $\Delta R$  of  $9 \pm 45$  ( $1\sigma$ ) y, based on the mean and standard deviation of  $\Delta R$  estimates from the Great Barrier Reef (GBR) region from the 14CHRONO marine reservoir database ([intcal.qub.ac.uk/marine/](http://intcal.qub.ac.uk/marine/)). Calibration was performed using the OxCal v4.1 software (Bronk Ramsey, 2009). Results of this calibration are presented in Table T11. Where calibrated  $^{14}\text{C}$  ages have polymodal probability distributions (Fig. F12), the quoted 95.4% probability range has been taken from the youngest end of the youngest window to the oldest end of the oldest window, ignoring any intermediate gaps of low probability. For the purposes of assigning an age for qualitative comparison, the mean of the distribution is taken.

Some of the radiocarbon ages are near the limit of the  $^{14}\text{C}$  chronometer and thus may be much older than the raw radiocarbon age suggests. This is particularly true for the deep offshore Hole M0058A, which has an uncalibrated age of  $48.0 \pm 0.5$  ( $1\sigma$ )  $^{14}\text{C}$

cal y BP for Section 325-M0058A-4R-2. This old age for the upper portion of this hole may be due to reworking and downslope transport of older material from the carbonate platform of the GBR to the continental slope, where it becomes incorporated in the younger sediment intersected by the drill core.

### Summary

The positions of coral samples for which chronological control now exists have been plotted on the core log sections for each of the four sites. Where ages are referenced in this report, they have been rounded to the nearest 1 cal y BP. In all but one of the dated holes (Hole M0037A), the ages of the samples are in stratigraphic order, providing some confidence on the accuracy of the dates and that the cores have sampled in situ reef framework, consistent with the sedimentological observations. Further evidence for the quality of the U-Th ages is given by the limited variation in the  $[^{234}\text{U}/^{238}\text{U}]_i$  and its approximation to what one might expect for seawater during sea level lowstands. The quality of the preliminary U-Th data illustrates the promise for the development of an absolute chronology, where thorough screening will be performed to identify more pristine samples. This screening will be especially important to avoid detrital contamination, as was evident in the high  $^{232}\text{Th}$  concentrations in the samples dated here.

The majority of the deeper holes have U-Th dates near their bases that indicate the Last Glacial Maximum (LGM) intersected 10 samples between 20 and 25 cal y BP. Shallower samples from these cores (dated by radiocarbon) range to as recent as 13–14 cal y BP, indicating that the early portion of the deglacial has also been captured by Expedition 325 drill cores. Holes drilled in shallower water have ages as young as 10 cal y BP, which indicate that periods postdating MWP-1A (Fairbanks, 1989) have also been sampled, opening up the possibility of comparison of this event in the GBR with other localities. There appears to be a sharp decline in the number of samples postdating 10 cal y BP (Fig. F13). This may reflect a reef drowning event at this time or may simply be an artifact of the relatively small dataset and/or a sampling bias.

U-Th ages prior to the LGM show promise for recovering high-quality material for U-Th dating of earlier periods in the Pleistocene. Holes M0032A, M0056A, and potentially M0033A have material from marine isotope Stages 4 and 3, whereas Hole M0042A may provide material from the transition between marine isotope Stages 7 and 6. Hole M0057A, although not yielding a closed system U-Th age, has U-Th isotope ratios that suggest that the age of the samples is older than the LGM and, given its intermediate

depth, may provide insight into glacial–interglacial transitions further back in time.

The offshore hole at Noggin Pass (Hole M0058A) produced a radiocarbon age close to the limit of the chronometer for a sample near the top of the hole. This suggests either a very slow sedimentation rate or that the sediment reaching this locality is reworked and hence much older than the age of sedimentation. If the latter is true, then establishing an accurate chronology for this core will not be possible using techniques that rely on the bulk isotopic compositions ( $^{14}\text{C}$  and U-Th) of precipitated mineral phases. Other methods such as paleomagnetism, microfossil isotope stratigraphy, or tuning to orbital chronologies may be more successful.

## Downhole logging

Downhole geophysical logging can provide continuous data throughout the length of a borehole, giving information on the physical, chemical, textural, and structural properties of the geological formations encountered. Where core recovery is poor, downhole geophysical logs may provide the only method of fully characterizing a borehole. In addition, downhole logs can allow more precise depth positioning of individual core pieces by visual (borehole images) or petrophysical correlation.

Usually, logging measurements are recorded in depth as the tools are pulled from the bottom of the borehole to the surface. Logging speeds are dependent on the physics of the specific tool that is deployed. For example, to obtain spectral gamma radioactivity data without excessive statistical variations, the tool must record a certain level of counts per second (cps). Therefore, where low radiating formations, such as carbonates, are being logged, higher count times at sampling points are required and logging speed is slower. Conversely, when logging high radiating formations such as clays and shales, a lower count time can be used and logging speed is therefore quicker. During Expedition 325, not all tools were deployed in each borehole (refer to individual transect chapters for details of logging tools deployed). With a shallow depth of penetration below seafloor (<50 m) and small-diameter holes (near 100 mm [HQ]–200 mm [American Petroleum Institute]), slimline downhole instruments were used. These slimline tools were run individually (no multiple-tool logging strings).

### Borehole geophysical instruments

The set of logging tools used during Expedition 325 was decided based on the scientific objectives of the



expedition and the limitations posed by the geological setting. The tool suite includes high-resolution borehole surface imaging tools, a borehole fluid sampling instrument, and a series of tools that allow determination of the borehole size and derivation of petrophysical or geochemical properties of the formations. These formation properties include porosity, electrical resistivity, acoustic velocities, magnetic susceptibility, and natural gamma radioactivity. Owing to the environmental constraints in place in the Great Barrier Reef Marine Park, no nuclear tools were deployed during Expedition 325. Most probes were run with Advanced Logging Technologies Ltd. (ALT) surface recording systems and combined ALT/Mount Sopris Instrument Company Inc. (Mount Sopris) recording systems.

### Optical Borehole Televiewer (OBI40)

The ALT Optical Borehole Televiewer (OBI40) (Fig. F14A) produces a millimeter-scale, high-resolution optical image of the borehole surface. A reflection cone placed at the bottom of the tool enables a vertical charge-coupled device camera located inside the tool to image the borehole surface directly. A 360° image of the borehole is captured. The tool has a built-in lighting system that illuminates the borehole surface, along with centralizers to optimize image precision. Image resolution is user-defined, with the highest quality images having a vertical sampling interval of 1 mm and 720 pixels taken around the borehole (every half-degree). Positioning of the images relative to magnetic north is possible using a set of triaxial magnetometers integrated in the tool. Data quality for OBI40 measurements is monitored by the logging engineer in real time from a computer display. Minor processing can improve color contrast, and interpolation may be necessary over data transmission errors. The resulting continuous digital image (in real color, calibrated from a Kodak reference plate) of the borehole can be used as an efficient tool for lithologic recognition and precise core-depth positioning. Consequently, it can be used directly for sedimentological and structural interpretation, as well as for meso- to macro-scale porosity quantification.

### Acoustic Borehole Televiewer (ABI40)

The ALT Acoustic Borehole Televiewer (ABI40) (Fig. F14B) generates centimeter-scale, high-resolution acoustic images of borehole surfaces. Similar to the OBI40 measurements, resulting data can be used directly for sedimentological and structural interpretation of a borehole, as well as for meso- to macro-scale porosity quantification. The ABI40 differs from

the OBI40 in that it is unaffected by possible murkiness of the borehole fluid or drilling mud.

A voltage is applied to the piezoelectric ceramic to produce acoustic waves (1.2 MHz) at regular intervals. On reaching the focalizing mirror, the acoustic waves are deflected perpendicularly to the wave source and toward the borehole surface. The focal point corresponds to the point of maximum energy. In a 100 mm diameter borehole, this gives a ~4 mm diameter footprint on the borehole wall. To obtain a 360° image, the mirror pivots on a central axis. Similar to the ABI40, the resolution is user-defined, with the highest quality images obtained while using a vertical sampling interval of 2 mm and a radial sampling of 288 shots per circumference.

The ABI40 produces two distinct images of the borehole surface, an acoustic impedance image and a distance (or traveltime) image. The acoustic impedance image (between the borehole fluid and borehole wall) is derived from the reflected wave amplitude obtained 72, 144, or 288 times around the hole. The amplitude ratio between the emitted wave and the reflected wave provides information on the formation's absorption capacity (low returned amplitude corresponds to a high capacity of absorption, i.e., soft formation). The distance image is derived from the reflected wave time of flight between the ceramic transducer to the borehole surface and back. This traveltime is directly proportional to the distance between the borehole wall and the probe. Similar to the OBI40 sonde, the ABI40 is equipped with magnetometers, as well as accelerometers for tool orientation with respect to magnetic north. The precision of measured inclination is 0.5°, and the precision measured azimuth is 1.5°. For each of the images, a set of false colors is assigned and a virtual image of the borehole wall depth is produced. This image is displayed as an unfolded representation in 360°. The magnetometers are factory calibrated in Luxembourg. Therefore, a postcruise recalibration file will be provided on return and recalibration.

### Hydrogeological probe

The ALT hydrogeological probe (IDRONAUT) (Fig. F14C) measures the hydrogeological properties of the borehole fluid, including the following.

#### *Borehole fluid pressure and temperature*

Fluid temperature can aid in the identification of inflow of water into the borehole and is also necessary to derive an accurate borehole fluid salinity from electrical conductivity measurements. Fluid pressure provides an indirect assessment of tool progress down and up the borehole, but it can also be inte-

grated to obtain fluid density in the borehole. The tool was calibrated for temperature by the manufacturer and checked on site using a thermometer. The precision of measured pressure is 0.01 dbar and the precision of measured temperature values is 0.004°C.

### **Electrical conductivity**

Conductivity is measured using seven platinum electrodes grouped within a cell. One central electrode emits an alternating current and six peripheral electrodes provide for current return and potential measurements. Electrical conductivity provides a means of identification of different fluid types in a borehole. Ultimately it can be used to derive borehole fluid salinity. The precision of measured electrical conductivity is 0.004 mS/cm.

### **Hydrogen concentration**

The hydrogen concentration (pH) is obtained using two electrodes, of which one is a reference. An electrical current is created between the electrodes. This current is a function of the amount of H<sup>+</sup> ions in the fluid. The resulting value is then amplified to acquire a precise signal. The precision of measured pH is 0.01 pH.

The tool was calibrated by the manufacturer prior to Expedition 325. Prior to each deployment of the tool, temperature was checked using a thermometer, and electrical conductivity, pH, and oxydo-reduction were checked using special reference liquids. Finally, the oxygen concentration was measured in air.

### **Spectral Natural Gamma Probe**

Unlike other slimline instruments recording total gamma ray emissions, the ANTARES Spectral Natural Gamma Probe (ASGR) Datensysteme GmbH (Fig. F14D) allows identification of the individual elements that emit gamma rays. Naturally occurring radioactive elements such as K, U, and Th emit gamma rays with a characteristic energy. K decays into two stable isotopes (argon and calcium), and a characteristic energy of 1.46 MeV is released. U and Th decay into unstable daughter elements also producing characteristic energies. In nature, U and Th decay chains contain many radioactive elements of which the final daughter elements are stable isotopes of lead. The most prominent of the gamma rays in the uranium series originate from the decay of <sup>214</sup>Bi (bismuth) and in the thorium series from the decay of <sup>208</sup>Tl (thallium). Because of the equilibrium relationship between the daughter product and parent, it is possible to compute the concentration of parent uranium (<sup>238</sup>U) and thorium (<sup>232</sup>Th) in the decay series

by counting gamma rays from <sup>214</sup>Bi and <sup>208</sup>Tl, respectively, if the probe has been properly calibrated.

The ASGR detector for gamma rays is a bismuth germanate (Bi<sub>4</sub>Ge<sub>3</sub>O<sub>12</sub>, also referred to as BGO) scintillation crystal which is optically coupled to a photomultiplier. The BGO detector has an absorption potential eight times greater than a more classic sodium iodide (NaI) crystal. As most of the spectral discrimination is performed in the high-energy range, only instruments equipped with BGO detectors prove to be sufficiently reliable for use in slimline downhole logging tools.

As the probe is pulled from the bottom of the hole to the surface, gamma rays are sorted according to their emitted energy spectrum (the tools available during Expedition 325 have 512 or 256 reference spectra in memory) and the number of counts in each of the three preselected energy intervals. These intervals are centered on the peak values of <sup>40</sup>K, <sup>214</sup>Bi, and <sup>208</sup>Tl. Tool output comprises K, U, and Th in becquerel/kilogram, and total counts gamma ray in counts per second. K, U, and Th values can also be presented as percent K and parts per million U and Th values. The vertical resolution of the tool is ~15 cm.

In reefal carbonates, the ASGR sonde provides a means of identifying clays (usually K rich and/or Th rich) from nearby terrestrial erosion and organic matter by the U band (or Th/U ratios).

The instrument was master-calibrated by the manufacturer. Prior to each deployment, the stability of the sensor was checked using a known volume of purest potassium.

### **Induction Conductivity Probe**

The ALT Induction Conductivity Probe (DIL45) (Fig. F15A) provides measurements of electrical conductivity. Variations of electrical conductivity correspond to variations in a number of factors including, but not limited to, lithology (composition and texture), formation porosity and saturation, and the nature of interstitial fluid.

An oscillator sends an alternating current of constant amplitude and frequency through an emitting coil. The electromagnetic field, created by the emitting coil, induces an alternating current as it runs through the receiving coil. This current is out of phase by 90°. The field, created by the Foucault currents, creates an alternating current when run through the receiving coil. This current has a phase in opposition with that of the emitting current. The Foucault currents are also out of phase with the emitting current by 90°. A phase sensitive detector enables the elimination of the “reactive” signal and

hence only keeps the signal induced by the field linked to the Foucault currents. In addition to the main receiving and emitting coils, induction probes also possess other secondary emitting and receiving coils (focalization solenoids), which act to reduce the effect of formations and drilling mud. The Foucault current is proportional to the formation conductivity and to the electromagnetic field induced in the solenoid.

The output of the tool comprises two logs:

1. Induction electrical conductivity of medium investigation depth (0.57 m) and
2. Induction electrical conductivity of greater investigation depth (0.83 m).

The instrument was master-calibrated against a Wenner array in a reference hole located in Campos, Mallorca (Spain). Validity of this master-calibration is checked on site using a reference coil.

### Full waveform sonic probe

The 2PSA-1000 sonic probe (SONIC) manufactured by Mount Sopris (Fig. F15B) measures compressional wave velocities of the formations encountered in the borehole. Used in combination with bulk density derived from core measurements, elastic properties, including bulk and shear moduli, as well as porosity can be derived from the sonic dataset. It is also possible to derive information on formation permeability from the analysis of surface waves in the hole (called Stoneley waves).

This sonic probe is composed of an acoustic transmitter and four receivers. The transmitter emits an acoustic signal that propagates through the borehole fluid to the fluid/rock interface, where some of the energy is critically refracted along the borehole wall. As a result of this wavefront spreading (Huygens principle), some of the refracted energy is transmitted back into the borehole. Each receiver picks up the transmitted signal, amplifies it, digitizes it, and sends the digitized signal to the surface via the wireline. The recorded waveforms are examined, and wave arrival times are selected (this process is known as “picking”). Arrival times are the transit times of the acoustic energy. By measuring the acoustic transit time and knowing the distance between receivers (1 ft), the fluid velocity, borehole diameter, and sonic velocity of the rock may be calculated. As a waveguide, the borehole propagates energy in many different modes, including the compressional and shear head waves, an infinite series of normal compressional and normal shear modes, and the Stoneley wave modes. All of these wave modes are excited when the source spectrum contains sufficiently high frequencies. The complexity of the received wave-

forms can be reduced by moderating the transmitted frequency band.

Normal modes (monopole surveys) are a result of constructive interference in the waveguides (borehole). For each normal mode, there exists a frequency below which the mode cannot be excited (cutoff frequency). The normal modes are highly dispersive, with their phase velocities approaching head wave velocities as frequency approaches the cutoff frequency. The optimal frequency band for producing head waves narrowly includes the cutoff frequencies for the first-order compressional and shear-normal modes. In this manner, unwanted modes are not excited and received head waves are high.

Calibration of the tool is performed either in water (1500 m/s for *P*-wave) or into a steel pipe (5440 m/s) while running downhole. The precision of acoustic traveltime measurements is ~5%.

### Magnetic susceptibility probe

The GEOVISTA EM51 (Fig. F15C) is an electromagnetic induction sonde designed to measure formation conductivity and magnetic susceptibility. The sonde includes two sets of two coils, one for conductivity measurement and the other for magnetic susceptibility measurement. Optimum operating conditions for the EM51 sonde are higher conductivity formations combined with low-conductivity borehole fluid (including air). Formation conductivity is typically measured in millisiemens per meter (or millimhos). Relationships between conductivity and resistivity are shown in Tables T12 and T13:

$$1 \Omega = (1/S) \rightarrow 1 \Omega\text{m} = [1/(S/\text{m})] \rightarrow 1 \text{ S/m} = (1/\Omega\text{m}) \rightarrow 1 \text{ mS/m} = (10^{-3}/\Omega\text{m}) = (1 \text{ mmho}).$$

A set of two calibration loops were used for calibration and testing of the electrical conductivity sensor. The equivalent conductivities of the calibration loops are 200 and 500 mS/m. A set of two calibration pieces was used for magnetic susceptibility sensor calibration and testing. The equivalent susceptibilities of the calibration pieces are  $1.7 \times 10^{-3}$  and  $5 \times 10^{-3}$  SI units. Prior to tool deployment, the calibration jigs must be placed over the middle of the respective TX-RX coil system. For conductivity, this is 100 cm from the bottom of the sonde. For magnetic susceptibility, the distance is 31 cm.

Magnetic susceptibility measures the degree of magnetization of a core in response to an applied magnetic field. It is a powerful tool for deciphering a formation's sedimentary provenance and/or diagenetic environment, and data derived from this tool are also invaluable when used for borehole correlation. Processes including diagenesis of earlier coral reef

generations (which can lead to coral dissolution) can result in a loss of magnetic susceptibility, and although these processes are poorly understood, often tracing where magnetic susceptibility is conserved allows sampling of well-preserved corals.

### Caliper probe

The 2PCA-100 from Mount Sopris (Fig. F15D) is a three-arm caliper tool (CAL3) that measures borehole diameter. The caliper measurement is made with the three arms attached to a mechanical assembly that drives a linear potentiometer. The three arms are linked mechanically, and therefore only the minimum diameter value is obtained for hole size. A constant reference voltage is applied across the potentiometer. The direct-current output voltage from the wiper of the potentiometer is converted to frequency. A microprocessor applies a quadratic correction to this frequency so that the frequency is linearly related to borehole diameter.

Calibration of the caliper tool is conducted using two cylindrical rings of known diameters before and after a logging run. The precision of the measurement is ~1 mm. The caliper log is essential for processing other logs and can be directly used in sedimentological and structural interpretation of the formation.

### Data quality

The quality of downhole logging data may be degraded by rapid changes in borehole diameter. Deep-investigation measurements such as induction resistivity are least sensitive to borehole conditions.

While deploying all the tools separately, a fixed zero depth position is maintained at the top of the drill pipe. Ship heave was minimized by attaching the winch (on the rooster box) to the drill pipe (placed into the seafloor), which is attached to a stabilization method depending on what logging was being conducted. When logging through API pipe, the drill pipe is attached to the heave-compensated part of the drill rig. When logging through HQ pipe, the HQ drill pipe is fixed in place in the top drive assembly, and so is attached to the heave-compensated part of the drill rig, and the API conductor pipe is clamped by the seabed template (Fig. F16).

### Data recording and processing offshore

Downhole geophysical logging aboard the *Greatship Maya* was provided by EPC. Each logging run was recorded and stored digitally. Data flow was monitored for quality in real time using tool-specific acquisition boxes and software. Table T14 summarizes the acquisition system for each tool.

After logging each borehole, data were preliminarily processed. WellCAD was used for visualization and plotting of the data. Processing was carried out using the WellCAD software package. The processing procedure is described below for standard logs (natural gamma radioactivity [ASGR], induction [DIL45], and magnetic susceptibility logs [EM51]), image data (ABI40 and OBI40), and sonic data (2PSA).

## Data processing onshore

### Depth adjustments

One main processing task involved evaluating the depth of each log run and referencing the data to seafloor. While deploying all the tools separately in the same section, a fixed zero depth position (loggers' zero) was maintained at the top of the drill pipe; hence, no depth shifting was necessary. Typical reasons for depth corrections include ship heave and tides, but as the logging for Expedition 325 was performed from a stable heave-compensated platform (see "Data quality"), no such corrections were necessary.

Using WellCAD, the original logs were depth adjusted to the seafloor (wireline log depth below seafloor [WSF]). This adjustment includes a couple of corrections:

1. Difference in zero tool depth. Discrepancies in depths between initial zeroing and zeroing on removal of the tool were generally <1 m.
2. Corrections specific to certain tools (e.g., matching down-logs to up-logs).

Logs were subsequently shifted to the seafloor (WSF) using the drillers depth from seafloor (DSF-A). Generally, discrepancies may exist between seafloor depths determined from the downhole logs and those determined by the drillers from the pipe length. This is because of the difficulty in obtaining an accurate seafloor from the "bottom felt" depth in soft sediment.

When necessary, logs have been manually adjusted by the log analyst to a reference log using distinctive peaks. In such cases, the gamma ray logs through pipe (or occasionally the induction logs) are taken as the reference logs (continuous). Generally, depth discrepancies between logs are <1.5 m. Matched log depths are referenced to seafloor and are referred to as wireline matched depth below seafloor (WMSF).

### Quality control

Data quality is assessed in terms of reasonable values for the logged formation and in this case repeatability between the gamma ray curves taken through pipe and in open hole. Considering the challenging borehole conditions, the overall quality of downhole

logging data is very good. Repeatability between data acquired on down and up acquisition of logs was checked by the log analyst and repeated well.

The quality of the ASGR spectral natural gamma data is good, even when logging through pipe and considering low counts. However, gamma ray logs recorded through drill pipe should only be used qualitatively because of attenuation of the incoming signal. Sections were acquired in open hole conditions in three holes (M0036A, M0042A, and M0054B) for through-pipe data calibration.

The quality of EM51 data is repeatable, with very low values recorded in each of the two logged holes (M0042A and M0054B).

The quality of DIL45 data is good. Induction resistivity is a deep-investigation measurement and is least sensitive to borehole conditions. Resistivity log values are within the expected range.

The quality of ABI40 varies from one hole to another. The distance to the borehole wall greatly affects the quality of this imaging log along with good centralization. Hole M0042A was an API diameter hole where it was not possible to both effectively centralize the tool in open hole and pass through the API bit. Additionally, this hole diameter is outside the normal operating range for this tool. These factors result in low-quality images containing dark lines oriented at 180°. For this reason, image data in these sections should be treated with great care. In Hole M0054B, acoustic images were acquired at high resolution and with HQ-appropriate centralizers, resulting in high-quality, high-resolution images.

The quality of the 2PSA (SONIC) data is variable. Measurements of compressional wave velocity are highly dependent on borehole conditions. Sonic measurements were taken in both API and HQ boreholes. The tool was not well centralized in the larger boreholes because of restrictions on deployment. Larger cavities cause the induced wave to scatter, and acoustic energy is lost more rapidly. The picked *P*-wave arrivals show variable values, and in Hole M0054B only 50% of the data were collected; it is unknown whether this collection rate was caused by borehole/formation factors or tool issues.

### ABI40 and OBI40 image data processing

Images have been oriented with respect to magnetic north. Additionally, images have been enhanced by optimizing the amplitude range (ABI40) or altering the brightness and contrast (OBI40). Images provided have been depth corrected to the seafloor and matched (WMSF). They are displayed as an unwrapped borehole cylinder. As such, a dipping plane in the borehole appears as a sinusoid on the image,

with the amplitude of this sinusoid proportional to the dip of the plane. Because of orientation of image logs with respect to magnetic north, the strike of dipping features can also be determined.

### 2PSA acoustic data

The 2PSA tool was run at a frequency of 15 kHz, and resultant logs can be used to calculate compressional wave velocities. The data were processed using the WellCAD logging package. For processing purposes, data were filtered (frequency filter) in such a way that only the energy around the induced frequency was analyzed. Waveform picking was done manually in the WellCAD logging package to ensure good quality data. Where no clear arrivals in the waveform were present in two receivers, a null value was entered in the dataset. Time picks were saved, and acoustic velocities were calculated. The precision of acoustic traveltime measurements is ~5%.

## Microbiology

During the offshore phase of Expedition 325, microbiology samples were collected at all sites with a suitable soft-sediment lithology. Fluorescent microspheres were used during the coring process to identify possible contamination from drilling fluids, which might adversely affect microbiological studies. A majority of samples were collected for DNA and RNA characterization of microbial populations. Additional samples were collected and preserved for cell enumeration. Further sample collections were made during the onshore phase to determine changes in the microbial community during core storage.

### Microbiological sediment sampling from soft sediments

#### Offshore science party sampling

##### *Cell enumeration—fresh samples*

For cell enumeration of fresh samples, 2 g of wet sediment was collected by penetrating a sterile syringe (the forepart of the syringe was cut off) into the fresh sediment core. Collected samples were transferred to a 10 mL plastic vial (prefilled with 2 mL of 4% formaldehyde). The vial was capped and mixed with gentle shaking. The vial was stored at 4°C and transported back to the Bremen Core Repository in the refrigerated container.

##### *Molecular-based community characterization and biomarker analysis*

A 5 cm long whole-round sample was sawed from the bottom of a core section, collected (with liner)

in Whirl-Pak bags (double bagged), and stored in a  $-80^{\circ}\text{C}$  freezer as soon as possible after the core was recovered onto the drill floor. Section lengths were specifically cut so that microbiology samples were not located midsection, which would have required the liner to be split. A list of samples is provided in Table T15. These samples were shipped directly to laboratories in China and the USA on dry ice at the end of the offshore phase of Expedition 325.

## Onshore Science Party sampling

### *Cell enumeration*

Core sections directly adjacent to the whole-round samples taken offshore were targeted for cell enumeration. Immediately following core splitting, the sediment was subsectioned using a 5 mL syringe with the end removed. From the syringe, 0.5 g of wet sediment was transferred to a glass vial containing 5 mL of preservation buffer (phosphate buffered saline containing 10% methanol and 10% formalin). Sediment was mixed thoroughly to maximize cell exposure to the preservation buffer. Vials were then frozen at  $-20^{\circ}\text{C}$  and shipped on dry ice to the receiving laboratory.

### *Molecular-based community characterization*

Sediment remaining from the cell enumeration sampling sections was collected for molecular-based community characterization. These approximate half-round sections were located adjacent to the molecular analysis whole-round samples removed offshore (see “[Molecular-based community characterization and biomarker analysis](#)”). The sediment was transferred to sterilized Whirl-Pak bags, frozen immediately at  $-80^{\circ}\text{C}$ , and shipped on dry ice to the receiving laboratory.

## Specialist sampling of massive corals

### Identification of massive corals

Massive corals suitable for paleoclimatic studies were visually identified in core sections through the transparent liners and from descriptions contained in the offshore visual core descriptions prior to core splitting. Those core sections containing massive corals longer than the core diameter (or shorter but apparently in good condition) were labeled prior to core splitting to prevent them from being split using the regular core-splitting procedure. The major goal was to recover pristine, long, continuous intervals of coral skeletons from individual colonies along the

major axis of growth. The regular core-splitting procedure does not take into account the major growth direction of coral colonies. The core axis, or holes within a colony as a result of bioerosion, can be different from the major growth direction and can interrupt an otherwise continuous interval of the coral skeleton. Therefore, having obtained permission from the Curatorial Advisory Board, the liner was split for core sections containing massive corals using a handheld electric saw. One half of the liner was removed, and photographs of the colonies in situ within the core were taken for reference. With the core open, a coral paleoclimate specialist examined the section of coral and identified the optimum axis and plane for cutting. This axis was marked on the coral with a red wax pencil, and the core was then rephotographed with the coral thus marked.

### Splitting of massive corals

After photographs were taken, massive corals were removed from the core liner and split along the plane of the corals' major growth direction using a rock saw with a 1 mm thick blade and tap water. This often resulted in two unequal parts, so the procedure outlined in Figure F17 was followed to preserve 50% of the core volume for the archive half. One part was declared to be the archive half of the coral colony and the other the working half. The parts of the core not containing any coral colonies were then cut in half using the regular core-splitting method, and the archive and working halves were placed in their respective D-tubes. Once the working half of the core reached the sampling table, a 0.8–1 cm thick slab was cut from the coral colony for paleoclimate studies. A second slab was cut from the working half for other purposes, including dating or geochemical studies. In cases where the second slab appeared to provide the better sample, it was selected for paleoclimate studies and the central slab was used for other purposes. The orientation of all samples was recorded on the outside of the coral slabs using a red wax pencil (arrow pointing toward the top of the core). Note that this arrow records orientation in the core and does not necessarily reflect the original growth direction (which was annotated on the visual core descriptions).

### Washing and drying of massive coral slabs for paleoclimatology

After slicing, coral slabs for paleoclimate studies were jet-washed with tap water (tap pressure focused using a nozzle) and dried at  $40^{\circ}\text{C}$  in an oven for ~12–24 h.

## References

- Andersen, M.B., Stirling, C.H., Porcelli, D., Halliday, A.N., Andersson, P.S., and Baskaran, M., 2007. The tracing of riverine U in Arctic seawater with very precise  $^{234}\text{U}/^{238}\text{U}$  measurements. *Earth Planet. Sci. Lett.*, 259(1–2):171–185. doi:10.1016/j.epsl.2007.04.051
- Blanchon, P., and Blakeway, D., 2003. Are catch-up reefs an artefact of coring? *Sedimentology*, 50(6):1271–1282. doi:10.1111/j.1365-3091.2003.00603.x
- Broecker, W.S., 1963. A preliminary evaluation of uranium series inequilibrium as a tool for absolute age measurement on marine carbonates. *J. Geophys. Res.*, 68(9):2817–2834. doi:10.1029/JZ068i009p02817
- Bronk Ramsey, C., 2009. Bayesian analysis of radiocarbon dates. *Radiocarbon*, 51(1):337–360. <http://digitalcommons.arizona.edu/restrictedobjectviewer?o=http://radiocarbon.library.arizona.edu/Volume51/Number1/0b094122-5128-4777-9edd-b4dad8f3864d>
- Camoin, G., Cabioch, G., Eisenhauer, A., Braga, J.-C., Hamelin, B., and Lericolais, G., 2006. Environmental significance of microbialites in reef environments during the last deglaciation. *Sediment. Geol.*, 185(3–4):277–295. doi:10.1016/j.sedgeo.2005.12.018
- Camoin, G.F., Gautret, P., Montaggioni, L.F., and Cabioch, G., 1999. Nature and environmental significance of microbialites in Quaternary reefs: the Tahiti paradox. *Sediment. Geol.*, 126(1–4):271–304. doi:10.1016/S0037-0738(99)00045-7
- Camoin, G.F., and Montaggioni, L.F., 1994. High energy corallgal-stromatolite frameworks from Holocene reefs (Tahiti, French Polynesia). *Sedimentology*, 41(4):655–676. doi:10.1111/j.1365-3091.1994.tb01416.x
- Cheng, H., Edwards, R.L., Hoff, J., Gallup, C.D., Richards, D.A., and Asmerom, Y., 2000. The half-lives of uranium-234 and thorium-230. *Chem. Geol.*, 169(1–2):17–33. doi:10.1016/S0009-2541(99)00157-6
- Chung, F.H., 1974. Quantitative interpretation of X-ray diffraction patterns of mixtures. I. Matrix-flushing method for quantitative multicomponent analysis. *J. Appl. Cryst.*, 7(6):519–525. doi:10.1107/S0021889874010375
- Delanghe, D., Bard, E., and Hamelin, B., 2002. New TIMS constraints on the uranium-238 and uranium-234 in seawaters from the main ocean basins and the Mediterranean Sea. *Mar. Chem.*, 80(1):79–93. doi:10.1016/S0304-4203(02)00100-7
- deMenocal, P., Bloemendal, J., and King, J., 1991. A rock-magnetic record of monsoonal dust deposition to the Arabian Sea: evidence for a shift in the mode of deposition at 2.4 Ma. In Prell, W.L., Niitsuma, N., et al., *Proc. ODP, Sci. Results*, 117: College Station, TX (Ocean Drilling Program), 389–407. doi:10.2973/odp.proc.sr.117.178.1991
- Dunham, R.J., 1962. Classification of carbonate rocks according to depositional texture. In Ham, W.E. (Ed.), *Classification of Carbonate Rocks*. AAPG Mem., 1:108–121.
- Ellwood, B.B., Balsam, W.L., and Roberts, H.H., 2006. Gulf of Mexico sediment sources and sediment transport trends from magnetic susceptibility measurements of surface samples. *Mar. Geol.*, 230(3–4):237–248. doi:10.1016/j.margeo.2006.05.008
- Ellwood, B.B., Brett, C.E., and MacDonald, W.D., 2007. Magnetostratigraphy susceptibility of the Upper Ordovician Kope Formation, northern Kentucky. *Palaeogeogr., Palaeoclimatol., Palaeoecol.*, 243(1–2):42–54. doi:10.1016/j.palaeo.2006.07.003
- Ellwood, B.B., Crick, R.E., El Hassani, A., Benoist, S.L., and Young, R.H., 2000. Magnetostratigraphy event and cyclostratigraphy method applied to marine rocks: detrital input versus carbonate productivity. *Geology*, 28(12):1135–1138. doi:10.1130/0091-7613(2000)28<1135:MEACMA>2.0.CO;2
- Ellwood, B.B., Stormer, J.C., Jr., and Whitney, J.A., 1989. Fish Canyon Tuff, Colorado: the problem of two magnetic polarities in a single tuff. *Phys. Earth Planet. In.*, 56(3–4):329–336. doi:10.1016/0031-9201(89)90167-2
- Embry, A.F., III, and Klovan, J.E., 1972. Absolute water depth limits of late Devonian paleoecological zones. *Geol. Rundsch.*, 61(2):672–686. doi:10.1007/BF01896340
- Esat, T.M., and Yokoyama, Y., 2006. Variability in the uranium isotopic composition of the oceans over glacial-interglacial timescales. *Geochim. Cosmochim. Acta*, 70(16):4140–4150. doi:10.1016/j.gca.2006.06.013
- Esat, T.M., and Yokoyama, Y., 2010. Coupled uranium isotope and sea level variations in the oceans. *Geochim. Cosmochim. Acta*, 74(24):7008–7020. doi:10.1016/j.gca.2010.09.007
- Expedition 302 Scientists, 2006. Methods. In Backman, J., Moran, K., McInroy, D.B., Mayer, L.A., and the Expedition 302 Scientists, *Proc. IODP, 302: Edinburgh (Integrated Ocean Drilling Program Management International, Inc.)*. doi:10.2204/iodp.proc.302.103.2006
- Fairbanks, R.G., 1989. A 17,000-year glacio-eustatic sea level record: influence of glacial melting rates on the Younger Dryas event and deep-ocean circulation. *Nature (London, U. K.)*, 342(6250):637–642. doi:10.1038/342637a0
- Fallon, S.J., Fifield, L.K., and Chappell, J.M., 2010. The next chapter in radiocarbon dating at the Australian National University: status report on the single stage AMS. *Nucl. Instrum. Methods Phys. Res., Sect. B*, 268(7–8):898–901. doi:10.1016/j.nimb.2009.10.059
- Grasshoff, K., 1983. Determination of oxygen. In Grasshoff, K., Ehrhardt, M., and Kremling, K. (Eds.), *Methods of Seawater Analysis* (2nd ed.): New York (Verlag Chemie).
- Hall, P.O.J., and Aller, R.C., 1992. Rapid, small-volume, flow injection analysis for  $\Sigma\text{CO}_2$  and  $\text{NH}_4^+$  in marine and freshwaters. *Limnol. Oceanogr.*, 37(5):1113–1119. doi:10.4319/lo.1992.37.5.1113
- Hallock, P., 1985. Why are larger foraminifera large? *Paleobiology*, 11(2):195–208.

- Holden, N.E., 1990. Total half-lives for selected nuclides. *Pure Appl. Chem.*, 62(5):941–958. doi:10.1351/pac199062050941
- Jaffey, A.H., Flynn, K.F., Glendenin, L.E., Bentley, W.C., and Essling, A.M., 1971. Precision measurements of half-lives and specific activities of U-235 and U-238. *Phys. Rev. C: Nucl. Phys.*, 4(5):1889–1906. doi:10.1103/PhysRevC.4.1889
- Jovane, L., Coccioni, R., Marsili, A., and Acton, G., 2009. The late Eocene greenhouse–icehouse transition: observations from the Massignano global stratotype section and point (GSSP). In Koeberl, C., and Montanari, A. (Eds.), *The Late Eocene Earth—Hothouse, Icehouse, and Impacts*. Spec. Pap.—Geol. Soc. Am., 452:149–168. doi:10.1130/2009.2452(10)
- Jovane, L., Florindo, F., Sprovieri, M., and Pälike, H., 2006. Astronomic calibration of the late Eocene/early Oligocene Massignano section (central Italy). *Geochem., Geophys., Geosyst.*, 7:Q07012. doi:10.1029/2005GC001195
- Jovane, L., Sprovieri, M., Coccioni, R., Florindo, F., Marsili, A., and Laskar, J., 2010. Astronomical calibration of the middle Eocene Contessa Highway section (Gubbio, Italy). *Earth Planet. Sci. Lett.*, 298(1–2):77–88. doi:10.1016/j.epsl.2010.07.027
- Kirschvink, J.L., 1980. The least-squares line and plane and the analysis of palaeomagnetic data. *Geophys. J. R. Astron. Soc.*, 62(3):699–718. doi:10.1111/j.1365-246X.1980.tb02601.x
- Kopp, R.E., and Kirschvink, J.L., 2008. The identification and biogeochemical interpretation of fossil magnetotactic bacteria. *Earth-Sci. Rev.*, 86(1–4):42–61. doi:10.1016/j.earscirev.2007.08.001
- Leroy, C.C., 1969. Development of simple equations for accurate and more realistic calculation of the speed of sound in seawater. *J. Acoust. Soc. Am.*, 46(1B):216–226. doi:10.1121/1.1911673
- Lund, S., Platzman, E., Thouveny, N., Camoin, G., Corsetti, F., and Berelson, W., 2010. Biological control of paleomagnetic remanence acquisition in carbonate framework rocks of the Tahiti coral reef. *Earth Planet. Sci. Lett.*, 298(1–2):14–22. doi:10.1016/j.epsl.2010.07.010
- Mason, A.J., and Henderson, G.M., 2010. Correction of multi-collector-ICP-MS instrumental biases in high-precision uranium-thorium chronology. *Int. J. Mass Spectrom.*, 295(1–2):26–35. doi:10.1016/j.ijms.2010.06.016
- McElhinny, M.W., 2007. Geocentric axial dipole hypothesis. In Gubbins, D., and Herrero-Ververa, E. (Eds.), *Encyclopedia of Geomagnetism and Paleomagnetism*. Berlin Heidelberg (Springer Verlag), 281–286.
- Ménabréaz, L., Thouveny, N., Camoin, G., and Lund, S.P., 2010. Paleomagnetic record of the late Pleistocene reef sequence of Tahiti (French Polynesia): a contribution to the chronology of the deposits. *Earth Planet. Sci. Lett.*, 294(1–2):58–68. doi:10.1016/j.epsl.2010.03.002
- Nagata, T., 1961. *Rock Magnetism*: Tokyo (Maruzen).
- Negre, C., Thomas, A.L., Mas, J.L., Garcia-Orellana, J., Henderson, G.M., Masqué, P., and Zahn, R., 2009. Separation and measurement of Pa, Th, and U isotopes in marine sediments by microwave-assisted digestion and multiple collector inductively coupled plasma mass spectrometry. *Anal. Chem. (Washington, DC, U. S.)*, 81(5):1914–1919. doi:10.1021/ac802341y
- Reimer, P.J., Baillie, M.G.L., Bard, E., Bayliss, A., Beck, J.W., Blackwell, P.G., Bronk, R.C., Buck, C.E., Burr, G.S., Edwards, R.L., Friedrich, M., Grootes, P.M., Guilderson, T.P., Hajdas, I., Heaton, T.J., Hogg, A.G., Hughen, K.A., Kaiser, K.F., Kromer, B., McCormac, F.G., Manning, S.W., Reimer, R.W., Richards, D.A., Southon, J.R., Talamo, S., Turney, C.S.M., van der Plicht, J., and Weyhenmeyer, C.E., 2009. Intcal09 and Marine09 radiocarbon age calibration curves, 0–50,000 years cal BP. *Radiocarbon*, 51(4):1111–1150. <http://digitalcommons.arizona.edu/restrictedobjectviewer?o=http://radiocarbon.library.arizona.edu/Volume51/Number4/49691745-6a68-4e2c-a26f-08f0a16c1a53>
- Robinson, L.F., Belshaw, N.S., and Henderson, G.M., 2004a. U and Th concentrations and isotope ratios in modern carbonates and waters from the Bahamas. *Geochim. Cosmochim. Acta*, 68(8):1777–1789. doi:10.1016/j.gca.2003.10.005
- Robinson, L.F., Henderson, G.M., Hall, L., and Matthews, I., 2004b. Climatic control of riverine and seawater uranium-isotope ratios. *Science*, 305(5685):851–854. doi:10.1126/science.1099673
- Studer, T., 1878. Zweite abtheilung der *Anthozoa polyactinia* welche während der Reise S.M.S. Corvette *Gazelle* um die Erde gesammelt wurden. *Monatsber. Dtsch. Akad. Wiss. Berlin*, 25:524–550.
- Valet, J.-P., 2003. Time variations in geomagnetic intensity. *Rev. Geophys.*, 41:1004. doi:10.1029/2001RG000104
- Valet, J.-P., Meynadier, L., and Guyodo, Y., 2005. Geomagnetic dipole strength and reversal rate over the past two million years. *Nature (London, U. K.)*, 435(7043):802–805. doi:10.1038/nature03674
- Veron, J.E.N., 2000. *Corals of the World*: Townsville, M.C. (Australian Inst. Mar. Sci.).
- Verosub, K.L., and Roberts, A.P., 1995. Environmental magnetism: past, present, and future. *J. Geophys. Res., [Solid Earth]*, 100(B2):2175–2192. doi:10.1029/94JB02713
- Vogt, C., 2009. Data report: semiquantitative determination of detrital input to ACEX sites based on bulk sample X-ray diffraction data. In Backman, J., Moran, K., McInroy, D.B., Mayer, L.A., and the Expedition 302 Scientists, *Proc. IODP, 302*: Edinburgh (Integrated Ocean Drilling Program Management International, Inc.). doi:10.2204/iodp.proc.302.203.2009
- Vogt, C., Lauterjung, J., and Fischer, R.X., 2002. Investigation of the clay fraction (<2 μm) of the clay mineral society reference clays. *Clays Clay Miner.*, 50(3):388–400. doi:10.1346/000986002760833765
- Von Herzen, R., and Maxwell, A.E., 1959. The measurement of thermal conductivity of deep-sea sediments by a needle-probe method. *J. Geophys. Res.*, 64(10):1557–1563. doi:10.1029/JZ064i010p01557
- Wallace, C.C., Chen, C.A., Fukami, H., and Muir, P.R., 2007. Recognition of separate genera within *Acropora* based on new morphological, reproductive, and genetic evidence from *Acropora togianensis*, and elevation of the subgenus *Isopora* Studer, 1878 to genus (Scleractinia):



- Astrocoeniidae; Acroporidae). *Coral Reefs*, 26(2): 231–239. doi:10.1007/s00338-007-0203-4
- Webster, J.M., Clague, D.A., Riker-Coleman, K., Gallup, C., Braga, J.C., Potts, D., Moore, J.G., Winterer, E.L., and Paull, C.K., 2004. Drowning of the –150 m reef off Hawaii: a casualty of global meltwater pulse 1A? *Geology*, 32(3):249–252. doi:10.1130/G20170.1
- Webster, J.M., and Davies, P.J., 2003. Coral variation in two deep drill cores: significance for the Pleistocene development of the Great Barrier Reef. In Blanchon, P., and Montaggioni, L. (Eds.), *Late Quaternary Reef Development*. Sediment. Geol., 159(1–2):61–80. doi:10.1016/S0037-0738(03)00095-2
- Weedon, G.P., Jenkyns, H.C., Coe, A.L., and Hesselbo, S.P., 1999. Astronomical calibration of the Jurassic timescale from cyclostratigraphy in British mudrock formations. *Philos. Trans. R. Soc., A*, 357(1757):1787–1813. doi:10.1098/rsta.1999.0401
- Wentworth, C.K., 1922. A scale of grade and class terms for clastic sediments. *J. Geol.*, 30(5):377–392. doi:10.1086/622910
- Yokoyama, Y., and Esat, T.M., 2004. Long term variations of uranium isotopes and radiocarbon in the surface seawater recorded in corals. In Shiyomi, M., Kawahata, H., Koizumi, H., Tsuda, A., and Awaya, Y. (Eds.), *Global Environmental Change in the Ocean and on Land*. Tokyo (TERRAPUB), 279–309.
- Yokoyama, Y., Esat, T.M., Lambeck, K., and Fifield, L.K., 2000. Last ice age millennial scale climate changes recorded in Huon Peninsula corals. *Radiocarbon*, 42(3):383–401. [http://digitalcommons.arizona.edu/objectviewer?o=http%3A%2F%2Fradiocarbon.library.arizona.edu%2FVolume42%2FNumber3%2Fazu\\_radiocarbon\\_v42\\_n3\\_383\\_401\\_v.pdf](http://digitalcommons.arizona.edu/objectviewer?o=http%3A%2F%2Fradiocarbon.library.arizona.edu%2FVolume42%2FNumber3%2Fazu_radiocarbon_v42_n3_383_401_v.pdf)
- Yokoyama, Y., Miyairi, Y., Matsuzaki, H., and Tsunomori, F., 2007. Relation between acid dissolution time in the vacuum test tube and time required for graphitization for AMS target preparation. *Nucl. Instrum. Methods Phys. Res., Sect. B*, 259(1):330–334. doi:10.1016/j.nimb.2007.01.176
- Yokoyama, Y., Koizumi, M., Matsuzaki, H., Miyairi, Y., and Ohkouchi, N., 2010. Developing ultrasmall-scale radiocarbon sample measurement at the University of Tokyo. *Radiocarbon*, 52(2):310–318. <http://digitalcommons.arizona.edu/restrictedobjectviewer?o=http://radiocarbon.library.arizona.edu/Volume52/Number2/ee7b1dd5-adf3-4690-b40b-3fb7034f532e>
- Zijderveld, J.D.A., 1967. AC demagnetization of rocks: analysis of results. In Collinson, D.W., Creer, K.M., and Runcorn, S.K. (Eds.), *Methods in Palaeomagnetism*: New York (Elsevier), 254–286.

**Publication:** 16 July 2011

**MS 325-102**

Figure F1. Schematic of IODP recovery and naming conventions used during Expedition 325.

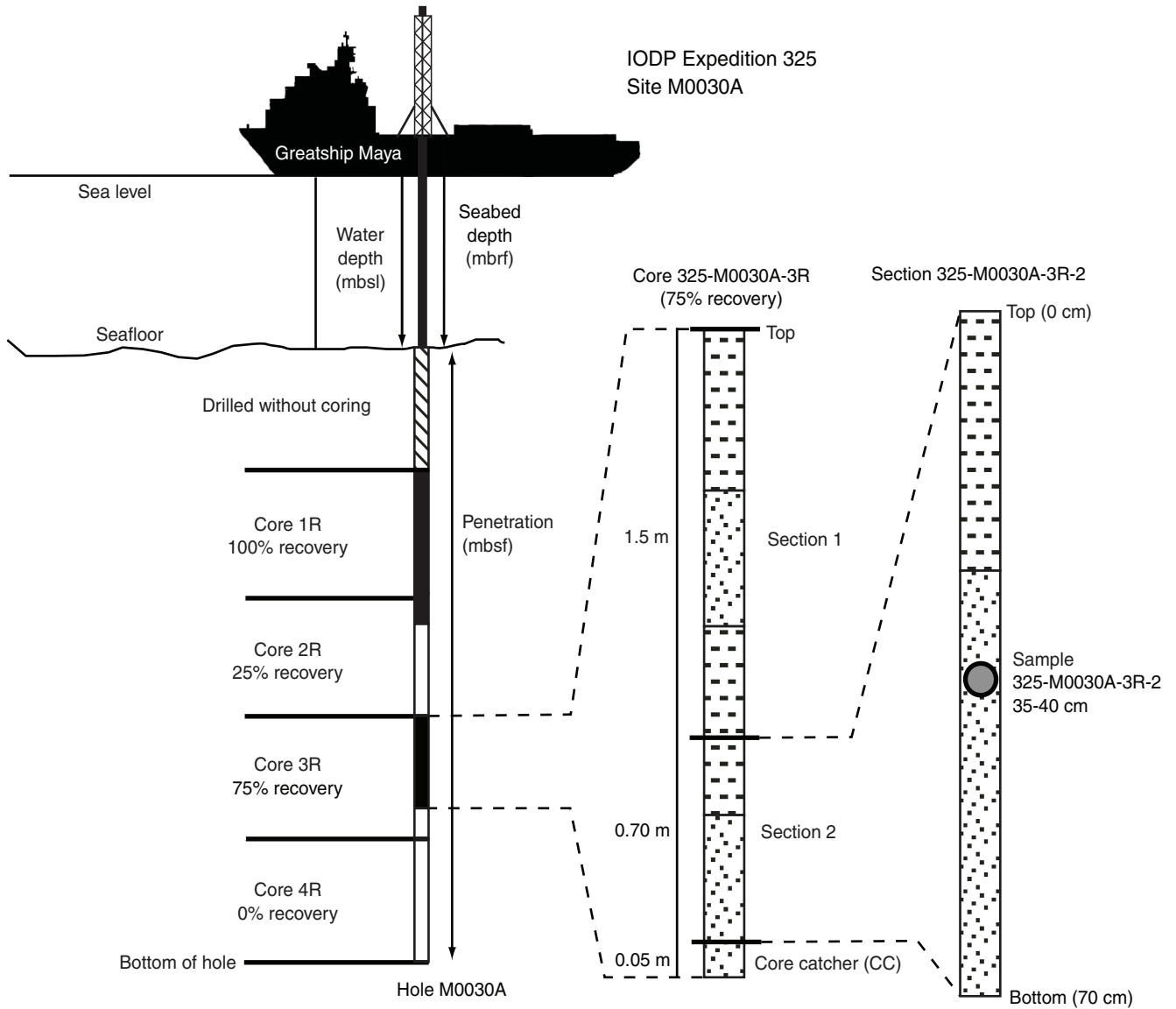


**Figure F2.** The *Greatship Maya*, Townsville, Australia, during Expedition 325. (Image courtesy of D.Potts@ECORD\_IODP.)



**Figure F3.** Layout of the ESO mobile offices and laboratories (turquoise containers) on the drill floor of the *Greatship Maya* during Expedition 325. (Image courtesy of G.Lott@ECORD\_IODP.)

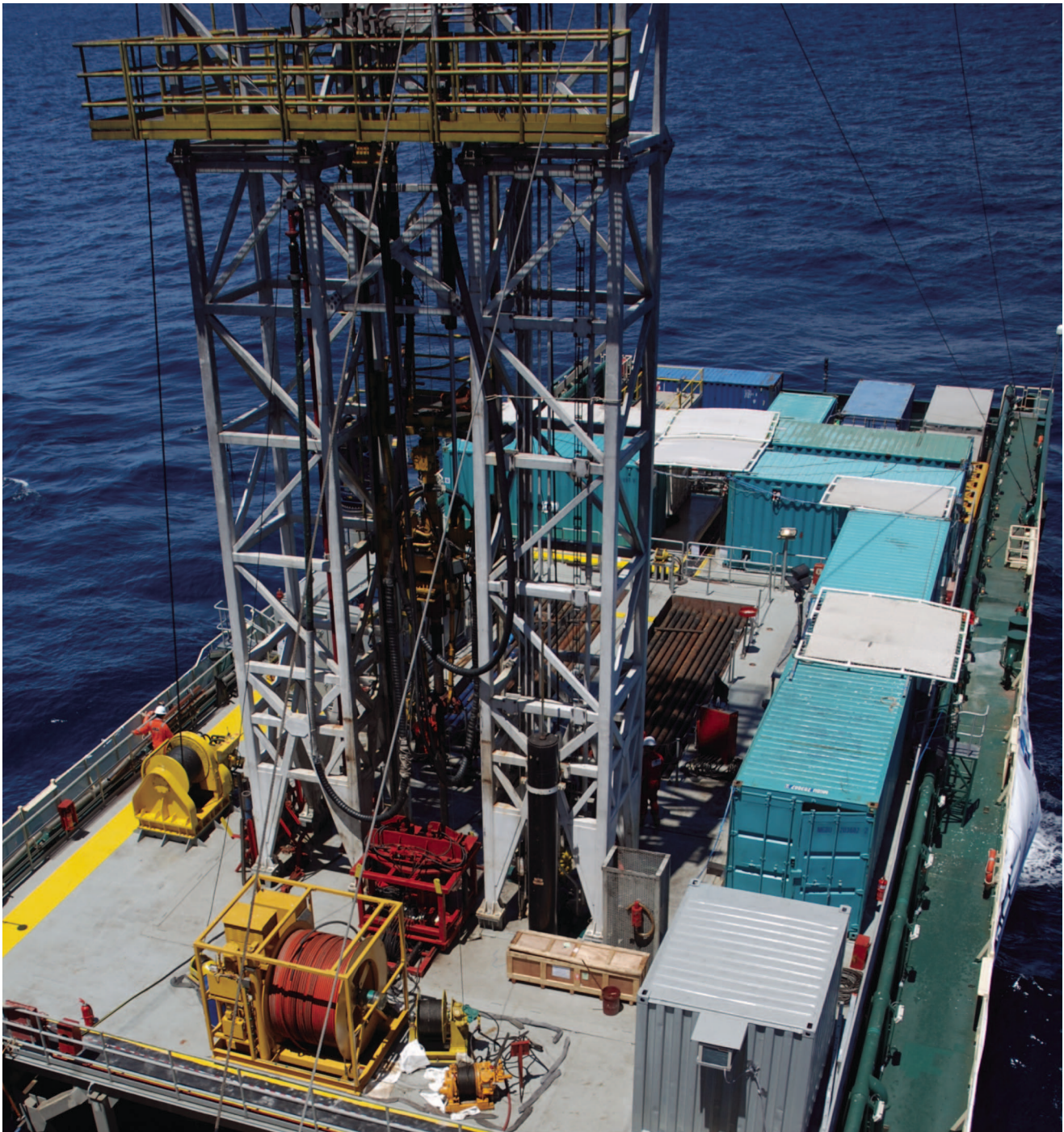


**Figure F4.** Image showing the mezzanine level drill floor and derrick during Expedition 325, with the seabed template positioned over the moonpool on the main deck level. (Image courtesy of C.Cotterill@ECORD\_IODP.)

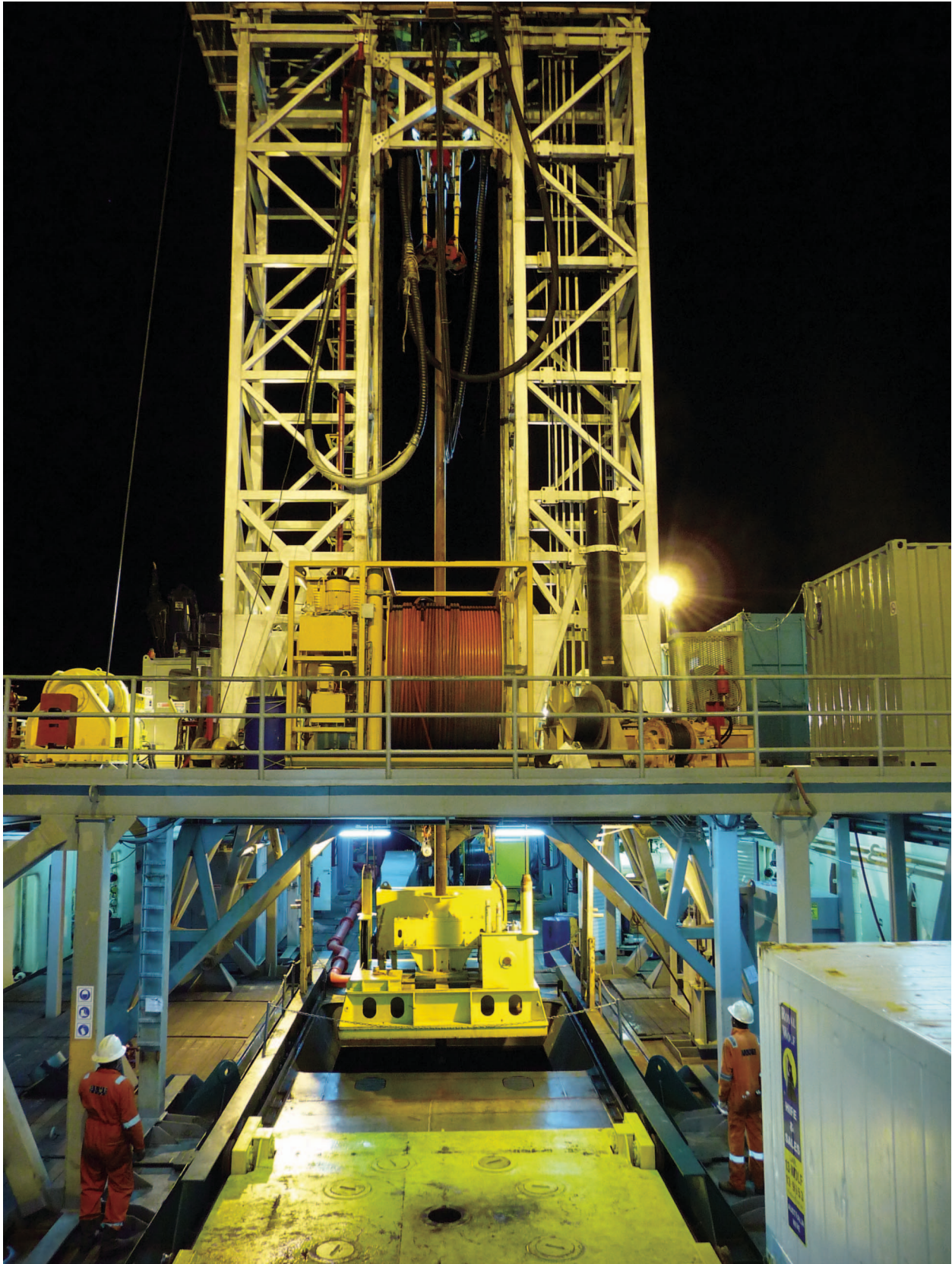


**Figure F5.** Bluestone TT150 derrick showing the rooster box from which downhole logging operations were conducted during Expedition 325. (Image courtesy of D.Smith@ECORD\_IODP.)



**Figure F6.** Downhole camera system and frame used to record pre- and postcoring video footage of the seabed during Expedition 325. (Image courtesy of D.Wallis@ECORD\_IODP.)





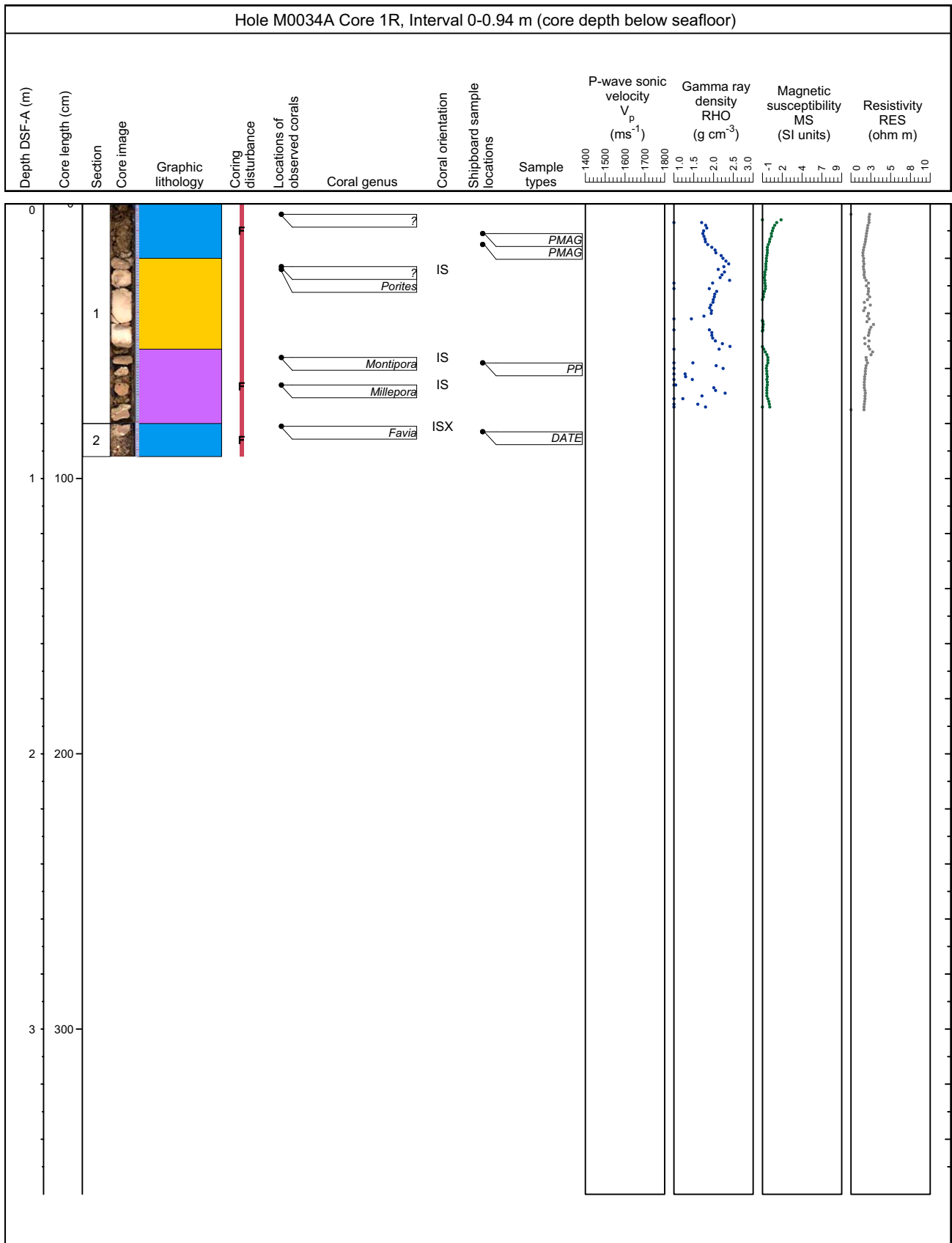








**Figure F7.** Example of a visual core description (VCD) sheet used during Expedition 325. F = fractured. IS = in situ, ISX = not in situ. PMAG = paleomagnetism, PP = physical properties, DATE = dating.





**Figure F8.** Summary of visual core description definitions used during Expedition 325.


## Lithology

	Modern		Rudstone
	Coralgal boundstone		Floatstone
	Coralgal-microbialite boundstone		Lime sand
	Microbialite boundstone		Mud
	Packstone		Unconsolidated sediment
	Grainstone		

## Orientation

IS	In situ
IS?	Possibly in situ
ISN	Status not known
ISX	Not in situ

## Disturbance

F	Fractured
S	Slight
B	Brecciated
	Bar with letter indicates extent of disturbance. Bar without letter indicates disturbance, but no further information provided.

## Sample

PMAG	Paleomagnetism	DATE	Dating
XRD	X-ray diffraction	IWRH	Interstitial water rhizome
TOC	Total organic carbon	HS	Headspace gas
PP	Physical properties	MBIO	Microbiology
MAD	Moisture and density	PAL	Micropaleontology

**Figure F9.** High-resolution line scan images of examples of core disturbance and downhole contamination (Sections 325-M0037A-9R-1 and 11R-1).

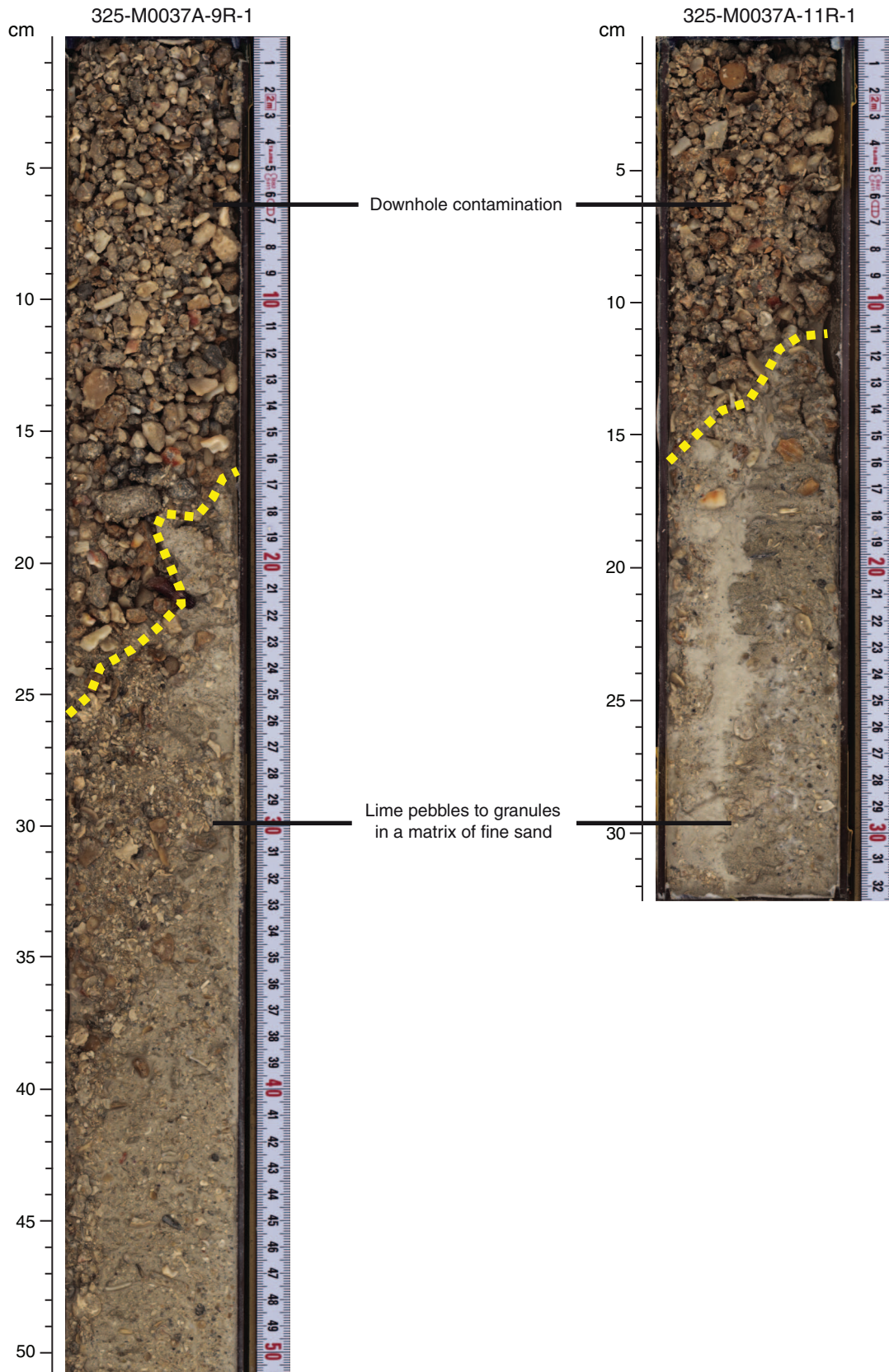


**Figure F10.** High-resolution line scan images of representative examples of the major lithologies. **A.** Coralgalmicrobialite boundstone (Section 325-M0035A-8R-1). **B.** Coral framestone with massive coral (Section 325-M0034A-11R-1). (Continued on next page.)

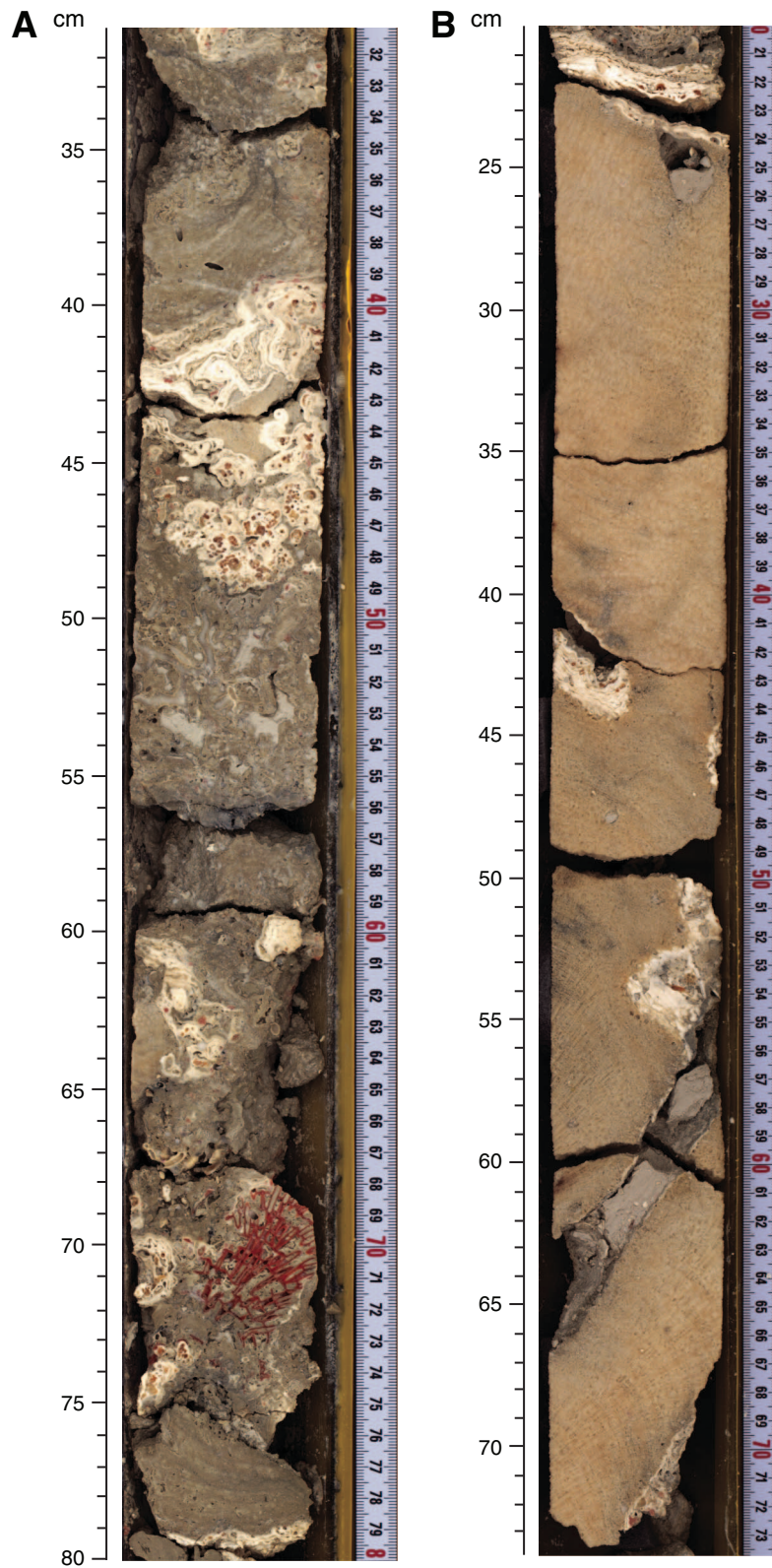


**Figure F10 (continued).** C. Bioeroded coralgall bindstone (Section 325-M0030A-1R-CC). D. Rudstone with bioclasts (Section 325-M0035A-9R-2). E. Grainstone with bioclasts (Section 325-M0039A-21R-CC). F. Packstone with bioclasts (Section 325-M0033A-22R-2).

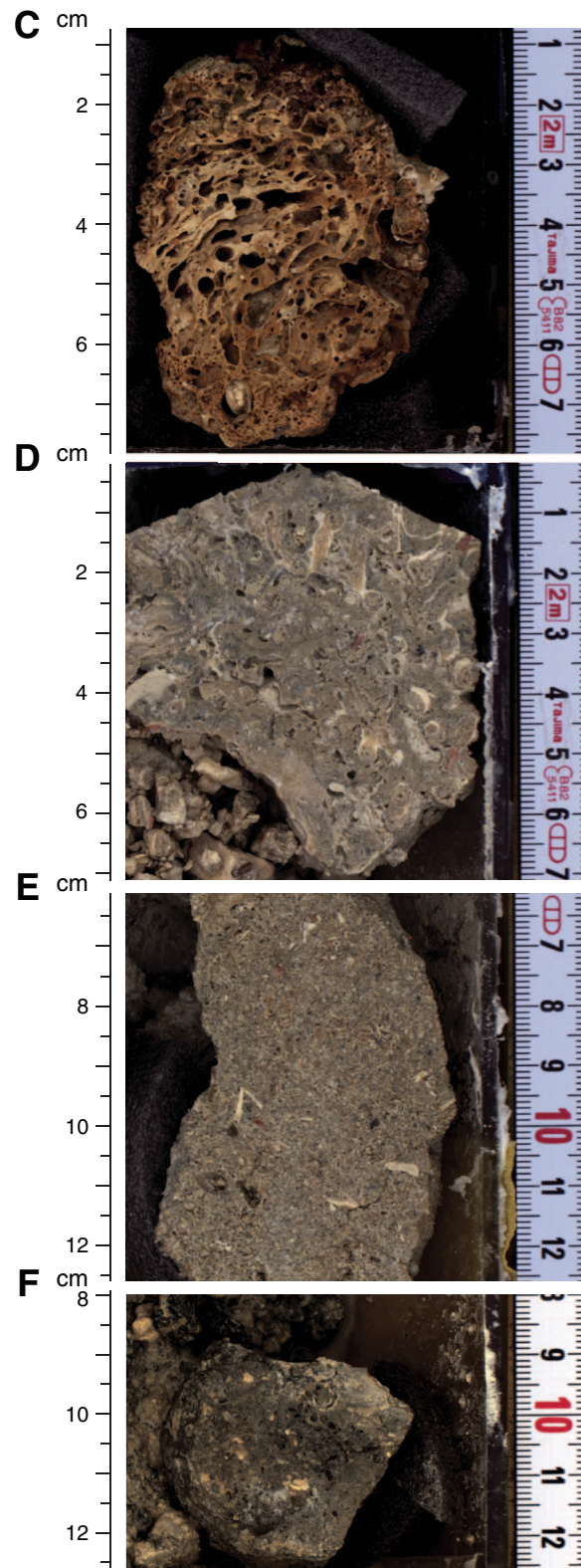




**Figure F11.** The effect of initial  $^{230}\text{Th}$  correction for Expedition 325 U-Th dated samples. Uncorrected ages (blue squares) and ages corrected for crustal (GeoRoc) contamination (purple circles) and seawater Th incorporation (red squares) are shown. Note the break and change in scale for the age axis. cal y BP = calibrated years before present (years before 1950 AD)

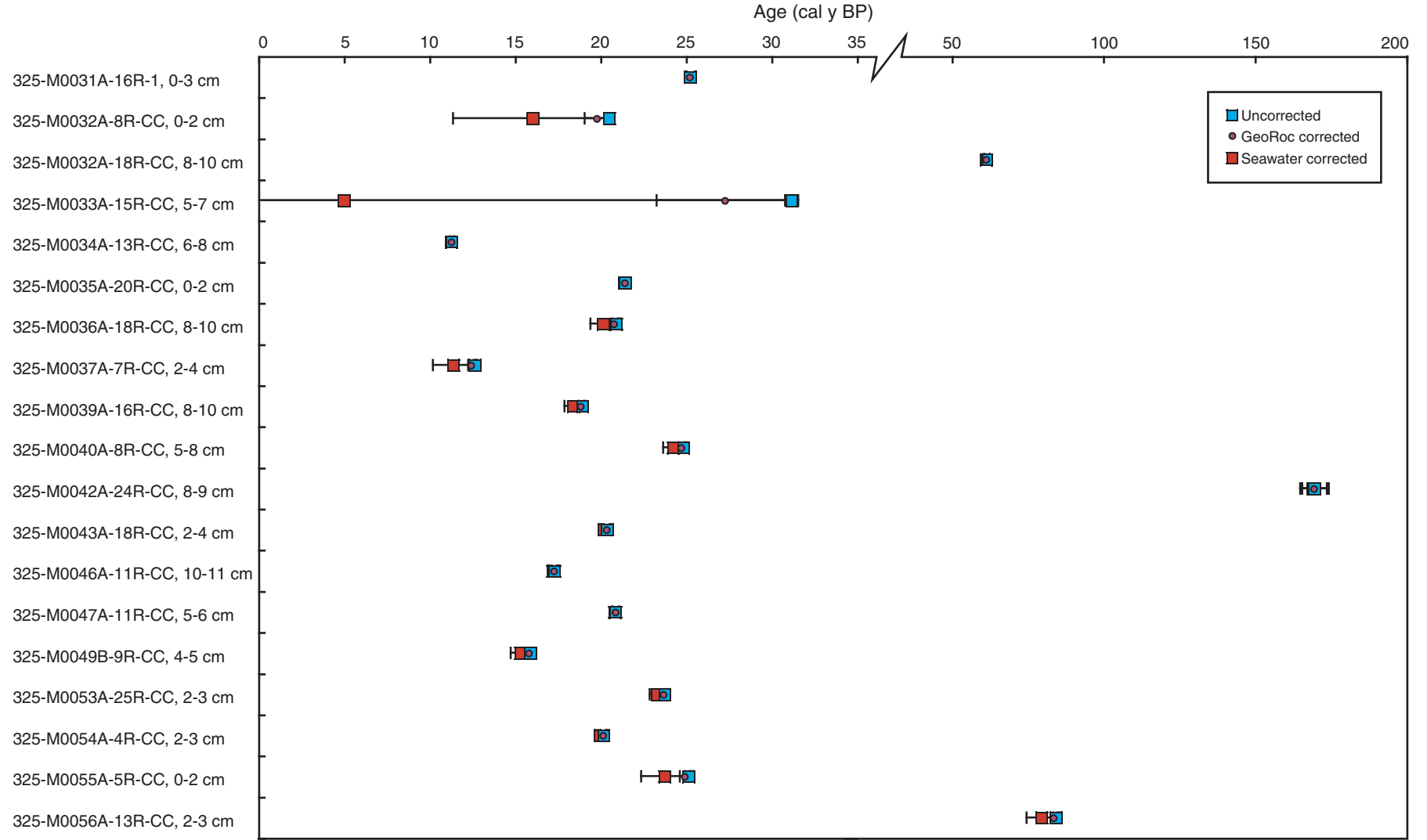


**Figure F12.** Illustration of the effect of radiocarbon calibration on the distribution of uncertainty in the calibrated ages of Expedition 325 corals. The uncalibrated radiocarbon age and uncertainty are shown as the red normal distribution, and the marine09 calibration curve representing the apparent radiocarbon age variability caused by changes in the marine  $\Delta^{14}\text{C}$  through time is shown in blue. The resultant calibrated age distribution is shown in gray, with the 95.4% and 68% probability bounds shown as bars below. For the purposes of comparing ages among corals, the mean calibrated age (white circle) is shown. It should be noted that in the summary plots where age interpretations are rounded to 1 k.y., this sample will be shown as 20 calibrated years before present (cal y BP; years before 1950 AD), whereas the calibrated age lies in the range 19.39–19.83 cal y BP. (See Bronk Ramsey [2009], as well as Bronk Ramsey [2010] at [c14.arch.ox.ac.uk/oxcal.html](http://c14.arch.ox.ac.uk/oxcal.html).)

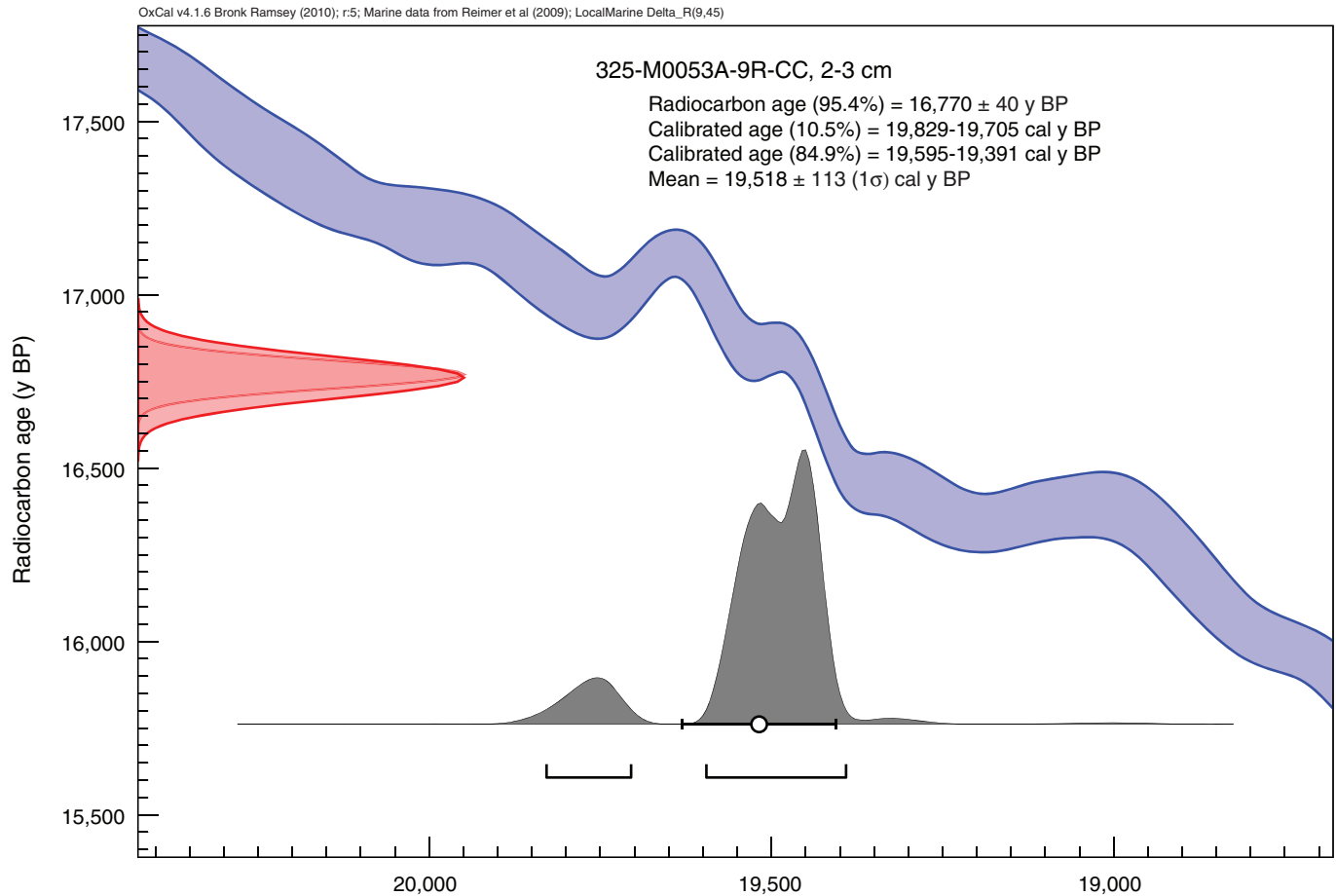


**Figure F13.** Histogram (1 k.y. bins) of the preliminary radiocarbon ages and U-Th ages for corals drilled during Expedition 325. U-Th = ages uncorrected for initial  $^{230}\text{Th}$ , Cal  $^{14}\text{C}$  = calibrated radiocarbon ages. cal y BP = calibrated years before present (years before 1950 AD)

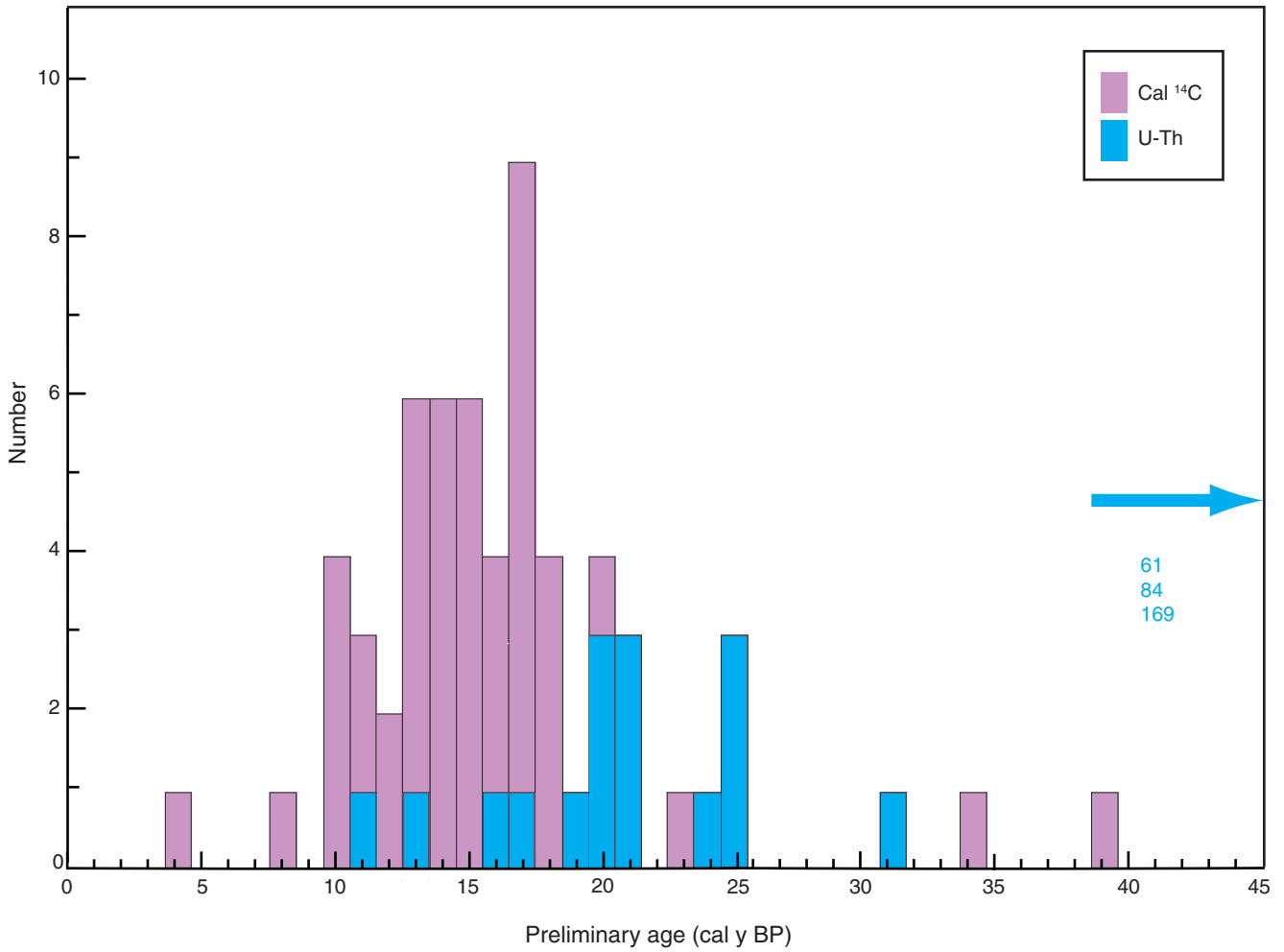




**Figure F14.** Diagrams of logging tools used during Expedition 325. **A.** Optical Borehole Imager (OBI40). **B.** Acoustic Borehole Imager (ABI40). **C.** Hydrogeological probe (IDRONAUT). **D.** Spectral Gamma Ray (ASGR).

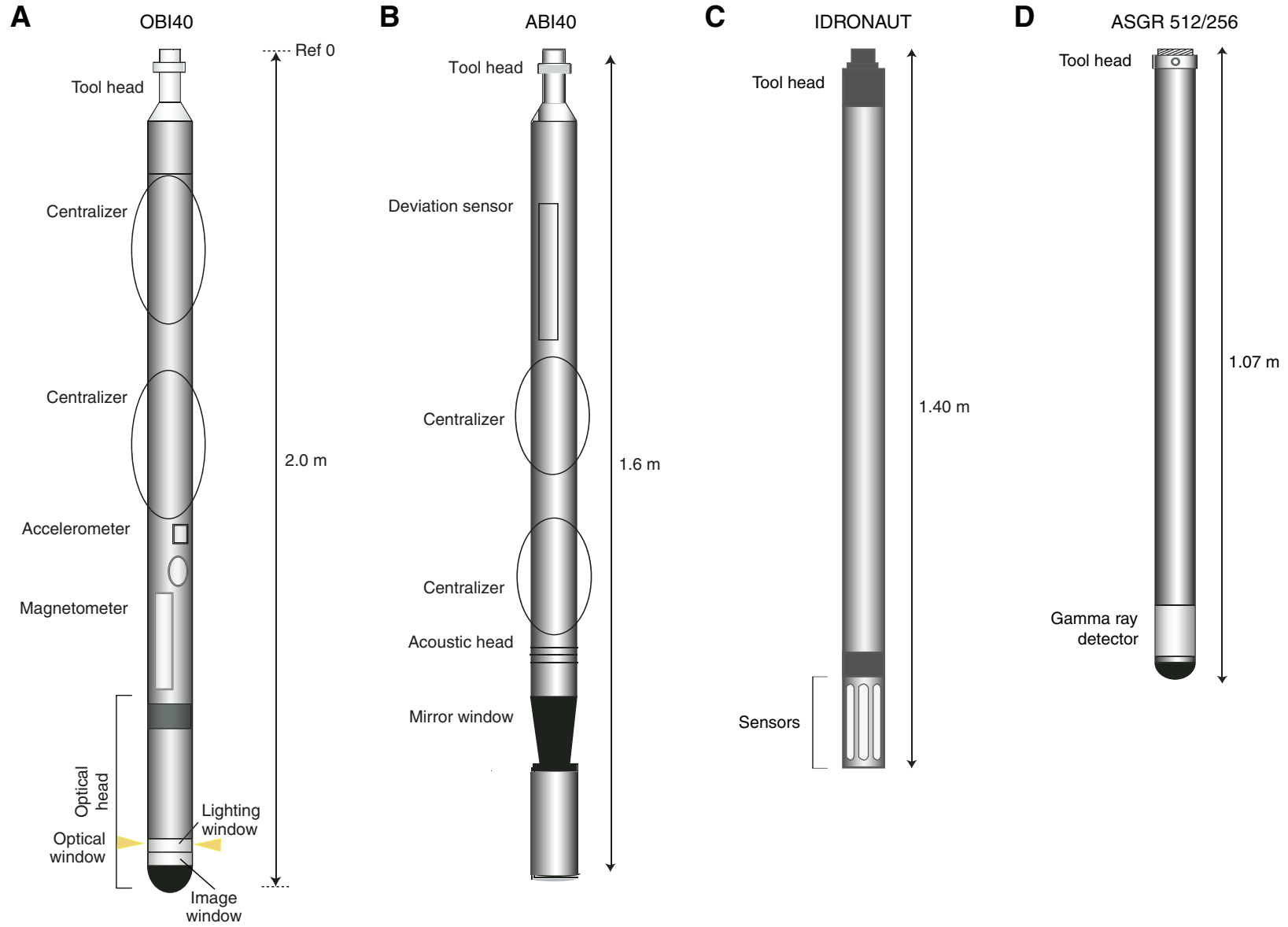






**Figure F15.** Diagrams of logging tools used during Expedition 325. **A.** Dual Induction Log (DIL 45). ILD = induction electrical conductivity of greater investigation depth, ILM = induction electrical conductivity of medium investigation depth. **B.** Full Wave Sonic (SONIC). **C.** Magnetic susceptibility tool (EM51). **D.** Borehole diameter tool (CAL3).

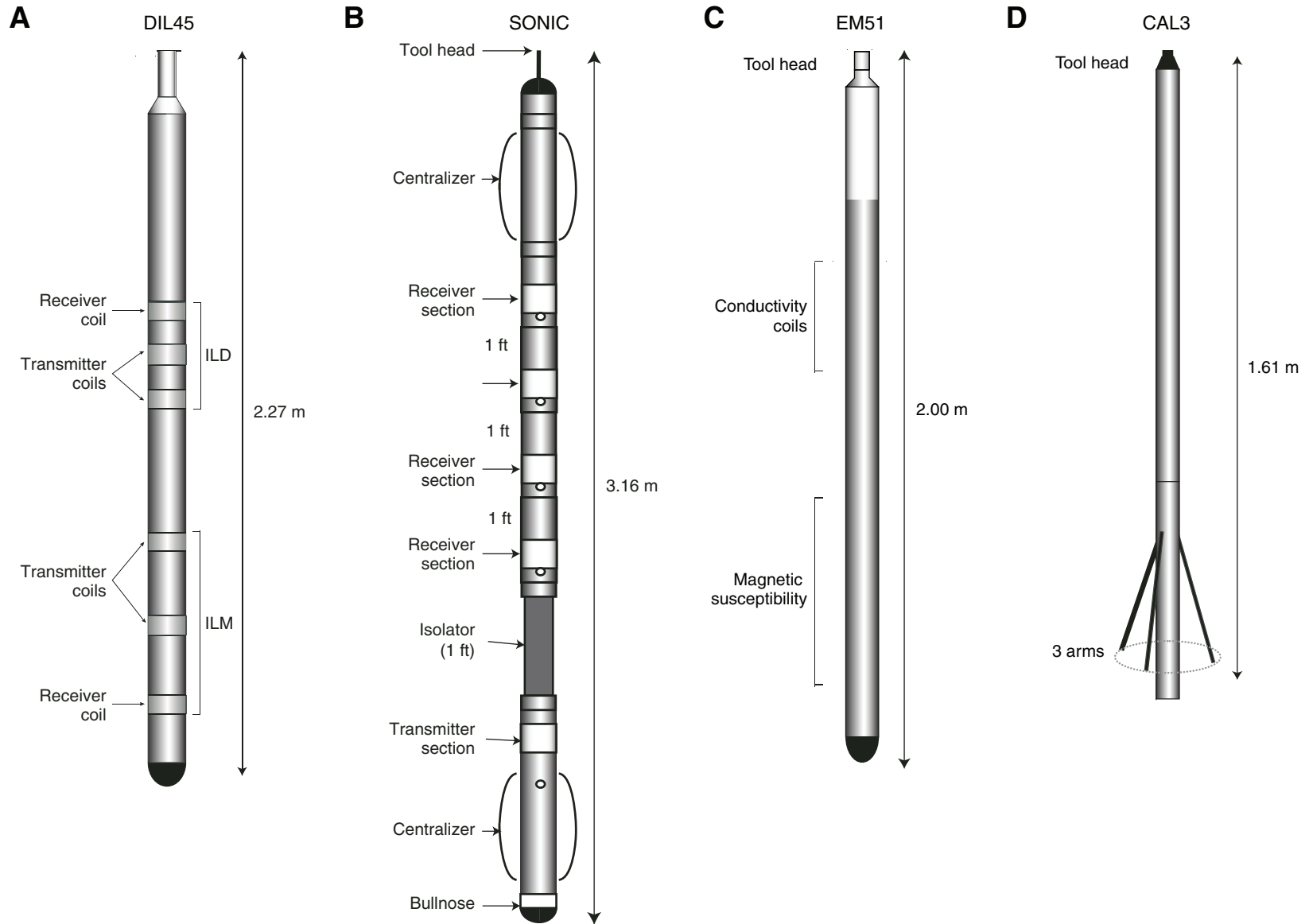


**Figure F16.** Schematic diagram (not to scale), showing how HQ and American Petroleum Institute (API) pipes were compensated during open hole logging in Hole M0054B.

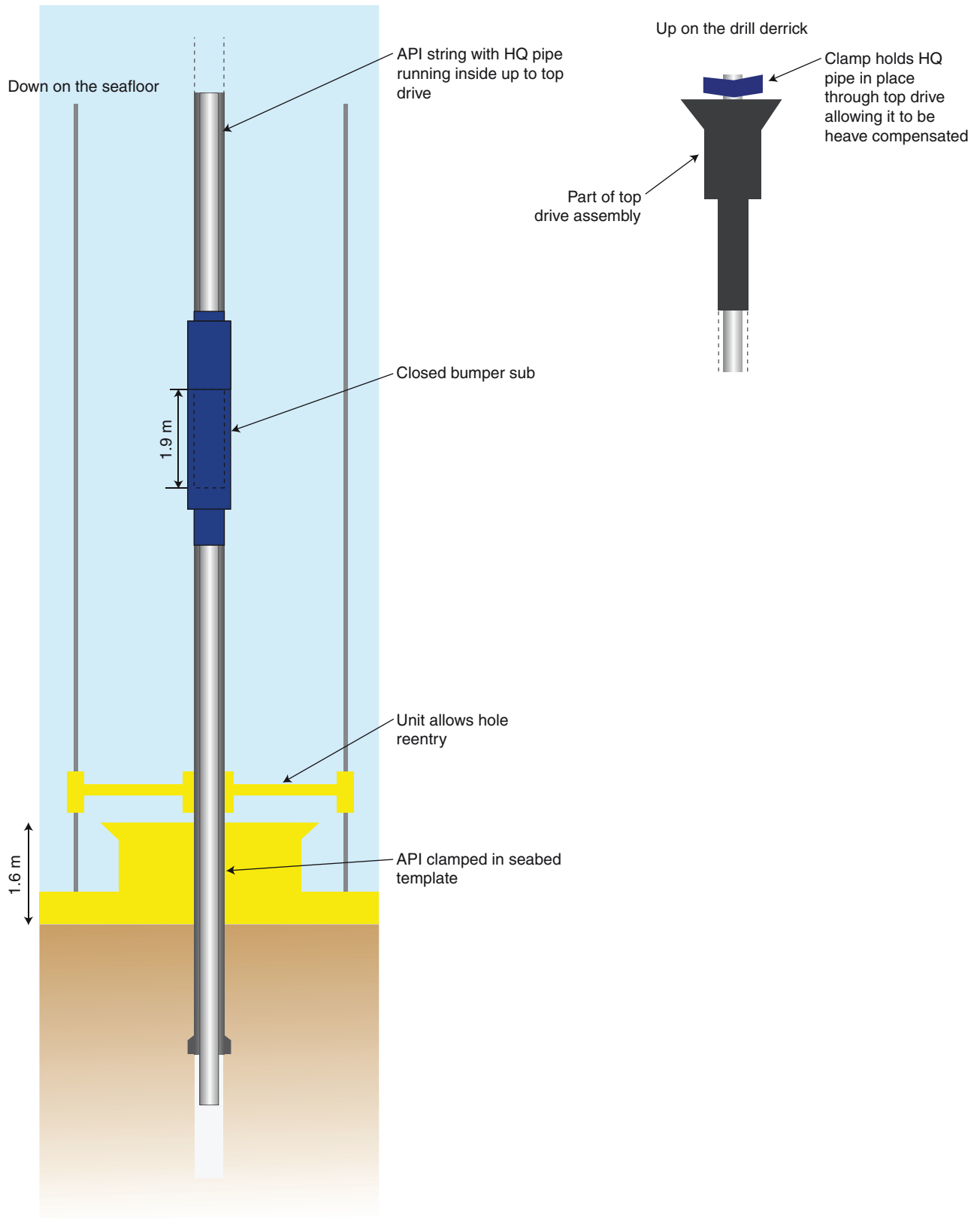


**Figure F17.** A–C. Schematic diagram illustrating placement of massive coral pieces after oblique cutting along the growth axis, Expedition 325. The corner piece of one half is added to the other half to ensure that both archive and working halves contain 50% of the original core volume. W = working half, A = archive half.

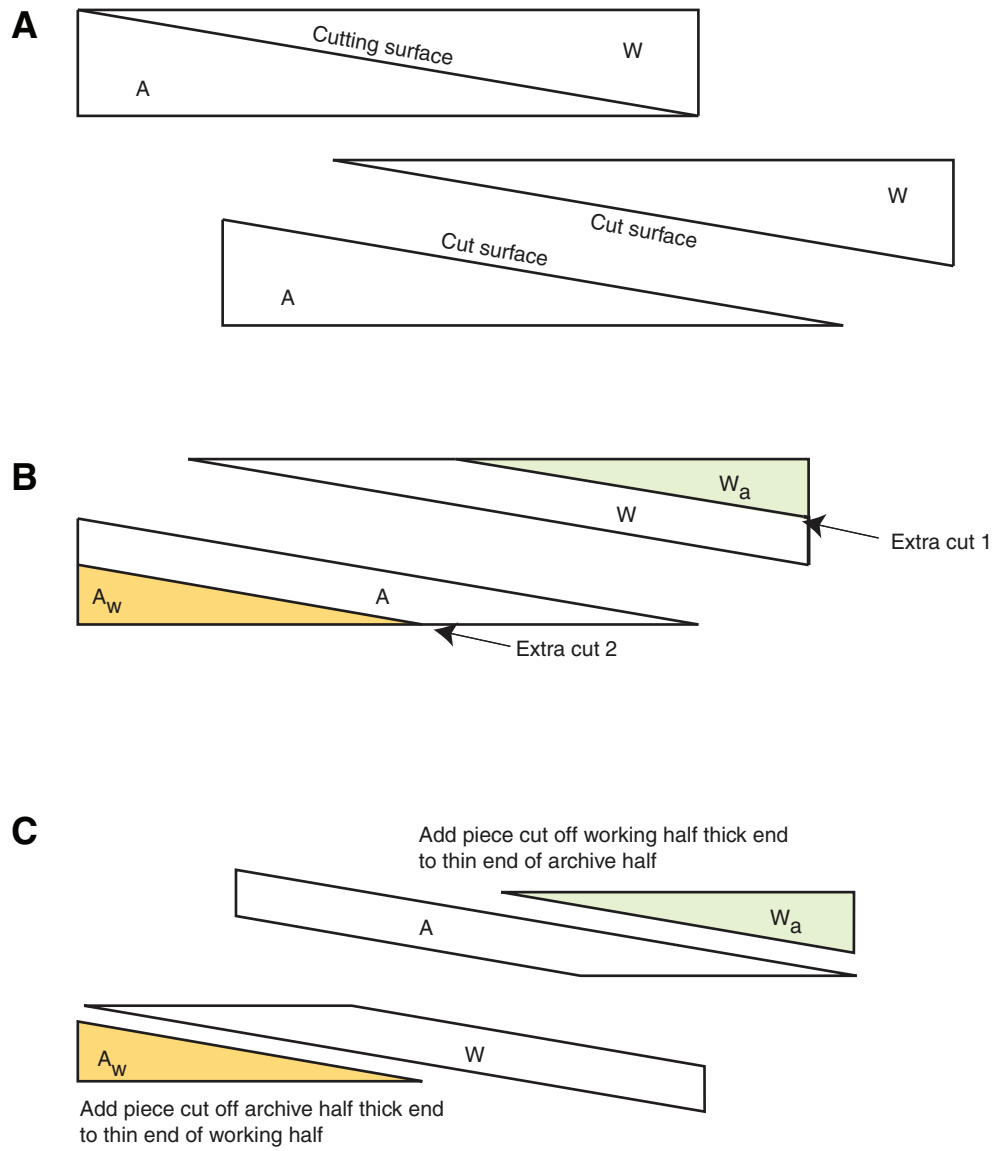




**Table T1.** Summary table showing all site locations, tidal states, dates, and times that the Conductivity, Temperature, and Depth (CTD) YSI 6600 V2-4 Sonde was deployed during Expedition 325. (See table note.)

Site	Hole	Latitude (°S)	Longitude (°E)	Date (2010)	Time (UTC)		File	Approximate tide cycle	Comments
					Start	End			
HYD-01C									
3	M0034A	19.6923	150.2303	18 Feb	1916	1923	CTD_1_M0034	Rising tide	
3	M0034A	19.6923	150.2303	19 Feb	0417	0425	CTD_2_M0034	Slack low tide	
3	M0034A	19.6923	150.2303	19 Feb	0826	0830	CTD_3_M0034	Rising tide	
3	M0034A	19.6923	150.2303	19 Feb	1054	1057	CTD_4_M0034	High tide	
3	M0034A	19.6923	150.2303	19 Feb	1500			Falling tide	Attempt abandoned because of strong surface currents.
3	M0034A	19.6923	150.2303	19 Feb	1729	1736	CTD_5_M0034	Low tide	
11	M0035A	19.6726	150.2438	28 Feb	0802	0810	CTD_6_M0035	High tide	Attempt abandoned—strong currents prevented anything deeper than 40 m.
11	M0035A	19.6726	150.2438	28 Feb	2200			Falling tide	Attempt abandoned because of currents off starboard side and positioning of winch.
11	M0036A	19.6724	150.2440	1 Mar	1902	1908	CTD_7_M0036	Rising tide	Attempt abandoned because of CTD failure at ~18 m.
9	M0037A	19.6707	150.2463	3 Mar	1654	1707	CTD_8_M0037	Slack low tide	
8	M0038A	19.6716	150.2449	4 Mar	1651	1656	CTD_9_M0038	Falling tide	Abandoned at 30 m because of strong current.
8	M0039A	19.6716	150.2449	5 Mar	0653	0705	CTD_10_M0039	Slack tide	Sonde to 100 m.
8	M0039A	19.6716	150.2449	5 Mar	0911	0919	CTD_11_M0039	Rising tide	Sonde to 100 m.
9	M0039A	19.6716	150.2449	5 Mar	1225	1243	CTD_12_M0039	High tide	Deployed to 60 m—ran out of cable!
HYD-02A									
10	M0040A	19.7963	150.4814	6 Mar	0739	0747	CTD_13_M0040	Slack tide	Sonde to 114 m.
10	M0041A	19.7963	150.4815	6 Mar	1545	1603	CTD_14_M0041	Falling tide	Sonde to 60 m, recovered because of proximity to other cable.
2	M0042A	19.8440	150.4480	8 Mar	0303	0307	CTD_15_M0042	Near high tide	Sonde to 51 m.
2	M0042A	19.8440	150.4480	8 Mar	1026	1029	CTD_16_M0042	1 h before low tide	Sonde to 50.6 m.
8	M0044A	19.7985	150.4796	10 Mar	0943	0953	CTD_17_M0044	Falling tide	Sonde to 97.5 m with 150 m cable out.
8	M0044A	19.7985	150.4796	11 Mar	1300	1304	CTD_18_M0044	Slack low tide	Sonde only deployed to 8 m because of swell and unpredictable current.
Test 1	Anchorage	19.1296	146.8307	15 Mar	0645	0648	CTD_anchorage	Rising tide	Sonde at sea surface measures 10.6 m, so deduct this from all depths. Date and time also incorrect.
Test 2	Anchorage	19.1296	146.8307	17 Mar	0630	0632	CTD_anchorage_2	Rising spring tide	Sonde now measuring correct depth after calibration—date and time still out.
RIB-02A									
4	M0049B	15.4724	145.8237	22 Mar	0530	0540	CTD_19_M0049	High tide (neaps)	Time incorrect again. Sonde to 52 m.
4	M0049B	15.4724	145.8237	22 Mar	0910	0920	CTD_20_M0049	Falling tide	Time incorrect again. Sonde to 89.9.
4	M0049B	15.4724	145.8237	22 Mar	1348	1415	CTD_21_M0049	Falling tide	Sonde to 90.3 m.
3	M0051A	15.4721	145.8230	23 Mar	0513	0520	CTD_22_M0051	Start of falling tide	Sonde to 77.6 m.
NOG-01B									
6	M0052C	17.1011	146.5763	27 Mar	0913	0921	CTD_23_M0052	Falling tide	Sonde to 98 m.
6	M0053A	17.1011	146.5763	28 Mar	0925	0934	CTD_24_M0053	Slack after high tide	Sonde to 107 m.
6	M0053A	17.1011	146.5763	28 Mar	1457	1517	CTD_25_M0053	Rising tide	Sonde to 102 m.
7	M0054A	17.1007	146.5767	29 Mar	0852	0859	CTD_26_M0054	High tide	Sonde to 104 m.
7	M0054A	17.1007	146.5767	29 Mar	1439	1507	CTD_27_M0054	Low tide	Sonde to 103.5 m.
7	M0054A	17.1007	146.5767	30 Mar	1120	1126	CTD_28_M0054	Falling tide	Sonde to 107 m.
7	M0054A	17.1007	146.5767	30 Mar	1651	1705	CTD_29_M0054	Rising tide	Sonde to 106.4 m.
7	M0054A	17.1007	146.5767	31 Mar	0908	0914	CTD_30_M0054	High tide	Sonde to 107 m.
5	M0056A	17.1022	146.5742	2 Apr	1659	1710	CTD_31_M0056	Low tide	Sonde to 83 m (now set to read every 2 s).
5	M0056A	17.1022	146.5742	2 Apr	1955	2008	CTD_32_M0056	Rising tide	Sonde to 81 m.
2	M0057A	17.1050	146.5640	3 Apr	1946	1953	CTD_33_M0057	Rising tide	Sonde to 36.9 m.
2	M0057A	17.1050	146.5640	4 Apr	0731	0734	CTD_34_M0057	Falling tide	Sonde to 47.4 m.
8	M0058A	17.0973	146.5893	4 Apr	2105	2108	CTD_35_M0058	Rising tide	Sonde only deployed 8 m because of unpredictable current and swells.
8	M0058A	17.0973	146.5893	5 Apr	0428	0436	CTD_36_M0058	High tide	Sonde to 132 m—ran out of cable!
8	M0058A	17.0973	146.5893	5 Apr	0810	0818	CTD_37_M0058	Falling tide	Sonde to 130 m.

Note: Comments field identifies if there were any specific issues, such as strong tidal currents, and the maximum depth reached by the sonde.

**Table T2.** Summary table detailing the sensor specifications, resolution, and accuracy for the Conductivity, Temperature, and Depth (CTD) YSI 6600 V2-4 sonde used during Expedition 325. (See table note.)

Sensor	Range	Resolution	Accuracy
Conductivity 6560 sensor (mS/cm)	0–100	0.001–0.1 (range dependent)	±0.5% of reading + 0.00
Salinity (ppt)	0–70	0.01	±1% of reading or 0.1, whichever is greater
Temperature 6560 sensor (°C)	–5 to +60	0.01	±0.15
Depth (m)			
Deep	0–200	0.001	±0.3
Medium	0–61	0.001	±0.12
Shallow	0–9.1	0.001	±0.02
Vented level	0–9.1	0.001	±0.018
Turbidity 6136 sensor (NTU)	0–1.000	0.1	±2% of reading or 0.3, whichever is greater
Chlorophyll 6025 sensor (µg/L Chl)	~0–400	~0.1	0.1
pH 6561 sensor (unit)	0–14	0.01	±0.2
ROX optical dissolved oxygen % saturation	0–500	0.1	0–200: ±1 of reading or 1 of air saturation, whichever is greater
BGA—Phycocyanin (cell/mL)	~0–200,000	~160	1 cell/mL

Note: NTU = nephelometric turbidity units, Chl = chlorophyll, ROX = luminescent dissolved oxygen sensor, BGA = blue-green algae.

**Table T3.** Major and minor components described during the Expedition 325 offshore and Onshore Science Party visual description of cores.

Component	Code used	Comments
Microbialite; undetermined	MB	
Microbialite; stromatolitic	MB-S	
Microbialite; dendritic	MB-D	
Coralline algae; undetermined	CA	
Coralline algae; crustose; thin	CA-t	<1 mm thick
Coralline algae; crustose; thick	CA-T	>1 mm thick
Coralline algae; branching	CA-B	
Coralline algae; nodule	CA-N	
Halimeda	HA	
Foraminifer; undetermined	FO	
Foraminifer; benthic (free)	FO-B	
Foraminifer; encrusting	FO-E	
Foraminifer; planktonic	FO-P	
Mollusk; undetermined	MO	
Mollusk; bivalve	MO-B	
Mollusk; gastropod	MO-G	
Mollusk; vermitid	MO-V	
Coral; undetermined	C	
Coral; encrusting	C-EN	<1 cm thick
Coral; submassive	C-SM	1–5 cm thick
Coral; massive	C-MA	>5 cm thick
Coral; foliaceous	C-FO	Free <5 mm thick
Coral; platy	C-PL	Free >5 mm thick
Coral; branching; fine	C-BF	<1 cm diameter
Coral; branching; medium	C-BM	1–3 cm diameter
Coral; branching; robust	C-BR	3–5 cm diameter
Coral; branching; columnar	C-BC	>5 cm diameter
Coral; tabular	C-T	
Coral; discoid	C-D	Free-living disks
Coral; fragments	C-FR	
Coral; ahermatypic/solitary	C-AS	Solitary or colonial; nonzooxanthellate; often deepwater forms
Coral; nonscleractinian	C-NS	(i.e., <i>Heliopora</i> , <i>Millepora</i> , and <i>Tubipora</i> )
Worm tube; undetermined	W	
Worm tube; serpulid	W-S	

**Table T4.** Sensor summary for the multisensor core logger, Expedition 325.

Sensor	Calibration pieces used		Acceptable departure from full calibration values	Sampling interval (cm)	Spatial resolution (cm)
	Full calibration	Calibration check			
Gamma density	Stepped Al/H <sub>2</sub> O (6, 5, 4, 3, 2, and 0 cm Al)	Distilled water	± 100 cps	1	0.5
P-wave velocity	Distilled water	Distilled water	± 1 μs	1	2
Noncontact resistivity	Saline fluids (35, 17.5, 8.75, 3.5, 1.75, and 0.35 g/L)	3.5 g/L saline fluid	± 10 mV	1	2
Magnetic susceptibility	Impregnated resin calibration piece	Impregnated resin calibration piece	± 5 SI	1	2–3

**Table T5.** Sample split priority for pore water samples, Expedition 325. (See table note.)

Sequential number	Split	Amount (mL)	Preservatives	Vial
1	Anions	0.1–10	—	Eppendorf 2 mL/Nalgene 8 mL
2	Alkalinity	0.3–1	—	Eppendorf 1.5 mL
3	NH <sub>4</sub>	0.5	—	Eppendorf 2 mL
4	Cations	1–10	10 μL HNO <sub>3</sub> per 1 mL of sample	Epp 2 mL/Nalgene 8 mL
5	δ <sup>13</sup> C	2	5 μL HgCl <sub>2</sub>	Crimp 1.8 mL
6	δ <sup>18</sup> O/δD	2	—	Crimp 1.8 mL
7	S/δ <sup>34</sup> S	2	40 μL ZnAc	Twist cap 2 mL
8	DOC/PO <sub>4</sub>	2	—	Crimp 1.8 mL

Note: — = none used.

**Table T6.** Wavelengths used for identifying major and trace elements by ICP-OES measurements, Expedition 325.

Element	Wavelength (nm)
Al	396.153
B	249.667
Ba	455.403
Ca	317.933
Fe	238.204
K	766.490
Li	670.784
Mg	280.271
Mn	257.610
Na	589.592
P	213.617
S	181.975
Si	251.611
Sr	407.771
Ti	334.940
As	193.696
Be	313.042
Cd	228.802
Co	228.616
Cr	267.716
Cu	324.752
Mo	202.031
Ni	231.604
U	385.958
V	310.230
Zn	213.856
Zr	343.823

Table T7. Concentrations of isotopes expressed as masses, Expedition 325. (See table notes.)

Core, section, interval (cm)	<sup>238</sup> U (ppm)	2σ	<sup>232</sup> Th (ppb)	2σ	( <sup>232</sup> Th/ <sup>238</sup> U)	2σ	( <sup>230</sup> Th/ <sup>238</sup> U)	2σ	( <sup>234</sup> U/ <sup>238</sup> U)	2σ
325-										
M0031A-16R-1, 0–3	3.106	0.011	0.20	0.00	0.0000208	0.0000005	0.2341	0.0020	1.1316	0.0007
M0032A-8R-3, 0–2	0.894	0.003	13.56	0.23	0.0049670	0.0000860	0.1944	0.0021	1.1332	0.0007
M0032A-18R-2, 8–10	2.241	0.008	0.99	0.02	0.0001448	0.0000026	0.4854	0.0048	1.1213	0.0007
M0033A-15R-2, 5–7	1.381	0.005	110.40	1.90	0.0261600	0.0004500	0.2815	0.0025	1.1294	0.0007
M0034A-13R-2, 6–8	2.734	0.009	0.17	0.00	0.0000208	0.0000005	0.1120	0.0011	1.1425	0.0007
M0035A-20R-2, 0–2	2.719	0.009	0.30	0.01	0.0000362	0.0000007	0.2024	0.0017	1.1335	0.0008
M0036A-18R-2, 8–10	3.939	0.014	10.39	0.17	0.0008640	0.0000140	0.1981	0.0017	1.1342	0.0007
M0037A-7R-2, 2–4	1.757	0.006	7.44	0.13	0.0013860	0.0000240	0.1241	0.0010	1.1362	0.0007
M0039A-16R-2, 8–10	4.007	0.014	7.22	0.12	0.0005900	0.0000100	0.1810	0.0014	1.1364	0.0007
M0040A-8R-2, 5–8	3.717	0.013	7.45	0.13	0.0006560	0.0000110	0.2304	0.0018	1.1300	0.0007
M0042A-24R-2, 8–9	1.344	0.005	2.87	0.05	0.0006990	0.0000120	0.8780	0.0100	1.0950	0.0007
M0043A-18R-2, 2–4	4.290	0.015	2.81	0.05	0.0002148	0.0000037	0.1934	0.0017	1.1340	0.0008
M0046A-11R-1, 10–11	4.088	0.014	1.55	0.03	0.0001243	0.0000022	0.1668	0.0015	1.1378	0.0007
M0047A-11R-2, 5–6	4.232	0.015	0.96	0.02	0.0000740	0.0000013	0.1978	0.0016	1.1348	0.0007
M0049B-9R-2, 4–5	3.356	0.012	6.83	0.12	0.0006670	0.0000120	0.1520	0.0014	1.1449	0.0007
M0053A-25R-2, 2–3	4.533	0.016	6.68	0.12	0.0004821	0.0000087	0.2217	0.0020	1.1315	0.0007
M0054B-4R-2, 2–3	3.682	0.013	2.71	0.05	0.0002414	0.0000043	0.1919	0.0015	1.1355	0.0008
M0055A-5R-3, 0–1	2.678	0.009	12.80	0.22	0.0015650	0.0000270	0.2332	0.0020	1.1307	0.0007
M0056A-13R-2, 2–3	1.674	0.006	26.90	0.50	0.0052610	0.0000930	0.6007	0.0051	1.1062	0.0007
M0057A-15R-3, 9–10	1.074	0.004	1.95	0.04	0.0005950	0.0000110	1.1730	0.0130	1.0868	0.0007

Notes: Uncertainties of concentrations include all weighing errors; isotope ratios are independent of weighing uncertainties. All isotope ratios are expressed as activities and are calculated using the decay constants of Cheng et al. (2000), Holden (1990), and Jaffey et al. (1971).

Table T8. Uncalibrated radiocarbon ages expressed in years before AD 1950, Expedition 325. (See table notes.)

Core, section, interval (cm)	Dated lithology	<sup>14</sup> C age	
		k.y. BP	1σ
325-			
M0031A-2R-2, 7-10	C	11.75	0.04
M0031A-8R-2, 7-9	C	13.83	0.05
M0032A-1R-2, 0-2	MB	11.36	0.04
M0032A-3R-2, 11-13	C	13.04	0.04
M0033A-3R-2, 4-6	C	12.52	0.04
M0033A-7R-2, 0-2	C	13.24	0.04
M0034A-1R-2, 2-4	C	9.36	0.04
M0034A-7R-2, 12-14	C	10.36	0.04
M0035A-3R-2, 2-4	C	13.03	0.04
M0035A-12R-2, 4-6	C	15.38	0.05
M0036A-8R-2, 2-4	C	14.05	0.04
M0036A-11R-2, 6-8	C	14.76	0.05
M0037A-4R-1, 6-8	C/b	7.60	0.04
M0037A-6R-2, 9-11	C	13.43	0.04
M0038A-1R-2, 2-4	C	11.70	0.04
M0039A-1R-2, 3-4	C	12.10	0.04
M0039A-9R-2, 9-10	C	14.73	0.05
M0040A-2R-1, 16-17	C	9.03	0.04
M0040A-4R-2, 7-8	C	13.24	0.04
M0041A-2R-2, 4-6	C	14.23	0.04
M0042A-1R-2, 2-3	C	9.03	0.03
M0042A-10R-1, 6-8	C	11.10	0.03
M0043A-2R-2, 3-4	C	12.85	0.04
M0043A-9R-2, 1-2	C	14.95	0.04
M0044A-2R-1, 0-1	C	12.77	0.04
M0044A-8R-2, 4-5	C	14.21	0.04
M0046A-6R-2, 4-5	C	13.36	0.04
M0046A-9R-2, 5-7	C	13.71	0.04
M0047A-3R-2, 6-8	C	12.95	0.05
M0047A-7R-2, 8-9	C	14.94	0.04
M0048A-2R-2, 7-8	C	12.75	0.04
M0049B-2X-1, 3-4	C	3.85	0.03
M0049B-4R-2, 6-7	C	10.69	0.03
M0050A-2R-2, 2-3	b	9.90	0.03
M0051A-2R-1, 0-1	C	9.54	0.03
M0052B-1R-2, 4-5	C	12.79	0.04
M0052C-1R-1, 3-4	C	14.72	0.03
M0053A-3R-1, 4-5	C	14.02	0.03
M0053A-9R-2, 2-3	C	16.77	0.04
M0054B-1W-1, 5-6	C	11.64	0.03
M0054B-3R-1, 7-8	C	15.65	0.04
M0055A-1R-2, 4-5	C	12.62	0.03
M0055A-4R-2, 150-151	C	19.69	0.05
M0056A-2R-1, 149-150	C	30.08	0.10
M0056A-5R-1, 68-69	C	34.25	0.15
M0057A-5R-1, 133-134	C	10.91	0.03
M0058A-4X-2, 0-2	*	48.03	0.53
M0058A-11X-4, 0-2	?	—	—

Notes: — = not calculated. C = coral, MB = microbiolite, b = bivalve, \* = shell fragment?



**Table T9.** Closed system age interpretations for U-Th dated samples, Expedition 325. (See table notes.)

Core, section, interval (cm)	Age (k.y. BP)	2 $\sigma$	[ <sup>234</sup> U/ <sup>238</sup> U] <sub>i</sub>	2 $\sigma$
325-				
M0031A-16R-1, 0–3	25.13	0.24	1.1413	0.0008
M0032A-8R-3, 0–2	20.42	0.24	1.1411	0.0007
M0032A-18R-2, 8–10	61.10	0.80	1.1442	0.0009
M0033A-15R-2, 5–7	31.07	0.32	1.1413	0.0008
M0034A-13R-2, 6–8	11.18	0.11	1.1471	0.0008
M0035A-20R-2, 0–2	21.33	0.20	1.1418	0.0008
M0036A-18R-2, 8–10	20.82	0.19	1.1423	0.0008
M0037A-7R-2, 2–4	12.54	0.11	1.1411	0.0008
M0039A-16R-2, 8–10	18.82	0.15	1.1439	0.0008
M0040A-8R-2, 5–8	24.73	0.22	1.1394	0.0008
M0042A-24R-2, 8–9	169.30	4.50	1.1533	0.0022
M0043A-18R-2, 2–4	20.28	0.20	1.1419	0.0008
M0046A-11R-1, 10–11	17.19	0.16	1.1446	0.0008
M0047A-11R-2, 5–6	20.78	0.19	1.1430	0.0008
M0049B-9R-2, 4–5	15.80	0.15	1.1515	0.0008
M0053A-25R-2, 2–3	23.65	0.24	1.1406	0.0008
M0054B-4R-2, 2–3	20.08	0.18	1.1434	0.0008
M0055A-5R-3, 0–1	25.05	0.25	1.1403	0.0008
M0056A-13R-2, 2–3	84.10	1.10	1.1347	0.0010
M0057A-15R-3, 9–10	No closed system age possible			

Notes: Ages are presented in thousands of years before AD 1950 so as to be comparable to calibrated radiocarbon ages. [<sup>234</sup>U/<sup>238</sup>U]<sub>i</sub> is [<sup>234</sup>U/<sup>238</sup>U] extrapolated back to the time of coral growth.

**Table T10.** Effect of correction for initial <sup>230</sup>Th for crustal contamination and (the worst case) seawater Th incorporation, Expedition 325. (See table notes.)

Core, section, interval (cm)	Dated lithology	<sup>232</sup> Th (ppb)	2 $\sigma$	U-Th age no correction		U-Th age crustal correction		U-Th age seawater correction	
				k.y. BP	2 $\sigma$	k.y. BP	2 $\sigma$	k.y. BP	2 $\sigma$
325-									
M0031A-16R-1, 0–3	C	0.20	0.00	25.13	0.24	25.1	0.2	25.1	0.2
M0032A-8R-3, 0–2	C	13.56	0.23	20.42	0.24	19.7	0.8	15.9	4.6
M0032A-18R-2, 8–10	C	0.99	0.02	61.10	0.80	61.1	0.8	61.0	0.8
M0033A-15R-2, 5–7	C	110.40	1.90	31.07	0.32	27.2	4.0	4.9	30.6
M0034A-13R-2, 6–8	C	0.17	0.00	11.18	0.11	11.2	0.1	11.2	0.1
M0035A-20R-2, 0–2	C	0.30	0.01	21.33	0.20	21.3	0.2	21.3	0.2
M0036A-18R-2, 8–10	C	10.39	0.17	20.82	0.19	20.7	0.2	20.1	0.8
M0037A-7R-2, 2–4	C	7.44	0.13	12.54	0.11	12.3	0.2	11.3	1.3
M0039A-16R-2, 8–10	C	7.22	0.12	18.82	0.15	18.7	0.2	18.3	0.6
M0040A-8R-2, 5–8	C	7.45	0.13	24.73	0.22	24.6	0.2	24.1	0.6
M0042A-24R-2, 8–9	C	2.87	0.05	169.30	4.50	169.2	4.4	168.7	4.4
M0043A-18R-2, 2–4	C	2.81	0.05	20.28	0.20	20.3	0.2	20.1	0.3
M0046A-11R-1, 10–11	C	1.55	0.03	17.19	0.16	17.2	0.2	17.1	0.2
M0047A-11R-2, 5–6	C	0.96	0.02	20.78	0.19	20.8	0.2	20.7	0.2
M0049B-9R-2, 4–5	C	6.83	0.12	15.80	0.15	15.7	0.2	15.2	0.6
M0053A-25R-2, 2–3	C	6.68	0.12	23.65	0.24	23.6	0.3	23.2	0.5
M0054B-4R-2, 2–3	C	2.71	0.05	20.08	0.18	20.1	0.2	19.9	0.3
M0055A-5R-3, 0–1	C	12.80	0.22	25.05	0.25	24.8	0.3	23.7	1.4
M0056A-13-2, 2–3	C/b	26.90	0.50	84.10	1.10	83.3	1.3	79.3	5.0
M0057A-15R-3, 9–10	C	1.95	0.04	No closed system age possible					

Notes: U-Th age interpretations are assumed to be a closed system. Three assumptions for the correction of initial <sup>230</sup>Th were made. First, no correction was made (this is the value, rounded to 1 ka, used for the purposes of preliminary dating). Second, two further age interpretations involving corrections for initial <sup>230</sup>Th were made, one assuming a detrital Th contamination from continental material ([<sup>230</sup>Th/<sup>232</sup>Th] = 1.030) and another assuming Th contamination scavenged from seawater ([<sup>230</sup>Th/<sup>232</sup>Th] = 9.250). BP = age before present (1950 AD). C = coral, b = bivalve.

Table T11. Calibrated radiocarbon ages, Expedition 325. (See table notes.)

Core, section, interval (cm)	Dated lithology	Age (cal y BP)			
		From	To	Mean	1 $\sigma$
325-					
M0031A-2R-2, 7-10	C	13.34	13.10	13.22	0.06
M0031A-8R-2, 7-9	C	16.87	15.99	16.53	0.22
M0032A-1R-2, 0-2	MB	13.06	12.64	12.82	0.10
M0032A-3R-2, 11-13	C	15.23	14.26	14.89	0.21
M0033A-3R-2, 4-6	C	14.13	13.79	13.95	0.09
M0033A-7R-2, 0-2	C	15.86	14.93	15.31	0.23
M0034A-1R-2, 2-4	C	10.38	10.03	10.20	0.08
M0034A-7R-2, 12-14	C	11.66	11.21	11.40	0.13
M0035A-3R-2, 2-4	C	15.22	14.26	14.87	0.21
M0035A-12R-2, 4-6	C	18.54	17.97	18.25	0.17
M0036A-8R-2, 2-4	C	16.98	16.58	16.78	0.10
M0036A-11R-2, 6-8	C	17.82	17.12	17.44	0.18
M0037A-4R-1, 6-8	C/b	8.18	7.93	8.05	0.07
M0037A-6R-2, 9-11	C	16.34	15.15	15.69	0.33
M0038A-1R-2, 2-4	C	13.33	12.98	13.18	0.07
M0039A-1R-2, 3-4	C	13.73	13.38	13.54	0.09
M0039A-9R-2, 9-10	C	17.77	17.07	17.41	0.18
M0040A-2R-1, 16-17	C	9.91	9.53	9.72	0.11
M0040A-4R-2, 7-8	C	15.86	14.93	15.31	0.23
M0041A-2R-2, 4-6	C	17.10	16.74	16.92	0.09
M0042A-1R-2, 2-3	C	9.89	9.54	9.72	0.10
M0042A-10R-1, 6-8	C	12.73	12.42	12.61	0.06
M0043A-2R-2, 3-4	C	15.00	14.14	14.54	0.24
M0043A-9R-2, 1-2	C	17.96	17.26	17.68	0.16
M0044A-2R-1, 0-1	C	14.91	14.04	14.42	0.24
M0044A-8R-2, 4-5	C	17.09	16.731	16.90	0.09
M0046A-6R-2, 4-5	C	16.18	15.07	15.55	0.30
M0046A-9R-2, 5-7	C	16.78	15.61	16.29	0.31
M0047A-3R-2, 6-8	C	15.11	14.22	14.70	0.24
M0047A-7R-2, 8-9	C	17.95	17.26	17.67	0.17
M0048A-2R-2, 7-8	C	14.89	14.02	14.39	0.24
M0049B-2X-1, 3-4	C	3.95	3.64	3.79	0.08
M0049B-4R-2, 6-7	C	12.30	11.76	12.04	0.12
M0050A-2R-2, 2-3	b	11.05	10.61	10.82	0.12
M0051A-2R-1, 0-1	C	10.51	10.24	10.38	0.07
M0052B-1R-2, 4-5	C	14.93	14.06	14.45	0.24
M0052C-1R-1, 3-4	C	17.72	17.05	17.39	0.17
M0053A-3R-1, 4-5	C	16.95	16.55	16.76	0.10
M0053A-9R-2, 2-3	C	19.83	19.39	19.52	0.11
M0054B-1W-1, 5-6	C	13.28	12.93	13.12	0.09
M0054B-3R-1, 7-8	C	18.68	18.07	18.45	0.18
M0055A-1R-2, 4-5	C	14.49	13.83	14.08	0.14
M0055A-4R-2, 150-151	C	23.39	22.58	22.97	0.23
M0056A-2R-1, 149-150	C	34.74	33.95	34.41	0.23
M0056A-5R-1, 68-69	C	39.28	37.98	38.73	0.25
M0057A-5R-1, 133-134	C	12.59	12.23	12.42	0.10
M0058A-4X-2, 0-2	*	49.17*	47.03*	48.08*	0.54*

Notes: \* = indicates age near the limit of radiocarbon dating. "From" and "To" are the limits of the upper and lowermost 95.4% confidence interval window(s). See Figure F12. C = coral, MB = microbiolite, b = bivalve, \* = shell fragment?

Table T12. EM51 magnetic susceptibility sonde measurement parameters, Expedition 325.

Parameter	Mnemonic	Depth offset	
		(cm)	Recommended unit
Conductivity	IL	100	mmho
Magnetic susceptibility	MSUS	31	mSI unit

**Table T13.** EM51 magnetic susceptibility sonde general specifications, Expedition 325.

Parameter	Induction	Magnetic susceptibility
Intercoil spacing (cm)	50	25
Operating frequency (kHz)	100	2
Measuring range	1–3000 mS/m (0.33–1000 $\Omega$ m)	10 <sup>-4</sup> to 2 SI unit
Accuracy (%)	100–1000 mS/m: 3; 1000–3000 mS/m: 10	3

**Table T14.** Logging tools, recording devices, and software used for data acquisition and processing, Expedition 325.

Number	Tool	Recording device	Software	Processing software
1	OBI40	ALT A-BOX or matrix	ALTLogger/matrix logger	WellCAD
2	ABI40	ALT A-BOX or matrix	ALTLogger/matrix logger	WellCAD
3	IDRONAUT	ALT A-BOX or matrix	ALTLogger/matrix logger	WellCAD
4	ASGR	ALT A-BOX	ALTLogger	WellCAD
5	DIL45	ALT A-BOX or matrix	ALTLogger/matrix logger	WellCAD
6	SONIC	Matrix	Matrix logger	WellCAD
7	EM51	Matrix	Matrix logger	WellCAD
8	CAL3	Matrix	Matrix logger	WellCAD

Table T15. Microbiology samples taken during the offshore phase of Expedition 325. (See table notes.)

Core, section, interval (cm)	Type	Volume (cm <sup>3</sup> )	Sample request	Half
325-				
M0033A-7R-1, 40–45	MBIO	160	546 IODP	WR
M0035A-19R-1, 63–68	MBIO	160	546 IODP	WR
M0036A-21R-2, 0–5	MBIO	160	546 IODP	WR
M0037A-9R-1, 57–62	MBIO	160	546 IODP	WR
M0037A-10R-1, 140–145	MBIO	160	546 IODP	WR
M0037A-13R-1, 36–41	MBIO	160	546 IODP	WR
M0040A-1R-2, 25–30	MBIO	160	546 IODP	WR
M0040A-10R-1, 46–51	MBIO	160	546 IODP	WR
M0040A-12R-1, 146–151	MBIO	160	546 IODP	WR
M0041A-1R-1, 46–51	MBIO	160	546 IODP	WR
M0041A-8R-1, 51–56	MBIO	160	546 IODP	WR
M0041A-10R-1, 81–86	MBIO	160	546 IODP	WR
M0041A-12R-1, 142–147	MBIO	160	546 IODP	WR
M0042A-29R-1, 42–47	MBIO	160	546 IODP	WR
M0053A-1X-1, 106–111	MBIO	160	546 IODP	WR
M0058A-2X-1, 94–99	MBIO	160	546 IODP	WR
M0058A-7X-1, 95–100	MBIO	160	546 IODP	WR
M0058A-10X-1, 118–123	MBIO	160	546 IODP	WR
M0058A-13X-1, 145–150	MBIO	160	546 IODP	WR
M0037A-7R-1, 0–4	MBIO	50	546 IODP	WR
M0055A-3R-2, 38–39	MBIO	30	546 IODP	WR
M0040A-1R-2, 30–35	MBIO	160	595 IODP	WR
M0041A-8R-1, 56–61	MBIO	160	595 IODP	WR
M0041A-10R-1, 86–91	MBIO	160	595 IODP	WR
M0041A-12R-1, 147–152	MBIO	160	595 IODP	WR
M0052A-1X-2, 0–5	MBIO	160	595 IODP	WR
M0053A-27R-1, 59–64	MBIO	160	595 IODP	WR
M0053A-27R-1, 54–59	MBIO	160	595 IODP	WR
M0053A-32R-1, 38–43	MBIO	160	595 IODP	WR
M0053A-32R-1, 43–48	MBIO	160	595 IODP	WR
M0055A-1R-1, 19–23	MBIO	140	595 IODP	WR
M0055A-1R-1, 23–27	MBIO	140	595 IODP	WR
M0058A-1X-1, 57–62	MBIO	160	595 IODP	WR
M0058A-1X-1, 62–67	MBIO	160	595 IODP	WR
M0058A-4X-1, 144–149	MBIO	160	595 IODP	WR
M0058A-4X-1, 149–154	MBIO	160	595 IODP	WR
M0058A-8X-1, 94–99	MBIO	160	595 IODP	WR
M0058A-8X-1, 99–104	MBIO	160	595 IODP	WR
M0058A-15X-1, 108–113	MBIO	160	595 IODP	WR
M0058A-15X-1, 113–118	MBIO	160	595 IODP	WR

Notes: MBIO = microbiology. WR = whole round. All samples taken were 5 cm in length.